8-15-2013

Structural and Functional Study of the Diheme Cytochrome c Subunit of the Cytochrome bc Complex in Heliobacterium modesticaldum

Hair Yue
Washington University in St. Louis

WASHINGTON UNIVERSITY IN ST. LOUIS

Department of Chemistry

Dissertation Examination Committee:

Robert E. Blankenship, Chair

Liviu Mirica

John-Stephen Taylor

Gary Patti

Himadri Pakrasi

Hani Zaher

Structural and Functional Study of the Diheme Cytochrome *c* Subunit of the Cytochrome *bc* Complex in *Heliobacterium modesticaldum*

by

Hai Yue

A dissertation presented to the
Graduate School of Arts and Sciences
of Washington University in
partial fulfillment of the
requirements for the degree of
Doctor of Philosophy

August 2013

St. Louis, Missouri

TABLE OF CONTENTS

LIST OF FIGURES

Chapter 1

Chapter 2

Acknowledgements

It would be impossible to thank everyone that helped me during the course of my thesis work. Several people really stand out though, and I will acknowledge them here. First and foremost is my thesis advisor and mentor, Professor Robert E. Blankenship, whose guidance and support made this thesis possible. His passion for science and most accessible personality made my life in graduate school filled with excitement and refreshing experiences. I must also express my eternal gratitude to my parents, who have always been supporting me and encouraging me to pursue my dream, without any hesitation. My research committee members, Professor Michael Gross and Professor Liviu Mirica have been taking time offering helpful suggestions and discussions for the past five years, for which I am forever grateful. Dr. Hao Zhang and Ms. Ying Zhang need to be thanked for their much needed help and patience in planning and discussing our mass spectromety work. Dr. Dariusz Niedzwiedzki, Dr. Haijun Liu, Dr. Xinliu Gao and Ms. Erica Majumder also contributed heavily to my understanding of protein biochemistry, biophysics and structural modeling with their insight into problems that I was unable to solve by myself. Dr. Aaron Collins's help in teaching me how to culture heliobacteria and use the anaerobic chamber properly when I first joined the group is deeply appreciated. I would also like to thank all of the people in the lab group that I had the opportunity to meet and work with, who created such a friendly and helpful environment that I have truly enjoyed. Finally, I would like to thank NASA, my favorite institution in the world, for the financial support.

Dedicated to my family, the ultimate sanctuary for my heart

“To strive, to seek, to find, and not to yield”

----*Ulysses*, by Lord Alfred Tennyson

ABSTRACT OF THE DISSERTATION

Structural and Functional Study of the Diheme

Cytochrome *c* Subunit of the Cytochrome *bc* Complex

in *Heliobacterium modesticaldum*

By

Hai Yue

Doctor of Philosophy in Chemistry

Washington University in St. Louis, 2013

Professor Robert E. Blankenship, Chair

This dissertation is focused on the structural and functional study of the unique diheme cytochrome *c* subunit of the cytochrome *bc* complex in *H. modesticaldum*, and its application in determining the stoichiometry between *H. modesticaldum*'s cytochrome *bc* complex and its reaction center. *Heliobacterium modesticaldum* is a gram positive, anaerobic, anoxygenic photoheterotrophic bacterium. Its cytochrome *bc* complex (Rieske/cyt *b* complex) has some similarities to cytochrome b_6f complexes from cyanobacteria and chloroplasts, and also shares some characteristics of typical bacterial cytochrome bc_1 complexes. One of the unique features of the heliobacterial cytochrome *bc* complex is the presence of a diheme cytochrome *c* instead of the monoheme cytochrome *f* in the cytochrome b_6f complex or the monoheme cytochrome c_1 in the bc_1 complex. To understand the structure and function of this diheme cytochrome *c* protein, we expressed the N-terminal transmembrane-helix-truncated soluble *H. modesticaldum* diheme cytochrome *c* in *Escherichia coli*. This 25 kDa recombinant protein possesses two *c*-type hemes,

confirmed by mass spectrometry and a variety of biochemical techniques. Sequence analysis of the *H. modesticaldum* diheme cytochrome *c* indicates that it may have originated from gene duplication and subsequent gene fusion, as in cytochrome c_4 proteins. The recombinant protein exhibits a single redox midpoint potential of + 71 mV vs NHE, which indicates that the two hemes are in very similar protein binding environments. Further studies by hydrogen/deuterium exchange mass spectrometry (HDX-MS) and ion mobility mass spectrometry (IM-MS) show unambiguously that there is a real structural conformational difference between the oxidized and reduced diheme cytochrome *c*. A smaller or more compact reduced form might have the function of bringing the two hemes closer to facilitate interheme electron transfer, which also implies a mechanism that is possibly sensitive to the distance between hemes. To determine the stoichiometry of heliobacterial reaction center (RC) and cytochrome *bc* complex, which is a crucial step toward building a more accurate heliobacterial cyclic electron transfer (CET) model, antibodies against the diheme cytochrome *c* was raised and quantitative Western blotting was performed to probe and calculate the content of the cytochrome *bc* complex. The amount of RC was determined by measuring the absorption spectrum of the Bchl *g* (Bchl *g*') in the cell methanol extract. A stoichiometry of 14 to 8 RCs per cytochrome *bc* complex catalytic center was estimated, a much larger number than previously reported, indicating a high turnover number of the cytochrome *bc* complex.

This research was supported by grant NNX08AP62G from the Exobiology program of NASA.

Chapter 1

Introduction

General introduction into photosynthesis

Photosynthesis is a biological process whereby the sun's energy is captured and stored by a series of events that convert the pure energy of light into the biochemical energy to power life [1, 2]. It is arguably the most important process ever to have evolved, and provides the foundation for essentially all life, all our food and most of our energy resources. Over the past billions of years of earth's geological evolution, photosynthesis profoundly altered the face of our planet [3].

Photosynthesis uses light from the sun to drive a series of chemical reactions. Although the sun produces a broad spectrum of light that ranges from gamma rays to radio waves, when the light reaches the surface of the earth, most of the ultraviolet part is absorbed by the ozone molecules in the atmosphere. The entire visible range of light, from 400 nm to 700 nm, and part of the near infrared range, from 700 nm to 1000 nm, are crucial in powering photosynthesis in most of the photosynthetic organisms [4]. The light quality, referring to the spectral content or color of the light, can vary a lot between different environments. One classic example is in a forest, while the upper part of the canopy receives the full solar spectrum, the floor receives only the light that is not absorbed above, therefore the one enriched in green and far red region. Interestingly, there are many elegant mechanisms different organisms use to adapt to changes in light quality [1].

In eukaryotic photosynthetic organisms, photosynthesis is localized in chloroplasts, which contains all the chlorophyll molecules and carry out most important reactions and stages of photosynthesis [5]. It is well established that chloroplasts were derived from symbiotic cyanobacteria through the process known as endosymbiosis [6]. Within chlorophlasts, an

extensive membrane system is found, the thylakoids, where light absorption and the early or primary reactions that transform light energy into biochemical energy happen [7, 8, 9].

In the more primitive prokaryotic photosynthetic organisms, photosynthesis takes place in the cytoplasmic membrane, or specialized membranes that are derived from it [10-14]. The carbon metabolism reactions happen in the cytoplasm, along with all the other crucial reactions for the cell's metabolism.

Starting with photon absorption, and ending with stable carbon products being synthesized, photosynthesis can be divided in convenience into four distinct temporal phases: (1) photon absorption and energy delivery by antenna systems, (2) primary electron transfer in reaction centers, (3) energy stabilization by secondary processes, and (4) synthesis and export of stable products [1].

The starting point of photosynthesis is the absorption of a photon of light, creating an excited state that eventually leads to charge separation in the reaction center. These two processes are facilitated by specialized protein complexes that bind pigments, such as chlorophyll and carotenoids as well as other cofactors [15]. Because the absorption of light and the electron transfer usually occur in separate protein complexes, they can be classified as the antenna system and the reaction center (RC). The function of the antenna is to increase the amount of energy that can be absorbed [16] which could be subsequently used by the RC. The RC traps and converts light energy into chemical energy.

In most instances, light is absorbed by antenna pigments located in peripheral pigment-binding complexes linked to the RC, or just inside the RC. The energy of the photon excites the pigment molecules to excited states, which can relax by different processes, including loss of energy as heat, emission of a fluorescent photon or promotion of chemical reactions such as

electron transfer. In intact photosystems, the dominant relaxation mechanism is excitation transfer to lower energy state pigments, eventually terminated at the primary donor of the RC where the energy is used for electron transfer reactions. The antenna systems don't carry out any chemical reactions, only energy transfer from one molecule to another, which is a pure physical process depending on a weak energetic coupling of the antenna pigments. Vectorial excitation transfer from antenna to RC is achieved by orienting the pigments with respect to the excited state energy: usually pigments with the lowest energy are near to the RC [17].

A variety of antennas are found in various photosynthetic organisms [18 - 24], and they can be broadly divided into integral membrane antenna complexes that cross the lipid bilayer, and peripheral membrane antenna complexes that are associated with components buried in the membrane. Fig. 1 shows two representative antenna protein-pigment complexes, the LH2 complex as integral membrane antenna, and the chlorosome as a peripheral membrane antenna. Although in most conditions, antenna systems' greatly increasing the amount of energy that can be absorbed is an advantage, in some cases, however, too much light energy input could lead to severe damage to the organisms. Therefore, antenna systems have extensive and multifunctional regulation, protection and repair mechanisms [25, 26, 27].

The transformation from pure energy of excited states to chemical changes in molecules happens in the RC complexes, which are integral membrane pigment-proteins that span the membrane in a vectorial fashion. All reaction centers conduct light driven electron transfer reactions, resulting in charge separation across the membrane [28]. Inside the RC, a specific pigment, known as the primary donor (P), traps the excitation passed from the antenna system. The energy is used to promote an electron from P to a higher energy orbital where it becomes an extremely strong reductant. In the ultrafast steps through a series of acceptors, an electron from

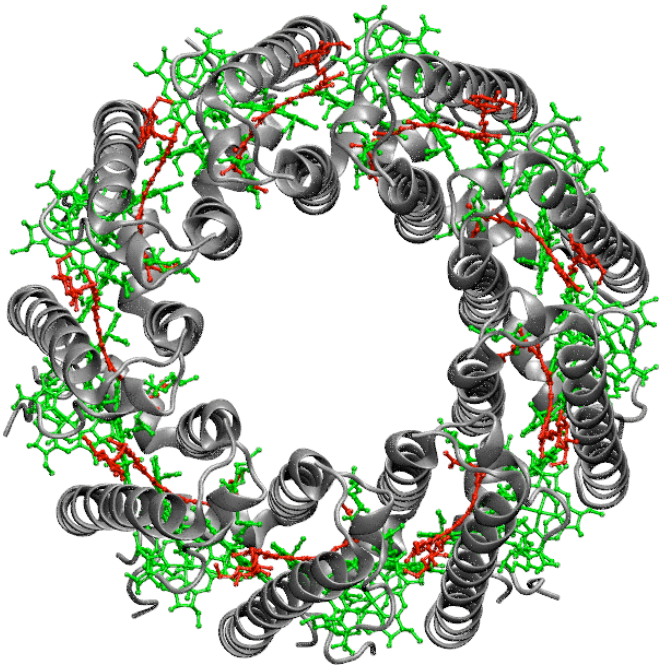

(**a**)

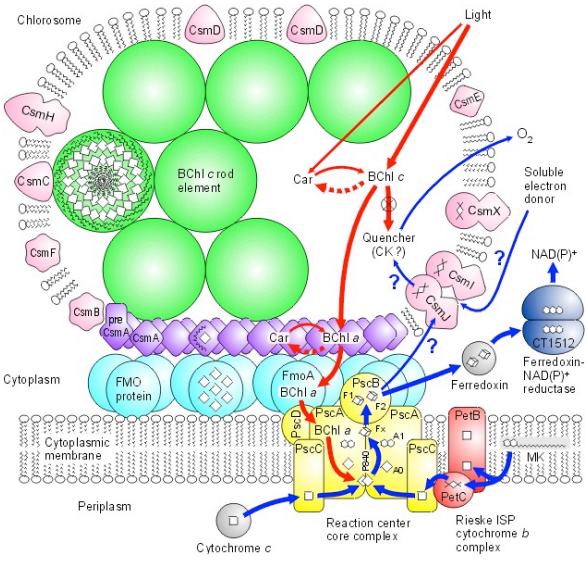

(**b**)

Fig. 1 Two representative antenna protein-pigment complexes. (a) Structure of the LH2 complex in *Rhodopseudomonas acidophila*. View perpendicular to the membrane plane, produced from Protein Data Bank file 1KZU. (b) Model of chlorosome from green sulfur bacteria [24].

the excited donor is spatially separated from P, creating a charge-separated state. At such point, the reaction could go to two possible directions: (1) the electron is transferred back to the donor and the energy of the photon is converted to heat; or (2) the oxidized and the reduced species are separated from each other through a series of ultrafast secondary electron reactions resulting in the separation of positive and negative charges. The rapidity of the secondary electron transfer reactions greatly decreases the chance of charge recombination and produces stable products [29]. The final result is that within a nanosecond, the oxidized and reduced species are separated by the thickness of the membrane (~30Å). After that, slower processes can take over and further stabilize the energy storage and convert it into more easily utilized forms. The system is so efficient in most cases that the quantum yield of products formed per photon absorbed is nearly 1.0.

Unlike the antenna complexes, which are highly diverse and different among species, reaction centers in photosynthetic species are generally homologous [30-34]. The reaction center complexes can be classified into two broad groups based on the identity of the early electron acceptors, Type I with iron-sulfur (FeS) cluster centers as acceptors and Type II with pheophytin and quinone as acceptors. Although functionally and structurally different from each other, structural and genetic analyses strongly indicate that both classes of reaction centers derived from a common ancestor [35, 36].

In the oxygen evolving form of photosynthesis, found in plants, algae, and cyanobacteria, water-splitting reaction ($2H_2O \rightarrow 4H^+ + 4e + O_2$) provides electrons that are eventually transferred to NADP. The removal of electrons from water leads to the release of oxygen and reduced NADP (NADPH) is used to reduce carbon dioxide (CO_2) to produce sugars. To accomplish this energetically uphill reaction, two types of RCs are linked in series,

Photosystem I and Photosystem II [37, 38]. In the anoxygenic form of photosynthesis found in bacteria, only one type of RC is used [39]. Purple bacteria and the chloroflexaceae contain Type II reaction centers, similar to Photosystem II [40, 41], and the green sulfur bacteria and heliobacteria contain Type I reaction center, similar to Photosystem I. The single photosystems found in anoxygenic photosynthetic bacteria are simpler than the more complex linked systems of oxygenic photosynthesis.

Following the primary electron transfer in RCs, the electron transfer will follow two different pathways, cyclic photosynthetic electron transfer and noncyclic photosynthetic electron transfer [1]. In cyclic electron flow, electrons begin in the RC complex, passing from the primary electron acceptor to a secondary acceptor, then returning to the RC complex. By coupling proton movement across the membrane with it, cyclic electron transfer stores the photon energy in the result of light-driven pH difference or electrochemical gradient generation, which is used to drive the synthesis of ATP [42]. Purple bacteria and filamentous anoxygenic phototrophs like chloroflexaceae are the typical species that carry out cyclic electron transfer. In higher plants, cyanobacteria and algae, in which noncyclic electron transfer happens, electrons get passed through a series of electron carriers and eventually to a terminal acceptor, like $NADP^+$. The pattern is less certain in heliobacteria, green sulfur bacteria and acidobacteria. Despite the vast differences between the two types of electron transfer pathways, they both couple with proton translocation which is the driving force for ATP synthesis. Fig. 2 shows a schematic diagram of the membrane architecture and electron transfer in a variety of phototrophic bacteria [43].

The final phase of photosynthetic energy storage involves the production of stable high-energy molecules and their utilization to power a variety of cellular processes. NADPH and ATP are used to reduce CO_2 to sugars.

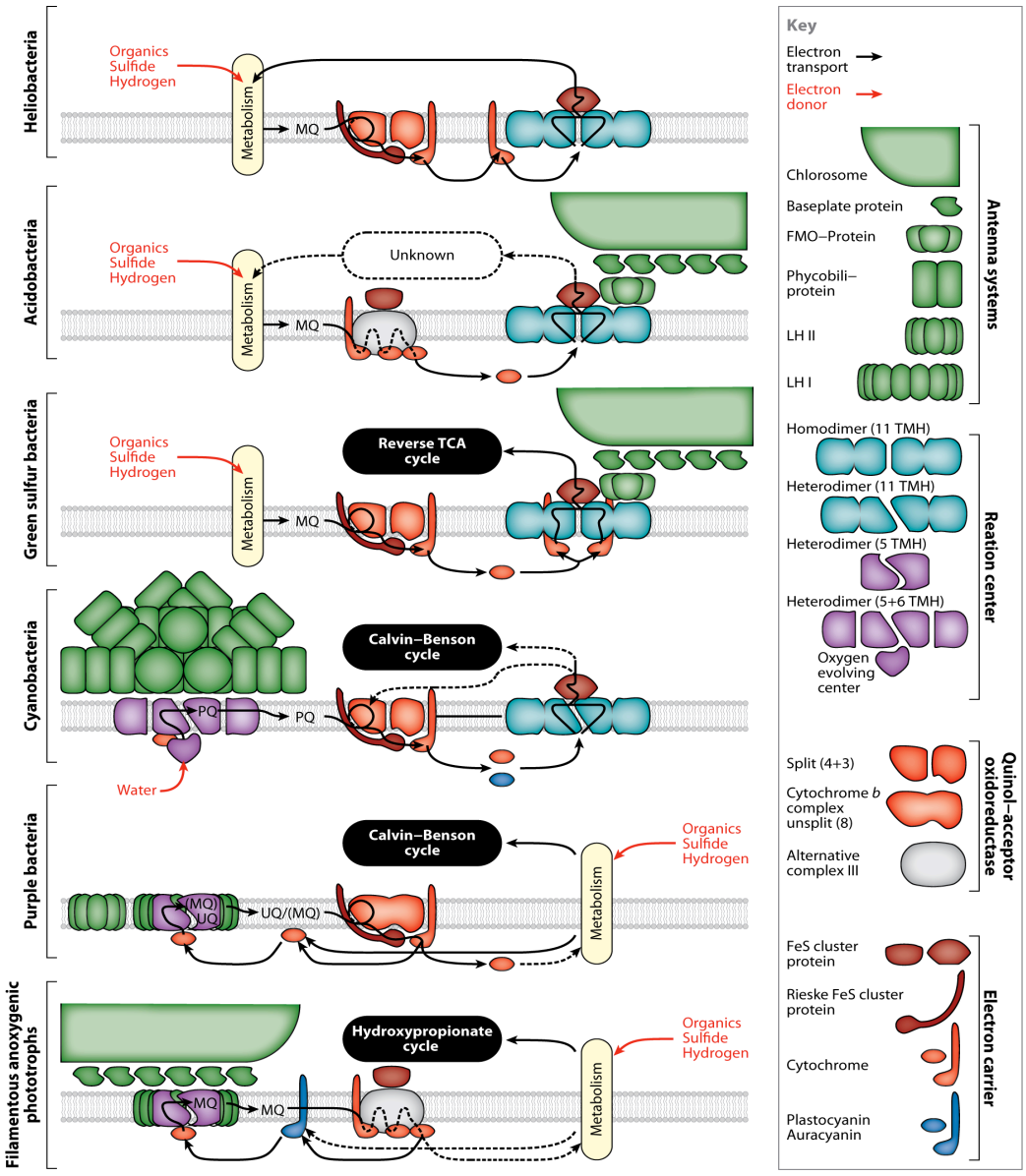

Hohmann-Marriott MF, Blankenship RE. 2011.
Annu. Rev. Plant Biol. 62:515–48

Fig. 2 Photosynthetic machinery and electron transport of photosynthetic bacteria, including a description of photosynthetic complexes. Abbreviations: LH, light harvesting; MQ, menaquinone; PQ, plastoquinone; TCA, tricarboxylic acid; TMH, transmembrane helix(ces); UQ, ubiquinone. Adapted from Hohmann-Marriott and Blankenship (2011).

Cytochrome *bc* complex in microorganisms

The ubihydroquinone:cytochrome *c* oxidoreductase, also called complex III or the cytchrome bc_1 complex, is a multi-subunit enzyme encountered in a very broad variety of organisms such as eukaryotes, like yeast or mammals, plants, or bacteria [44-48]. While mitochondria and some bacteria, e. g. purple bacteria, have related cytochrome bc_1 complexes, plant and algeal chloroplasts and cyanobacteria contain a related yet distinct complex called the plastohydroquinone:plastocyanin oxidoreductase or the cytochrome b_6f complex [49]. The cyt bc_1 complex and cyt b_6f complex are essential components of the energy transduction machinery of the vast majority of photosynthetic organisms. From an evolutionary perspective, these complexes have in common a pair of cytochrome *b* hemes and a [2Fe-2S] Rieske iron-sulfur cluster [50, 51, 52]. In addition to this catalytic core, most complexes possess structurally variable, or non-conserved secondary electron carriers, usually a *c*-type cytochrome or functionally equivalent redox carriers, while some contain an additional *c*-type heme bound to the cyt *b* protein [53, 54]. Fig. 3 shows the core structures of cyt b_6f and cyt bc_1 complex side by side and the cofactors they bind with.

The primary roles of the cytochrome *bc* complexes are: (1) to make an electronic connection between the two-electron chemistry of the quinone pool and the one-electron chemistry of the downstream electron transfer chain; and (2) to translocate protons across the bioenergetic membrane, thus storing a portion of the potential energy from the two electron-two proton oxidation reaction in the electrochemical proton gradient, or proton motive force (*pmf*) [55, 56]. The *pmf* in turn drives the synthesis of ATP by the ATP synthase. A general equation for the overall reaction catalyzed by the cyt *bc* complex can be summarized as:

$$QH_2 + 2C(oxi) + H^+(n) <=> Q + 2C(red) + 2H^+(p)$$

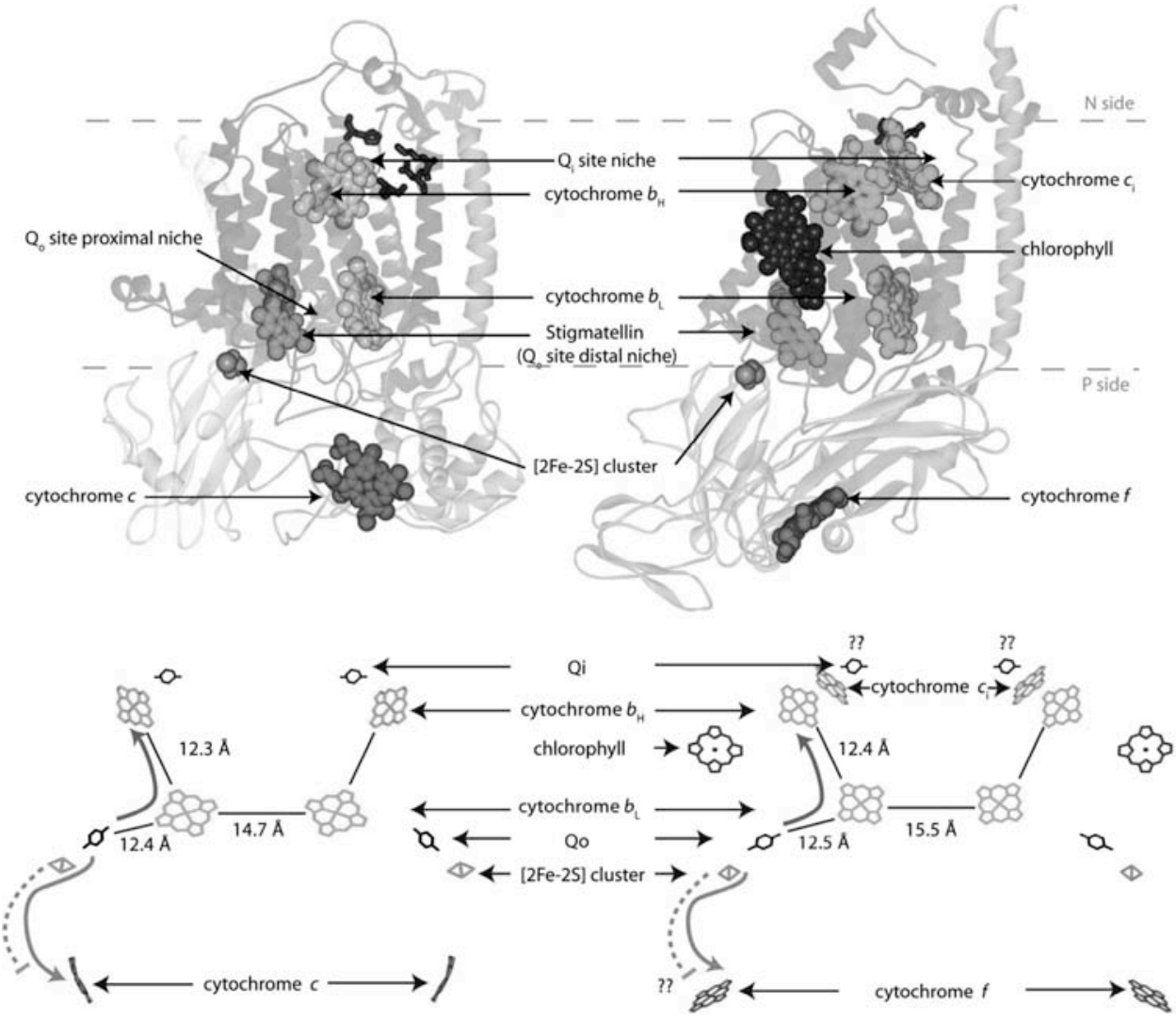

Fig. 3 Similarities and differences in the electron transfer chains and core structures of the cyt bc_1 and cyt b_6f complexes. The gross functional monomeric structures of the cyt *b*, cyt *c* and the iron-sulfur protein coordinating portions of the cyt bc_1 (left) or cyt b_6f -type (right) complexes are illustrated side-by-side as matching ribbon structures with the cofactors coordinated in each drawn as space filled spheres. The glaring differences of the presence of an extra *c*-type heme (heme c_i) adjacent to the Q_i (or Q_N) site of the cyt b_6f, as well as the presence of the non-redox active chlorophyll molecule in the same complex are readily seen in these side-by-side

illustrations. However, in each case, a similar high and low potential chain of cofactors facilitating bifurcated electron flow following QH_2 oxidation is easily envisioned. Both types of complex are shown with the inhibitor, stigmatellin bound at the Q_o (or Q_p) site as well as amino acids, pictured as stick models, thought to be important for Q_i (or Q_N) site substrate binding to aid in visually identifying the two spatially distinct Q binding sites. The illustrations have been worked up from the *Rba. capsulatus* and *Mastigocladus laminosus* derived atomic coordinate files 1ZRT.pdb and 1VF5.pdb, respectively. The entire illustration is adapted from D. M. Kramer, W. Nitschke, J. W. Cooley, The Purple Phototrophic Bacteria, *Advances in Photosynthesis,* (2009).

Where QH_2 and Q are the reduced and oxidized forms of the native quinone, e.g. ubiniquinole (UQH_2) or menaquinol (MH_2). C(oxi) and C(red) are oxidizd and reduced downstream electron carriers, e.g. cytochrome c_2 in purple bacteria, or membrane anchored cytochrome c_{553} in heliobacteria. H^+(n) and $2H^+$(p) are aqueous protons on the positively and negatively charged sides of the energy transducing membrane.

The path of electron transfer from quinol to the soluble or membrane anchored cyt *c* through the *bc* complex is called the protonmotive Q-cycle. The Q-cycle model postulates two separate quinone/quinol binding sites, Q_o (quinol-oxidizing site) and Q_i (quinone-reducing site), showed in Fig. 4. The Q_o site is located near the positive side of the membrane (periplasmic side); Q_i site is located near the negative side of the membrane (cytoplasmic side). The Q-cycle is initiated when a QH_2 molecule is bound at the Q_o site with the [2Fe-2S] cluster and the heme b_L in their oxidized forms, allowing a bifurcated oxidation of QH_2, with one electron going to the high potential chain (Rieske FeS protein and cyt *c*/*f*), and the other going to the low potential chain (Fig. 4). The first electron is transferred to the [2Fe-2S] cluster. At the same time the quinol will transiently form a semiquinone (SQ) species at the Q_o site, which in turn reduces heme b_L, a process that involves proton transfer from QH_2 and SQ species to protein residues [57, 58]. The electron on the [2Fe-2S] cluster is transferred to the secondary high potential chain carrier, cyt c_1 in the cyt bc_1 complex, or cyt *f* in the cyt b_6f complex. This electron transfer step is facilitated by a large scale pivoting of the Rieske FeS protein from the 'b' position at cyt *b* surface to the 'c' position in contact with the cyt *c*/*f* subunit [59]. From cyt *c*/*f*, electrons are transferred to a downstream, tertiary carrier and then to a source of oxidant (e.g., the photosynthetic reaction center). The electron passed from SQ to heme b_L is passed to heme b_H, driven by a substantial difference of potentials between the two hemes [60]. In the case of the cyt

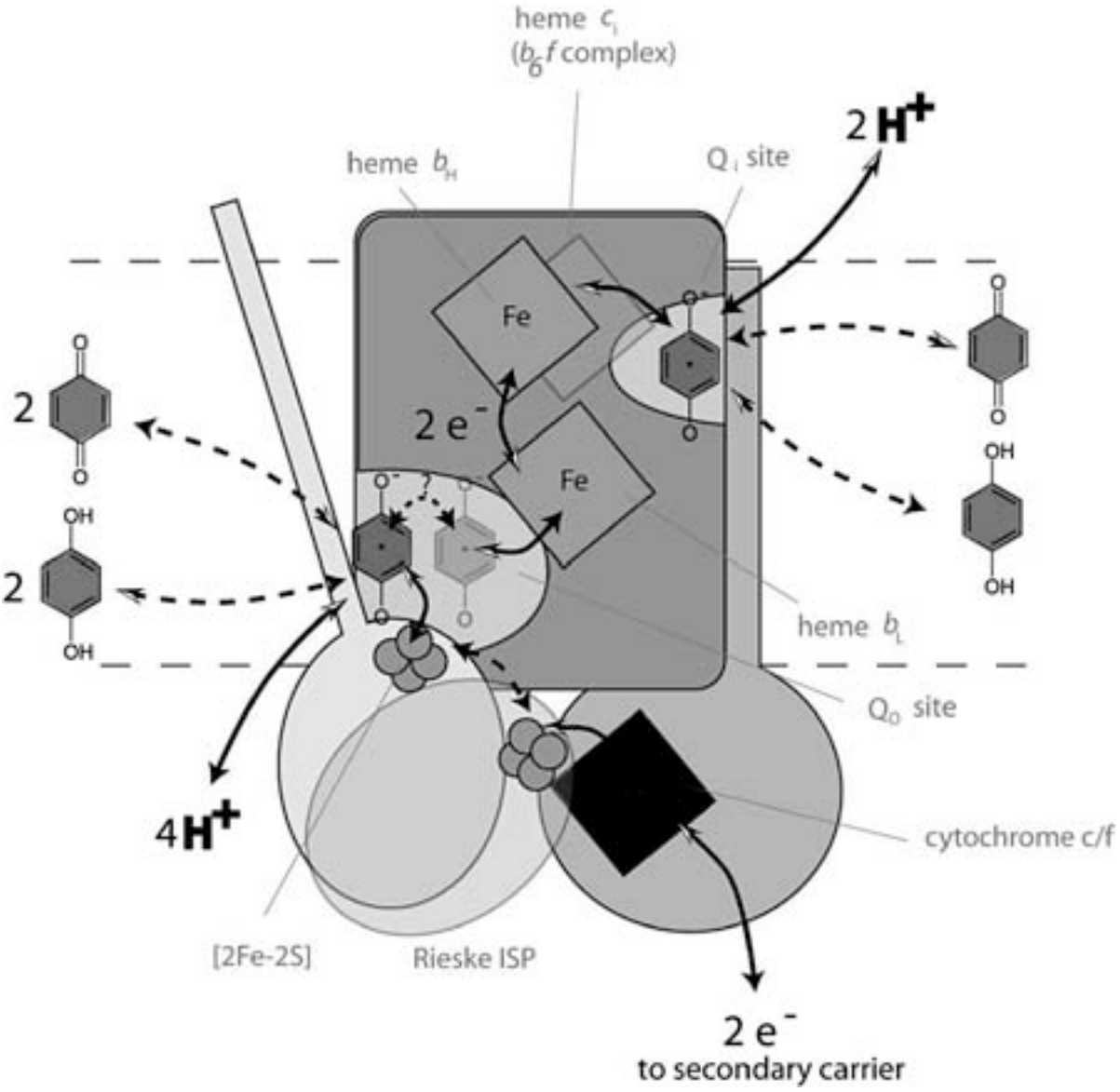

Fig. 4 The general Q-cycle framework. Shown is a cartoon depicting the common 'wiring diagram' of the *bc* complexes, known as the Q-cycle. Key functional components of both the cyt bc_1 and cyt b_6f complex are included. The Q-cycle mechanism is described in detail in the text. Adapted from D. M. Kramer, W. Nitschke, J. W. Cooley, The Purple Phototrophic Bacteria, *Advances in Photosynthesis,* (2009).

bc_1 complex, electrons from heme b_H are transferred to a quinone bound at the Q_i site forming a stabilized SQ. The process of oxidizing the cyt *b* hemes is clearly different in the case of the cyt b_6f and related complexes, e.g. heliobacterial cytochrome *bc* complex, and likely involves a third heme between heme b_H and a quinone species bound at the Q_i site. In either case, oxidation of a second QH_2 molecule at the Q_o site is required to introduce a second electron into the low potential chain [53], which, together with the first electron, reduces a quinone to a QH_2 at the Q_i site with an uptake of two protons from the *n*-side of the membrane. The bifurcated oxidation of QH_2 at the Q_o site results in the net release of two protons into the *p*-side of the membrane and the generation of *pmf* is used to generate chemical energy in the form of ATP.

Though intensively studied for decades, there are still many open questions about the structural functional relationship of the *bc* complex. In the cyt b_6f complex's case, the exact function of the Q_i site and heme c_i is not clear [50, 61-65]. And the role of the carotenoid and chlorophyll seen in the crystal structure is not known either [53, 66-70].

Heliobacteria and their photosystem

Heliobacteria are photosynthetic bacteria that uniquely employ bacteriochlorophyll (Bchl) *g* as the major pigment and primary electron donor within their type I reaction centers [71-77]. This pigment is related to chlorophyll *a* but has an ethylidine functional group at the C-8^1 position and is esterified with farnesol rather than phytol [78, 79]. An oxidized form of chlorophyll *a*, 8^1-hydroxy-chlorophyll *a*, is the primary electron acceptor from the reaction center special pair [80]. Unlike other anoxygenic phototrophic bacteria, e.g. purple bacteria or green bacteria, heliobacteria have no Bchl-containing internal membranes, such as lamellae (purple bacteria) and chlorosomes (green bacteria). In heliobacteria, photosynthetic pigments are

confined to RCs in the cytoplasmic membrane [81, 82]. Carotenoids are also unusual in heliobacteria in that they consist of C_{30} pigments rather than the C_{40} derivatives that are observed in all other phototrophs [83]. The dominant carotenoid in all species of heliobacteria is 4,4′-diaponeurosporene [84]. Although the vast majority of phototrophic bacteria are autotrophic, heliobacteria are obligate heterotrophs [85, 86]. Growth occurs either photoheterotrophically on a limited range of organic substrates or by fermentation of pyruvate in darkness [87, 88]. Phylogenetically, heliobacteria are the only phototrophic organisms that group with the low GC Gram-positive bacteria in 16S rRNA gene sequence analyses [89]. It has been suggested that a strong tie may exist to cyanobacteria [90]. In addition, heliobacteria are unique among all phototrophic organisms in that they can undergo endosporulation [91].

Like all known heliobacteria, *Heliobacterium modesticaldum* is an active dinitrogen fixer [92, 93, 94]. *H. modesticaldum* shares the distinction with the green sulfur bacterium *Chlorobaculum tepidum* of being the only cultured anoxygenic phototrophs capable of N_2-fixation above 50 °C [93]. Nitrogen fixation in heliobacteria is regulated using a “switch off” mechanism, in which the presence of excess ammonia inhibits nitrogenase activity. The unique photosynthetic features, physiological characters and phylogenetic affiliation of heliobacteria make this group of organisms an obvious research subject. In 2008, the genome of *H. modesticaldum* strain Ice1 was sequenced and annotated, which is a major step in the study of heliobacteria [95, 96]. Based on the genome annotation, combined with the previously available biochemical and biophysical studies, a putative photosystem electron transfer model was proposed [97]. Fig. 5 shows the photosynthetic reaction chain core proteins, which have been the focus of many heliobacterial bioenergetic studies [85]. The absence of separate antenna systems

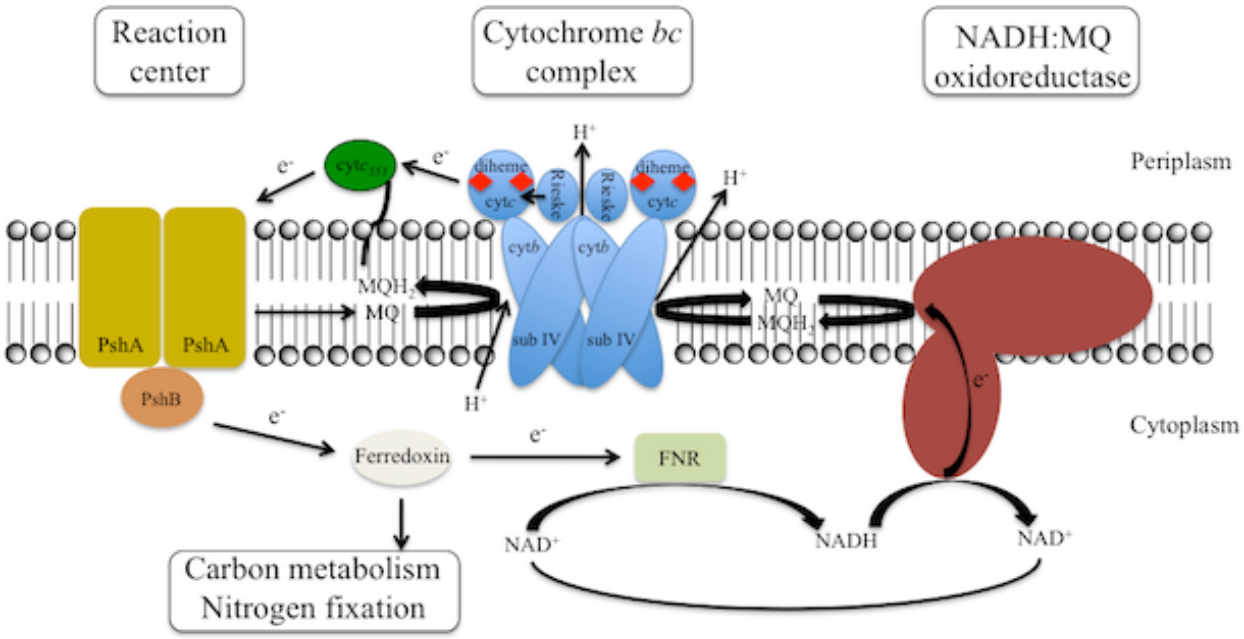

Fig. 5 Photosynthetic reaction chain core proteins in *Heliobacterium modesticaldum*. Reaction center, cytochrome *bc* complex and NADH:menaquinone oxidoreductase (complex I) protein complexes in the membrane based on genetic components present in *Heliobacterium modesticaldum*. The cytochrome *bc* complex is here presented as a dimmer based on its structural similarity to the cytochrome bc_1 and b_6f complex.

provides a certain advantage for spectroscopic investigation of the electron transfer chain, but the organism's high sensitivity to oxygen complicates these studies [98]. Furthermore, there have been reports that the rest of the electron transfer chain except the RCs can be only studied in whole cells, because any cell disturbance or membrane preparation would disrupt the function [99].

The RCs are the major proteins in the cytoplasmic membrane for *H. modesticaldum* cells grown photosynthetically. Its core is composed of the 67-kDa PshA polypeptide, which is predicted to span the membrane 11 times, like PsaA and PsaB of photosystem I. The RC form a homodimer structure made of an identical pair of core proteins, as in the case of the green sulfur bacterial RCs [100, 101], all of which suggests that heliobacteria are one of the most primative photosynthetic organisms known. All known type II RCs are heterodimeric, like the ones in purple bacteria and chloroflexi. The structural and functional relationships in the homodimeric type I RCs remain poorly understood [102, 103, 104].

Heliobacterial cytochrome *bc* complex

Enzymes homologous to the cyt bc_1 and b_6f complexes are found in almost all major phyla of the tree of life, including photosynthetic organisms like heliobacteria. They function in diverse types of energy conserving chains, such as photosynthetic electron transport. The subunit composition of the enzyme family is somewhat variable with respect to the subunits analogous to cyt c_1 or cyt *f* but strictly conserved regarding the functional core, which contains cyt *b* or cytb_6/subunit IV, and the iron sulfur protein (Rieske protein). In *H. modesticaldum*, the four genes proposed to encode for the cyt *bc* complex were identified in the same operon, *petC* (Rieske iron sulfur protein), *petB* (cytochrome *b*), *petD* (subunit IV) and *petA* (diheme

cytochrome *c*) [95]. Inhibitor studies showed that heliobacterial cyt *bc* complex is sensitive to stigmatellin [105, 106], an inhibitor of Q_o-site, but not to antimycin A. All of the above indicates that the heliobacterial *bc* complex resembles the b_6f-type complex. Heme c_i, which is attached to the protein by a single cysteine residue and present in the cyt b_6 subunit in b_6f complex, was also detected in heliobacterial *bc* complexes, using SDS-PAGE followed by heme-staining [107, 108]. Three enrichment protocols of the heliobacterial *bc* complex have been published so far [106, 108, 109], yet none of which could yield an intact enzyme, in contrast to what has been achieved for the b_6f complex [110]. The lack of purified intact protein and 3D structure makes the exact function of the complex remain unknown.

The gene encoding cyt c_{553} (*petJ*), which re-reduces the RC after its primary donor is light-oxidized [99], is located upstream of the *petCBDA* operon, implying that cyt c_{553} is functionally related to the cyt *bc* complex. Cyt c_{553} also has close functional links to the reaction center, so the *bc* complex should work with reaction center closely as well. So far, based on limited studies on the heliobacterial *bc* complex, the function is similar to the b_6f complex in cyanobacteria in general.

Different from the case in cyt c_1 or cyt *f*, a diheme cytochrome *c* plays the role of the terminal electron acceptor in the high-potential electron transfer chain of the *bc* complex in heliobacteria [108, 111]. This cytochrome is of the c_4 type, and the sequence comparisons of the two monoheme domains suggest that it probably results from gene duplication and subsequent gene fusion [112]. Possessing such a diheme cyt *c* subunit differentiates the heliobacterial *bc* complex from those of all other anoxygenic phototrophs, and presents a burning yet interesting question: what exactly is the structural and functional role of it? In fact, diheme cytochromes, attached to the hydrophobic part of the *bc* complexes via a transmembrane helix, are widespread

among actinobacteria, where a fusion of two different monoheme cytochromes was put forward [113, 114], and ε-proteobacteria where sequence analysis indicated that they also have a c_4-type fold [115]. Cyt c_1 also seems to originate from a c_4-type cytochrome by losing one heme-binding site, then a consequent collapse of part of the cytochrome c_4 structure results in the current cyt c_1 [115]. On the other hand, the structure of cyt *f* is completely unrelated to c_1 or c_4 type (diheme cyt *c*) cytochromes [116]. All of the information above puts the diheme cyt *c* subunit and the entire heliobacterial cytochrome *bc* complex in a very unique evolutionary position.

Statement of thesis

This dissertation is focused on the structural and functional study of the unique diheme cytochrome *c* subunit, and its further application in the understanding of the relationship between *H. modesticaldum*'s cytochrome *bc* complex and its reaction center. To achieve these goals, multi-disciplinary approaches were employed, including biochemical, biophysical, spectroscopic and molecular biological techniques. In Chapter 2, the diheme cytochrome *c* subunit was expressed in *E. coli* and characterized with multiple techniques. The potentiometric titration showed a single redox midpoint potential, which leads to the proposal of an inter- and intra-electron transfer mechanism. Chapter 3 further elaborated diheme cytochrome *c*'s redox state related structural changes by studying the protein with ion mobility mass spectrometry and hydrogen-deuterium exchange mass spectrometry under chemically controlled reduced and oxidized states, which provided more structural details to support the hypothesis proposed in Chapter 2. In Chapter 3, using the antibodies raised against diheme cytochrome *c*, we utilized immunoblotting to quantify the cyt *bc* complex. By comparing it to the reaction center measured by absorption spectroscopy, we provide the first biochemical/biophysical *in vitro* quantification

of the stoichiometry of the heliobacterial *bc* complex and reaction center. Chapter 5 gives a short conclusion and prospectus.

References:

[1] R. E. Blankenship, Molecular mechanisms of photosynthesis 1st ed., *Blackwell Science* (2002), pp. 1-10.
[2] R. H. Garrett, C. M. Frisham, Principles of biochemistry with a human focus 1st ed., *Thomson Learning* (2002).
[3] R. E. Blankenship, Early evolution of photosynthesis, *Plant Physiology* **154** (2010), pp. 434-438.
[4] B. A. Osborne, J. A. Raven, Light absorption by plants and its implications for photosynthesis, *Biological reviews* **61** (1986), pp. 1-60.
[5] E. Gantt, Oxygenic photosynthesis and the distribution of chloroplasts, *Photosyn. Res.* **107** (2011), pp. 1-6.
[6] W. Martin, C. Schnarrenberger, The evolution of the Calvin cycle from prokaryotic to eukaryotic chromosomes: a case study of functional redundancy in ancient pathways through endosymbiosis, *Curr. Genet.* **32** (1997), pp. 1-18.
[7] K. J. van Wijk, Plastid proteomics, *Plant. Physiol. Biochem.* **42** (2004), pp. 963-977.
[8] G. Friso, L. Giacomelli, A. J. Ytterberg, J. B. Peltier, A. Rudella, Q. Sun, K. J. van Wijk, In-depth analysis of the thylakoid membrane proteome of *Arabidopsis thaliana* chloroplasts: new proteins, new functions, and a plastid proteome database, *Plant Cell* **16** (2004), pp. 478-499.
[9] T. Kleffmann, M. Hirsch-Hoffman, W. Gruissem, S. Baginsky, Plprot: a comprehensive proteome database for different plastid types, *Plant Cell physiol.* **47** (2006), pp. 432-436.
[10] D. A. Bryant, N. U. Frigaard, Prokaryotic photosynthesis and phototrophy illuminated, *Trends Microbiol.* **14** (2006), pp. 488-496.
[11] R. E. Blankenship, Origin and early evolution of photosynthesis, *Photosynth. Res.* **33** (1992), pp. 91-111.
[12] R. E. Blankenship, Protein structure, electron transfer and evolution of prokaryotic photosynthetic reaction centers. *Antonie van Leeuwenhoek* **65** (1994), pp. 311-329.
[13] R. S. Gupta, T. Mukhtar, B. Singh, Evolution relationships among photosynthetic prokaryotes (*Heliobacterium chlorum, Chloroflexus aurantiacus, cyanobacteria, Chlorobium tepidum* and proteobacteria): implications regarding the origin of photosynthesis. *Mol. Microbiol.* **32** (1999), pp. 893-906.
[14] R. S. Gupta, Evolutionary relationships among photosynthetic bacteria. *Photosynth. Res.* **76** (2003), pp. 173-183.
[15] R. E. Blankenship, Early evolution of photosynthesis, *Plant Physiology* **154** (2010), pp. 434-438.
[16] H. Tamiaki, Function and structure of photosynthetic antenna, *CSJ Current Review* **2** (2010), pp. 52-58.
[17] R. van Grondelle, H. Bergstrom, V. Sundstrom, R. J. van Dorssen, M. Vos, C. N. Hunter, Photosynthetic light-harvesting systems: organization and function, *de Gruyter & Co., Berlin*, (1988), pp. 519-530.
[18] R. MacColl, Cyanobacterial phycobilisomes, *J. Structural Biology* **124** (1998), pp. 311-334.
[19] E. Wientjes, G. T. Oostergetel, S. Jansson, E. J. Boekema, R. Croce, The role of Lhca complexes in the supramolecular organization of higher plant photosystem I, *J. Biol. Chem.* **273** (1998), pp. 16122-16127.
[20] Z. Liu, H. Yan, K. Wang, T. Kuang, J. Zhang, L. Gui, X. An, W. Chang, Crystal structure

of spinach major light-harvesting complex at 2.72 Å resolution. *Nature* **428** (2004), pp. 287-292.
[21] A. W. Roszak, T. D. Howard, J. Southall, A. T. Gardiner, C. J. Law, N. W. Isaacs, R. J. Cogdell, Crystal structure of the RC-LH1 core complex from *Rhodopseudomonas palustris*, *Science* **302** (2003), pp. 1969-1972.
[22] G. McDermott, S. M. Prince, A. A. Freer, A. M. Hawthornthwaite-Lawless, M. Z. Papiz, R. J. Cogdell, N. W. Isaacs, Crystal structure of an integral membrane light harvesting complex from photosynthetic bacteria, *Nature* **374** (1995), pp. 517-521.
[23] J. Wen, H. Zhang, M. L. Gross, R. E. Blankenship, Surface mapping of the FMO antenna protein on the native membrane from *Chlorobium tepidum* by a combination of chemical labeling and mass spectrometry, *Proc. Natl. Acad. Sci. U. S. A.* **106** (2009), pp. 6134-6139.
[24] R. E. Blankenship, K. Matsuura, Antenna complexes from green photosynthetic bacteria, in *Light-Harvesting Antenna,* Kluwer, Dordrecht, pp. 195-217.
[25] W. I. Gruszecki, Light-driven regulatory mechanisms in the photosynthetic antenna complex LHCII, *Biochem. Soc. Trans.* **38** (2010), pp. 702-704.
[26] D. Kramer, R. Bassi, X. P. Li, A. M. Gilmore, S. Caffarri, T. Golan, K. K. Niyogi, Regulation of photosynthetic light harvesting involes intrathylokoid lumen pH sensing by the PsbS protein, *J. Biol. Chem.* **279** (2004), pp. 22866-22874.
[27] C. Kulheim, J. Agren, S. Jansson, Rapid regulation of light harvesting and plant fitness in the field, *Science* **297** (2002), pp. 91-93.
[28] W. Hillier, G. T. Babcock, Photosynthetic reaction centers, *Plant Physiol.* **125** (2001), pp. 33-37.
[29] C. Kirmaier, D. Holten, Primary photochemistry of reaction centers from photosynthetic purple bacteria, *Photosynth. Res.* **13** (1987), pp. 225-260.
[30] A. Amunts, O. Drory, N. Nelson, The structure of a plant photosystem I supercomplex at 3.4 Å resolution, *Nature* **447** (2007), pp. 58-63.
[31] B. Loll, J. Kern, W. Saenger, A. Zouni, J. Biesiadka, Towards complete cofactor arrangement in the 3.0 Å resolution structure of photosystem II, *Nature* **438** (2005), pp. 1040-1044.
[32] K. N. Ferrerira, T. M. Iverson, K, Maghlaoui, J. Barber, S. Iwata, Architecture of the photosynthetic oxygen-evolving center, *Science* **303** (2004), pp. 1831-1838.
[33] P. Jordan, P. Fromme, H. T. Witt, O. Klukas, W. Saenger, N. Krauss, Three-dimensional structure of cyanobacterial photosystem I at 2.5 Å resolution, *Nature* **411** (2001), pp. 909-917.
[34] J, Deisenhofer, H. Michel, The photosynthetic reaction center from the purple bacterium *Rhodopseudomonas viridis*, *Science* **245** (1989), pp. 1463-1473.
[35] W. D. Schubert, O. Klukas, W. Saenger, H. T. Witt, P. Fromme, N. Krauss, A common ancestor for oxygenic and anoxygenic photosynthetic systems: a comparison based on the structural model of photosystem I, *J. Mol. Biol.* **280** (1998), pp. 297-314.
[36] S. Sadekar, J. Raymond, R. E. Blankenship, Conservation of distantly related membrane proteins: photosynthetic reaction centers share a common structural core, *Mol. Biol. and Evolution* **23** (2006), pp. 2001-2007.
[37] J. H. Golbeck, Structure, function and organization of the photosystem I reaction center complex, *Biochem. Biophys. Acta* **895** (1987), pp. 167-204.
[38] Y. Umena, K. Kawakami, J. R. Shen, N. Kamiya, Crystal structure of oxygen-evolving photosystem II at a resolution of 1.9 Å, *Nature* **473** (2011), pp. 55-60.
[39] D. A. Bryant, N. U. Frigaard, Prokaryotic photosynthesis and phototrophy illuminated, *Trends in Microbiology* **14** (2006), pp. 488-496.

[40] J. Barber, Light-Energy transduction in photosynthesis: Higher plant and bavterial models, *The American Society of Plant Physiologists, Rockville MD,* (1988), pp. 178-196.
[41] R. E. Blankenship, Electron transport in green photosynthetic bacteria, *Photosynth. Res.* **6** (1985), pp. 317-333.
[42] Y. Anraku, Bacterial electron transport chains, *Ann. Rev. of Biochem.* **57** (1988), pp. 101-132.
[43] M. Hohmann-Marriott, R. E. Blankenship, Evolution of photosynthesis, *Ann. Rev. Plant Biol.* **62** (2011), pp. 515-548.
[44] R. B. Gennis, B. Barquera, B. Hacker, S. R. Doren, S. Arnaud, A. R. Crofts, E. Davidson, K. A. Gray, F. Daldal, The bc_1 complexes of *Rhodobacter sphaeroides* and *Rhodobacter capsulatus*, *J. Bioenerg. Biomembr.* **25** (1993), pp. 195-209.
[45] K. A. Gray, F. Daldal, Mutational studies of the cytochrome bc_1 complexes. *Anoxygenic Photosynthetic Bacteria, Kluwer Academic Publishers,* pp. 747-777.
[46] A. R. Crofts, E. A. Berry, Structure and function of the cytochrome bc_1 complex of mitochondria and photosynthetic bacteria, *Curr. Opin. Struct. Biol.* **8** (1998), pp. 501-509.
[47] L. Yu, S. C. Tso, S. K. Shenoy, B. N. Quinn, D. Xia, The role of the supernumerary subunit of Rhodobacter sphaeroides cytochrome bc_1 complex. *J. Bioenerg. Biomembr.* **31** (1999), pp. 251-257.
[48] E. A. Berry, M. Guergova-Kuras, L. S. Huang, A. R. Crofts, Structure and function of cytochrome *bc* complexes, *Annu. Rev. Biochem.* **69** (2000), pp. 1005-1075.
[49] W. A. Cramer, G. Soriano, M. Ponomarev, D. Huang, H. Zhang, S. Martinez, J. Smith, Some new structural aspects and old controversies concerning the cytochrome b_6f complex of oxygenic photosynthesis, *Annu. Rev. Plant. Physiol.* **47** (1996), pp. 477-508.
[50] J. L. Smith, H. Zhang, J. Yan, G. Kurisu, W. A. Cramer, Cytochrome *bc* complexes: a common core of structure and function surrounded by diversity in the outlying provinces, *Curr. Opin. Struc. Biol.* **14** (2004), pp. 432-439.
[51] W. A. Cramer, H. Zhang, J. Yan, G. Kurisu, J. L. Smith, Evolution of photosynthesis: Time-independent structure of the cytochrome b_6f complex, *Biochemistry* **43** (2004), pp. 5921-5929.
[52] C. Hunte, S. Solmaz, H. Palsdottir, T. Wenz, A structural perspective on mechanism and function of the cytochrome bc_1 complex, in *Bioenergetics, Springer-Verlag,* Berlin Heidelberg, (2007).
[53] D. Stroebel, Y. Choquet, J. L. Popot, D. Picot, An atypical haem in the cytochrome b_6f complex, *Nature* **426** (2003), pp. 413-418.
[54] W. A. Cramer, H. Zhang, Consequences of the structure of the cytochrome b_6f complex for its charge transfer pathways. *Biochim. Biophys. Acta.* **1757** (2006), pp. 339-345.
[55] A. R. Crofts, Proton-coupled electron transfer at the Q_o site of the bc_1 complex contros the rate of ubihydroquinone oxidation, *Biochim. Biophys. Acta.* **1655** (2004), pp. 77-92.
[56] J. L. Cape, M. K. Bowman, D. M. Kramer, Understanding the cytochrome *bc* complexes by what they don't do. The Q-cycle at 30, *Trends Plant Sci.* **11** (2006), pp. 46-55.
[57] B. L. Trumpower, R. B. Gennis, Energy transduction by cytochrome complexes in mitochondrial and bacterial respiration: The enzymology of coupling electron transfer reactions to transmembrane proton translocation. *Annu. Rev. Biochem.* **63** (1994), pp. 675-716.
[58] D. M. Kramer, A. G. Roberts, F. Muller, J. Cape, M. K. Bowman, Q-cycle bypass reactions at the Q_o site of the cytochrome bc_1 (and related) complexes. *Methods in Enzymology* **382** (2003), pp. 21-45.

[59] Z. Zhang, L. Huang, V. Shulmeister, Y. Chi, K. Kim, L. Hung, A, Crofts, E. Berry, S. Kim, Electron transfer by domain movement in cytochrome bc_1, *Nature* **392** (1998), pp. 677-684.
[60] W. Nitschke, D. M. Kramer, A, Riedel, U. Liebl, From Naphtho- to benzoquinones-(r)evolutionary reorganizations of electron transfer chains, *Photosynthesis: From Light to Biosphere*, *Kluwer Academic Press, Dordrecht*, (1995), pp. 945-950.
[61] J. Alric, Y. Pierre, D. Picot, J. Lavergne, F, Rappaport, Spectral and redox characterization of the heme c_i of the cytochrome $b_6 f$ complex, *Proc. Natl. Acad. Sci. U. S. A.* **102** (2005), pp. 15860-15865.
[62] F. Baymann, F. Giusti, D. Picot, W. Nitschke, The c_i/b_H moiety in the $b_6 f$ complex studied by EPR: A pair of strongly interacting hemes. *Proc. Natl. Acad. Sci. U. S. A.* **104** (2007), pp. 519-524.
[63] G. M. Soriano, M. V. Ponamarev, C. J. Carrell, D. Xia, J. L. Smith, W. A. Cramer, Comparison of the cytochrome bc_1 complex with the anticipated structure of the cytochrome $b_6 f$ complex: De plus ça change de plus c'est la même chose. *J. Bioenerg. Biomemb.* **31** (1999), pp. 201-213.
[64] A. I. Zatsman, H. Zhang, W. A. Gunderson, W. A. Cramer, M. P. Hendrich, Heme-heme interactions in the cytochrome $b_6 f$ complex: EPR spectroscopy and correlation with structure. *J. Am. Chem. Soc.* **128** (2006), pp. 14246-14247.
[65] H. Zhang, A. Primak, J. Cape, M. K. Bowman, D. M. Kramer, W. A. Cramer WA, Characterization of the high-spin heme x in the cytochrome b_6 f complex of oxygenic photosynthesis, *Biochemistry* **43** (2004), pp. 16329-16336.
[66] G. Kurisu, H. Zhang, J. Smith, W. A. Cramer, Structure of the cytochrome $b_6 f$ complex of oxygenic photosynthesis: tuning the cavity, *Science* **302** (2003), pp. 1009-1014.
[67] N. Dashdorj, H. Zhang, H. Kim, J. Yan, W. A. Cramer, The single chlorophyll a molecule in the cytochrome $b_6 f$ complex: unusual optical properties protect the complex against singlet oxgen, *Biophys. J.* **88** (2005), pp. 4178-4187.
[68] P. Zuo, B. X. Li, X. H. Zhao, Y. S. Wu, X. C. Ai, J. P. Zhang, L. B. Li, T. Y. Kuang, Ultrafast carotenoid-to-chlorophyll singlet energy transfer in the cytochrome $b_6 f$ complex from *Bryopsis corticulans*, *Biophys. J.* **90** (2006), pp. 4145-4154.
[69] Y. Pierre, C. Breyton, Y. Lemoine, B. Robert, C. Vernotte, J. L. Popot, On the presence and role of a molecule of chlorophyll *a* in the cytochrome $b_6 f$ complex, *J. Biol. Chem.* **272** (1997), pp. 21901-21908.
[70] J. Yan, N. Dashdorj, D. Baniulis, E. Yamashita, S. Savikhin, W. E. Cramer, On the structure role of the aromatic residue environment of the chlorophyll in the b_6 f complex, *Biochemistry* **47** (2008), pp. 3654-3661.
[71] H. Gest, J. Favinger, *Heliobacterium chlorum*, an anoxygenic brownish-green photosynthetic bacterium containing a "new" form of bacteriochlorophyll, *Arch. Microbiol.* **136** (1983), pp. 11-16.
[72] C. R. Woese, B. A. Derbunner-Vossbrinck, H. Oyaizu, E. Stackebrandt, W. Ludwig, Gram-positive bacteria: possible photosynthetic ancestry, *Science* **229** (1985), pp. 762-765.
[73] M. Kobayashi, E. J. van de Meent, C. Erkelens, J. Amesz, I. Ikegami, T. Watanabe, Bacterioclorophyll *g* epimer as a possible reaction center component of heliobacteria, *Biochim. Biophys. Acta.* **1057** (1991), pp. 89-96.
[74] R. C. Prince, H. Gest, R. E. Blankenship, Thermodynamic properties of the photochemical reaction center of *Heliobacterium chlorum*, *Biochim. Biophys. Acta.* **810** (1985), pp. 377-384.

[75] T. Noguchi, Y. Fukami, H. Oh-oka, Y. Inoue, Fourier transform infrared study on the primary donor P798 of *Heliobacterium modesticaldum*: cysteine S-H coupled to P798 and molecular interactions of carbonyl groups, *Biochemistry* **36** (1997), pp. 12329-12336.
[76] J. T. Trost, D. C. Brune, R. E. Blankenship, Protein sequences and redox titrations indicate that the electron acceptors in reaction centers from heliobacteria are similar to Photosystem I. *Photosynth Res* **32** (1992), pp. 11-22.
[77] J. T. Trost, R. E. Blankenship, Isolation of a photoactive photosynthetic reaction center-core antenna complex from *Heliobacillus mobilis*, *Biochemistry* **28** (1989), pp. 9898-9904.
[78] M. T. Madigan, The Prokaryotes, *Springer, New York* **4** (2006), pp. 951-964.
[79] T. Mizoguchi, H. Oh-Oka, H. Tamiaki H, Determination of stereochemistry of bacteriochlorophyll g_F and 8^1-hydroxy-chlorophyll a_F from *Heliobacterium modesticaldum*, *Photochem. Photobiol.* **81** (2005), pp. 666-673.
[80] E. J. van de Meent, M. Kobayashi, C. Erkelens, P. A. van Veelen, J. Amesz, T. Watanabe, Identification of 8^1-hydroxychlorophyll *a* as a functional reaction center pigment in heliobacteria, *Biochim. Biophys. Acta.* **1058** (1991), pp. 356-362.
[81] K. Miller, J. S. Jacob, U. Smith, S. Kolaczkowski, M. K. Bowman, *Heliobacterium chlorum*: cell organization and structure, *Arch. Microbiol.* **146** (1986), pp.111-114.
[82] R. C. Fuller, S. G. Sprague, H. Gest, R. E. Blankenship, A unique photosynthetic reaction center from *Heliobacterium chlorum*, *FEBS Lett*. **182** (1985), pp. 345-349.
[83] S. Takaichi, in The Photochemistry of Carotenoids: Applications in Biology, *Kluwer, Dordrecht*, (1999), pp. 39-69.
[84] S. Takaichi, K. Inoue, M. Akaike, M. Kobayashi, H. Oh-oka, M. T. Madigan, The major carotenoid in all known species of heliobacteria is the C_{30} carotenoid 4,4′-diaponeurosporene, not neurosporene, *Arch. Microbiol.* **168** (1997), pp. 277-281.
[85] K. H. Tang, H. Yue, R. E. Blankenship, Energy metabolism of *Heliobacterium modesticaldum* during phototropic and chemotrophic growth, *BMC Microbiol.* **10** (2010), pp. 150.
[86] A. K. Stevenson, L. K. Kimble, C. R. Woese, M. T. Madigan, Characerization of new phototrophic heliobacteria and their habitats, *Photosynth. Res.* **53** (1997), pp. 1-12.
[87] M. T. Madigan, J. G. Ormerod, in Anoxygenic Photosynthetic Bacteria, *Kluwer, Dordrecht*, (1995), pp. 17-30.
[88] L. K. Kimble, A. K. Stevenson, M. T. Madigan, Chemotrophic growth of heliobacteria in darkness, *FEMS Microbiol. Lett.* **115** (1994), pp. 51-55.
[89] I. A. Bryantseva, V. M. Gorlenko, E. I. Kompantseva, L. A. Achenbach, M. T. Madigan, *Heliorestis daurensis*, gen. nov. sp. nov., an alkaliphilic rod-to-coiled-shaped phototrophic heliobacterium from a Siberian soda lake, *Arch. Microbiol*. **172** (1999), pp. 167-174.
[90] W. F. J. Vermaas, Evolution of heliobacteria: implications for photosynthetic reaction center complexes, *Photosynth. Res.* **41** (1994), pp. 285-294.
[91] L. K. Kimble, M. T. Madigan, Molecular evidence that the capacity for endosporulation is universal among phototrophic heliobacteria, *FEMS Microbiol. Lett.* **199** (2001), pp. 191-195.
[92] J. Enkh-Amgalan, H. Kawasaki, T. Seki, NifH and NifD sequences of heliobacteria: a new lineage in the nitrogenase phylogeny, *FEMS Microbiol. Lett.* **243** (2005), pp. 73-79.
[93] L. K. Kimble, L. Mandelco, C. R. Woese, M. T. Madigan MT, *Heliobacterium modesticaldum*, sp. nov., a thermophilic heliobacterium of hot springs and volcanic soils, *Arch. Microbiol*. **163** (1995), pp. 259-267.
[94] L. K. Kimble, M. T. Madigan, Nitrogen fixation and nitrogen metabolism in heliobacteria.

Arch. Microbiol. 158 (1992), pp. 155-161.
[95] W. M. Sattley, M. T. Madigan, W. D. Swingley, P. C. Cheung, K. M. Clocksin, A. L. Conrad, L. C. Dejesa, B. M. Honchak, D. O. Jung, L. E. Karbach, A. Kurdoglu, S. Lahiri, S. D. Mastrian, L. E. Page, H. L. Taylor, Z. T. Wang, J. Raymond, M. Chen, R. E. Blankenship, J. W. Touchman, The genome of *Heliobacterium modesticaldum*, a phototrophic representative of the firmicutes containing the simplest photosynthetic apparatus, *J. Bacteriol.* **190** (2008), pp. 4687-4696.
[96] W. M. Sattley, R. E. Blankenship, Insights into heliobacterial photosynthesis and physiology from the genome of *Heliobacterium modesticaldum*, *Photosynth. Res.* **104** (2010), pp. 113-122.
[97] H. Yue, Y. Kang, H. Zhang, X. Gao, R. E. Blankenship, Expression and characterization of the diheme cytochrome *c* subunit of the cytochrome *bc* complex in *Heliobacterium modesticaldum*, *Arch. Biochem. Biophys.* **517** (2012), pp. 131-137.
[98] T. J. Michalsky, J. E. Hunt, M. K. Bowman, U. Smith, K. Bardeen, H. Gest, J. R. Norris, J. J. Katz, Bacteriopheophytin *g*: Properties and some speculations on a possible primary role for bacteriochlorophylls *b* and *g* in the biosynthesis of chlorophylls, *Proc. Natl. Acad. Sci. U. S. A.* **84** (1987), pp. 2570-2574.
[99] M. H. Vos, H. E. Klaasen, H. J. Gorkom, Electron transport in *Heliobacterium chlorum* whole cells studied by electroluminescence and absorbance difference spectroscopy, *Biochim. Biophys. Acta* **973** (1989), pp. 163-169.
[100] M. Buttner, D. L, Xie, H. Nelson, W. Pinther, G. Hauska, N. Nelson, Photosynthetic reaction center genes in green sulfur bacteria and in photosystem I are related, *Proc. Natl. Acad. Sci. U. S. A.* **89** (1992), pp. 8135-8139.
[101] G. Hauska, T. Schoedl, H. Remigy, G. Tsiotis, The reaction center of green sulfur baceria, *Biochim. Biophys. Acta* **1507** (2001), pp. 260-277.
[102] H. Oh-oka, Type I reaction center of photosynthetic heliobacteria, *Photochem. Photobiol.* **83** (2007), pp. 177-186.
[103] M. Heinnickel, J. H. Golbeck, Heliobacterial photosynthesis, *Photosynth. Res.* **92** (2007), pp. 35-53.
[104] S. P. Romberger, J. H. Golbeck, The bound iron-sulfur clusters of Type-I homodimeric reaction centers, *Photosynth. Res.* **104** (2010), pp. 333-346.
[105] U. Liebl, W. Rutherford, W. Nitschke, Evidence for a unique iron-sulfur centre in *Heliobacterium chlorum*, *FEBS Lett.* **261** (1990), pp. 427-430.
[106] D. M. Kramer, B. Schoepp, U. Leibl, W. Nitschke, Cyclic electron transfer in *Heliobacillus mobilis* involving a menaquinol-oxidizing cytochrome *bc* complex and an RCI-type reaction center, *Biochemistry* **36** (1997), pp. 4203-4211.
[107] W. Nitschke, U. Liebl, K. Matsuura, D. M. Kramer, Membrane-bound *c*-type cytochromes in *Heliobacillus mobilis*. *In vivo* study of the hemes involved in electron donation to the photosynthetic reaction center. *Biochemistry* **34** (1995), pp. 11831-11839.
[108] A. L. Ducluzeau, E. Chenu. L. Capowiez, F. Baymann, The Rieske/cytochrome *b* complex of Heliobacteria, *Biochim. Biophys. Acta* **1777** (2008), pp. 1140-1146.
[109] U. Liebel, S. Pezennec, A. Riedel, E. Kellner, W. Nitschke, the Rieske FeS center from the gram-positive bacterium PS3 and its interaction with the menaquinone pool studied by EPR, *J. Biol. Chem.* **267** (1992), pp. 14068-14072.
[110] D. Baniulis, H. Zhang, T. Zakharova, S. S. Gasan, W. A. Cramer, Purification and crystallization of the cyanobacterial cytochrome b_6f complex, in *Photosynthesis Research*

Protocols, Methods in Molecular Biology, **684** (2011), pp. 65-77.
[111] J. Xiong, K. Inoue, C. E. Bauer, Tracking molecular evolution of photosynthesis by characterization of a major photosynthesis gene cluster from *Heliobacillus mobilis*, *Proc. Natl. Acad. Sci. U. S. A.* **95** (1998), pp. 14851-14856.
[112] J. van Beeumen, Primary structure diversity of prokaryotic diheme cytochrome *c*, *Biochim. Biophys. Acta* **1058** (1991), pp. 56-60.
[113] N. Sone, K. Nagata, H. Kojima, J. Tajima, Y. Kodera, T. Kanamaru, S. Noguchi, J. Sakamoto, A novel hydrophobic diheme ctype cytochrome. Purification from *Corynebacterium glutamicum* and analysis of the QcrCBA operon encoding three subunit proteins of a putative cytochrome reductase complex. *Biochim. Biophys. Acta*. 1503 (2001), pp. 279-290.
[114] N. Sone, M. Fukuda, S. Katayama, A. Jyoudai, M. Syugyou, S. Noguchi, J. Sakamoto J, QcrCAB operon of a nocardia-form actinomycete *Rhodococcus rhodochrous* encodes cytochrome reductase complex with diheme cytochrome cc subunit. *Biochim. Biophys. Acta*. 1557 (2003), pp. 125-131.
[115] F. Baymann, E. Lebrun, W. Nitschke, Mitochondrial cytochrome c_1 is a collapsed diheme cytochrome, *Proc. Natl. Acad. Sci. U. S. A.* **101** (2004), pp. 17737-17740.
[116] S. E. Martinez, D. Huang, A. Szczepaniak, W. A. Cramer, J. L. Smith, Crystal structure of chloroplast cytochrome *f* reveals a novel cytochrome fold and unexpected heme ligation, *Structure* **2** (1994), pp. 95-105.

Chapter 2

Expression and characterization of the diheme cytochrome *c* subunit of the cytochrome *bc* complex in *Heliobacterium modesticaldum*

[Portions of this work have been published previously as Hai Yue, Yisheng Kang, Hao Zhang, Xinliu Gao, Robert E. Blankenship, *Archives of Biochemistry and Biophysics* **2012**, 517, 131-137.]

Abstract

Heliobacterium modesticaldum is a gram positive, anaerobic, anoxygenic photoheterotrophic bacterium. Its cytochrome *bc* complex (Rieske/cyt *b* complex) has some similarities to cytochrome b_6f complexes from cyanobacteria and chloroplasts, and also shares some characteristics of typical bacterial cytochrome bc_1 complexes. One of the unique features of the heliobacterial cytochrome *bc* complex is the presence of a diheme cytochrome *c* instead of the monoheme cytochrome *f* in the cytochrome b_6f complex or the monoheme cytochrome c_1 in the bc_1 complex. To understand the structure and function of this diheme cytochrome *c* protein, we expressed the N-terminal transmembrane-helix-truncated soluble *H. modesticaldum* diheme cytochrome *c* in *Escherichia coli*. This 25 kDa recombinant protein possesses two *c*-type hemes, confirmed by mass spectrometry and a variety of biochemical techniques. Sequence analysis of the *H. modesticaldum* diheme cytochrome *c* indicates that it may have originated from gene duplication and subsequent gene fusion, as in cytochrome c_4 proteins. The recombinant protein exhibits a single redox midpoint potential of + 71 mV vs NHE, which indicates that the two hemes are in very similar protein binding environments.

Introduction

Cytochrome *bc* complex (Rieske/cytochrome *b* complex) in Heliobacteria is a crucial component completing cyclic electron transfer and generating proton gradient. The genes proposed to code for *H. modesticaldum* cytochrome *bc* complex encode four protein subunits: Rieske iron sulfur protein (*petC*), cytochrome *b* (*petB*), subunit IV (*petD*) and diheme cytochrome *c* (*petA,* NC 010337, NCBI Genome database). Moreover, it has been shown that heliobacterial cytochrome *b* is a cytochrome b_6-like protein [1]. This suggests that *H. modesticaldum* cytochrome *bc* complex is structurally organized similarly to the cytochrome b_6f complex in cyanobacteria and chloroplasts with cytochrome b_6 and subunit IV [2]. However, instead of the cytochrome *f* found in the b_6f complex, heliobacterial *bc* complexes appear to use the diheme cytochrome *c* as a replacement, which is a unique feature also differentiating them from bacterial cytochrome bc_1 complexes possessing cytochrome c_1 [3]. Sequence alignment and structure modeling analysis [4] of the diheme cytochrome *c* show two important characters: (a) It is predicted to be an α-helix rich globular protein with an N terminal transmembrane helix, which is similar to cytochrome c_1 rather than to the β-sheet rich cytochrome *f*; (b) The N- and C-terminal heme-binding domains share high sequence similarity, which makes it a cytochrome c_4-type protein. Cytochromes c_4 are diheme proteins believed to have originated from a gene duplication event, giving rise to two heme-binding domains with each domain resembling a typical type I monoheme cytochrome. Interestingly, cytochrome c_1 of proteobacteria and mitochondria also has been suggested to evolve from cytochrome c_4 by the loss of one heme-binding domain followed by a collapse of part of the cytochrome c_4 structure [5]. This in turn suggests that the cytochrome *bc* complex of heliobacteria is potentially an evolutionary prototype for other similar complexes.

The possible shared origin of heliobacterial *bc* complex's diheme cytochrome *c* subunit and cytochrome c_1, and the general similarity of the rest of its subunits with those of the b_6f complex place it at a very interesting evolutionary position and make the structure, function and bioenergetics of diheme cytochrome *c* an important topic to explore. In this study, we report the successful expression of recombinant heliobacterial diheme cytochrome *c* in *E. coli*. Its size and binding with *c*-type hemes were confirmed by gel electrophoresis, including SDS-PAGE, western blot analysis and heme staining. Mass spectrometry and pyridine hemochrome analysis were used to investigate the details of the heme binding and extinction coefficient. The redox potential of the recombinant diheme cytochrome was determined by potentiometric titration.

Materials and methods

Growth of H. modesticaldum and cell lysis

H. modesticaldum was grown in PYE medium, which is composed of (per liter) K_2HPO_4 (1.0 g), $MgSO_4 \cdot 7H_2O$ (0.2 g), $CaCl_2 \cdot 2H_2O$ (20 mg), $Na_2S_2O_3 \cdot 5H_2O$ (0.2 g), sodium pyruvate (2.2g), yeast extract (4.0 g), $(NH_4)_2SO_4$ (1.0 g), chelated iron solution [6] (2 mL), D-biotin (15 μg), vitamin B12 (20 μg) and trace element solution (1 mL) with the final pH adjusted to pH 6.9–7.0. The composition of the trace element solution was reported previously [6]. All cultures were grown anaerobically in a Coy anaerobic chamber at temperatures ranging from 46–50 °C in the light (10 ± 1 W/m^2). 500 μL of overnight (18 hours) culture was harvested by centrifugation at 13,000 rpm and re-suspended in 50 μL 20 mM Tris buffer (pH 8.0). The cell suspension was heated to 98 °C for 5 min and quickly chilled on ice to disrupt the cells. Another 5 min 13,000 rpm centrifugation was performed to remove unbroken cell debris. The cell lysate

was frozen at – 20 °C for further use.

E. coli cell strains and plasmids

Escherichia coli stain DH5α from Invitrogen (Carlsbad, California) was used for DNA ligation and sequencing steps. *E. coli* strain BL21 (DE3) *Δccm* (cytochrome *c* maturation genes knock-out), courtesy of Prof. Robert Kranz from Washington University in St. Louis, was used for the expression of the recombinant diheme cytochrome *c*. The plasmid pTEV [7], which bears T7 promoter, gentamicin resistance gene, and the replication origin ColE1, was used to construct the expression vector. *H. modesticaldum* petA coding sequence was PCR amplified using TaKaRa Ex Taq (Takara Bio company) DNA polymerase. Genomic DNA in *H. modesticaldum* cell lysate acquired by the heat-shock method was used as PCR template. The recombinant diheme cytochrome *c* gene was constructed by replacing its original N-terminal transmembrane helix with the signal sequence of *Thiobacillus versutus* cytochrome c_{550} [8]. It was then digested and cloned into similarly digested pTEV to obtain the expression vector pTEV-petA, which has a sequence fused with the insertion allowing a C-terminal poly-histidine (His_6) tag to be co-expressed to facilitate purification. A plasmid containing *ccmABCDEFGH* (pSysI) genes was co-transformed with the expression vector to the host cells [8]. Routine techniques were performed to handle DNA. The final sequence was confirmed by determining the nucleotide sequences of both strands.

E. coli cell growth and harvest

E. coli cell strain BL21 (DE3) *Δccm*, carrying both pTEV-petA and pSysI plasmids, was grown aerobically in 1 liter LB medium [9]. The culture was vigorously agitated at 16 °C until the optical density at 600 nm (OD600) reached 0.7. The protein expression was induced by adding IPTG (isopropyl-β-D-thiogalactopyranoside) to a final concentration of 300 μM. The cultivation was then continued for another 6 hrs. With this culture, cells were pelleted by centrifugation at 7,100 × g for 20 min at 16 °C. The pellet was stored in −80 °C if not used immediately. Ampicillin, gentamicin, and kanamycin were used to final concentrations of 100, 20, and 25 μg/mL, respectively, wherever was needed.

Purification of recombinant diheme cytochrome c

E. coli cells were re-suspended in buffer A (50 mM sodium phosphate, 500 mM NaCl, 5 mM imidazole, 1 mM phenylmethylsulfonyl fluoride, pH 7.2) at 4 °C and disrupted by sonication. The cell extract was centrifuged at 7,100 × g for 20 min to pellet the unbroken cell debris. The supernatant was ultracentrifuged for 2 hrs at 150,000 × g to pellet the membrane fraction from the supernatant of the previous step. The supernatant of the ultracentrifugation, containing the recombinant diheme cytochrome *c* and other *E. coli* soluble proteins, was filtered through a 0.45 μm filter and directly loaded onto a HisTrap HP (GE Healthcare) Co^{2+} chelated column. The column was washed with 10-column volumes of 20 mM imidazole in buffer A. The protein was then eluted with 50 mM imidazole in buffer A. The eluted protein was exchanged into buffer B (20 mM Tris-HCl, 800 mM ammonium sulfate, pH 8.0) and loaded onto a HiTrap phenyl HP column (GE Healthcare). A linear ammonium sulfate concentration gradient from 800 mM to 0 mM was performed and the pure recombinant diheme cytochrome *c* protein was

obtained in the 450 mM to 350 mM ammonium sulfate fractions.

SDS-PAGE, Western blot and Heme stain

SDS-PAGE analysis was performed to determine the purity of the samples, following the protocol described by Marshak et al. [10]. Samples dissolved in SDS–PAGE coomassie brilliant blue dye containing buffer were boiled for 5 minutes and used for heme stains and western blots. Anti-His antibody was diluted 5000 times (Sigma Aldrich, USA). Chemiluminescence was used for both heme stain and anti-His western blot using the SuperSignal Femto kit (Pierce) and detected in an LAS-1000plus detection system (Fujifilm).

Protein concentration assay and heme analysis

The concentration of recombinant protein was determined by the bicinchoninic acid protein assay (BCA assay kit, Pierce). The pyridine hemochrome analysis, as previously reported by Berry et al. [11] was used in this study.

In-gel protein digestion

After SDS-PAGE and gel staining, the bands were carefully excised and cut into small pieces with a diameter roughly 1 mm. The samples were then washed with 50 % acetonitrile (ACN) in 50 mM ammonium bicarbonate (NH_4HCO_3) aqueous solution. Proteins were reduced with 10 mM dithiothreitol (DTT) in 100 mM NH_4HCO_3 for 30 min and then the cysteines in the proteins were alkylated by 55 mM iodoacetamide in 100 mM NH_4HCO_3 for another 30 min.

Trypsin (20μg/mL, Sigma Aldrich) in 9 % ACN 40 mM NH_4HCO_3 aqueous solution was added to the excised gel mixture and the digestion reaction was conducted at 37 °C for 12 hrs. The peptides were then extracted by 0.5 % trifluoroacetic acid (TFA) 60 % ACN buffer at 37 °C for 1 hr. The solution containing the extracted peptides was dried in a bench-top speed-vacuum and stored at -20 °C for further analysis.

Mass Spectrometry

In-gel digested protein samples were used for MALDI-TOF mass spectroscopic analysis. The protocol was reported previously and followed in this work [12]. For ESI mass spectrometry, the protein sample was desalted by a home-packed C18 tip. The eluate with 75% acetonitrile 25% water 0.1% formic acid was collected. The protein solution was delivered by syringe pump at a flow rate of 400 nL/min. Mass spectra were acquired with a Waters SYNAPT G2 Q-TOF (Waters Corporation, Milford, MA) mass spectrometer equipped with a nanoESI source. The protein spectrum was acquired at sensitive mode ("V" mode) with the capillary voltage 1.8 kV, cone voltage 30 V and source temperature 100 °C.

Room temperature and low temperature UV-Vis spectroscopy

The UV-Vis spectra of oxidized and reduced forms of recombinant diheme cytochrome *c* at room temperature and 78 K (liquid nitrogen cooling) were taken with a Perkin Elmer Lambda 950 UV-Vis spectrophotometer and analyzed by Perkin Lambda UV WinLab Explorer software.

Potentiometric Titration

Potentiometric titrations were performed to determine the midpoint potential (Em) of the recombinant diheme cytochrome *c*. The general protocol was described previously [13] and was followed in this study with some modifications. The redox potential of the sample was controlled by a CH 620C potentiostat (CH instruments), and the spectral changes of diheme cytochrome *c* upon oxidation and reduction were monitored at 550 nm in a Perkin Elmer Lambda 950 UV-Vis spectrophotometer. The electrodes used for this analysis were platinum gauze working electrode, Ag/AgCl reference electrode, and a platinum wire auxiliary electrode. The titration was performed at room temperature with the following redox mediators: anthraquinone-2-sulfonic acid (Em = -255 mV), anthraquinone-2, 6-disulfonic acid disodium salt (Em = -184 mV), 2-hydroxy-1,4-naphthoquinone (Em = -145 mV), 2, 5-dihydroxy-p-benzoquinone (Em = -60 mV), phenazine methosulfate (Em = 8 mV), phenazine ethosulfate (Em = 60 mV), Fe (III) EDTA (Em = 117 mV), 1, 2-naphthoquinone-4-sulfonic acid (Em = 215 mV), 2, 3, 5, 6-tetramethyl-p-phenylenediamine (Em = 260 mV), and N, N-dimethyl-1, 4-phenylenediamine dihydrochloride (Em = 371 mV). Recombinant diheme cytochrome *c* was dissolved in 50 mM sodium phosphate pH 7.2 buffer at a final concentration of 2 mg/mL. Then a final concentration of 150 mM NaCl and 40 μM each of the mediators were added to the working solution. The calculation and equations used for fitting the data were described in Bell et al. [13].

Results

Recombinant diheme cytochrome c expression, purification and identification

The coding sequence of the diheme cytochrome *c* of *H. modesticaldum*'s cytochrome *bc*

complex was directly obtained from the NCBI genome database (NC 010337). Based on secondary structure prediction (SOSUI engine ver. 1.11, Nagoya University), starting from the N-terminus, the first 22 amino acids form a single transmembrane helix, and the rest of the protein is hydrophilic (Fig. 1a), which is consistent with the fact that this cytochrome *c* is part of the cytochrome *bc* complex and does not function independently as some other soluble diheme cytochrome *c* proteins do, which therefore do not require such a structural feature [14, 15, 16]. This N-terminal transmembrane helix probably functions as an anchor to bind the diheme cytochrome *c* with the cytochrome *bc* complex, but its presence will likely complicate both protein expression and purification. We therefore replaced the codons for the first 22 amino acids with the ones that will be translated as the signal peptide from *Thiobacillus versutus* cytochrome c_{552} (Fig. 1b). Two previous reported successful cases regarding the expression of *c*-type cytochrome proteins in *E. coli* using the *T. versutus* signal peptide made it a favored choice [8, 17]. To facilitate detection and purification of the recombinant protein, a poly-histidine tag (His_6) was added to the C-terminus of the protein linked with a TEV-protease cutting site (Fig. 2).

A Co^{2+} chelated affinity column was used in the first purification step. Compared to Ni^{2+} columns, Co^{2+} columns showed better resolution and less protein impurities in our studies (data not shown). We also compared the affinity column purification result at 4 °C with ones at room temperature (25 °C) and found no difference, which is an indication of the stability of the recombinant diheme cytochrome *c* protein. After affinity chromatography, anti-His western blot and heme staining were used to confirm the expression of a *c*-type heme-binding protein with poly-histidine tag (Fig. 3a, 3b). The samples for both tests were under denatured conditions. Therefore, the existence of *c*-type hemes in His-tagged proteins was detected. The molecular mass of the protein showed on both anti-His western blot and heme staining gels are 25 kDa

MFGSTGLLLAGILLAPTWQAQGELVRGHELYKTHCASCHGEDGKGVQGVK
AATLNNEGFLKVASDDYLLKSIRLGRPSLATNAMPHFDTQKLPDEKVNLIIKNM
RSWHPEISAPVETGEKVAGDPVKGEAFYKTACAACHGQKGEGGIGA ALLDP
GYLNSASDEFILQSIIMGRPGTNMPPYPDSPDIRNVVAFLRSKQVPYDPAEKK
EEGKAKSKDTGAADGDKKQ

(a)

MKISIYATLAALSLALPAGAELVRGHELYKTHCASCHGEDGKGVQGVKAATLN
NEGFLKVASDDYLLKSIRLGRPSLATNAMPHFDTQKLPDEKVNLIIKNMRSWH
PEISAPVETGEKVAGDPVKGEAFYKTACAACHGQKGEGGIGAALLDPGYLNS
ASDEFILQSIIMGRPGTNMPPYPDSPDIRNVVAFLRSKQVPYDPAEKKEEGKA
KSKDTGAADGDKKQ***ENLYFQG****HHHHHH*

(b)

Fig. 1 Amino acid sequence from N- to C- terminus of (a) original *H. modesticaldum* diheme cytochrome *c* (two heme binding motifs were highlighted by red characters) of the cytochrome *bc* complex and (b) recombinant diheme cytochrome *c*. The amino acids forming the transmembrane helix (panel a in bold characters) are replaced by *T. thermophilus* cytochrome c_{552} signal peptide (panel b in bold characters). The TEV cutting site and the poly histidine tag (His_6) are shown in bold italic and italic forms respectively.

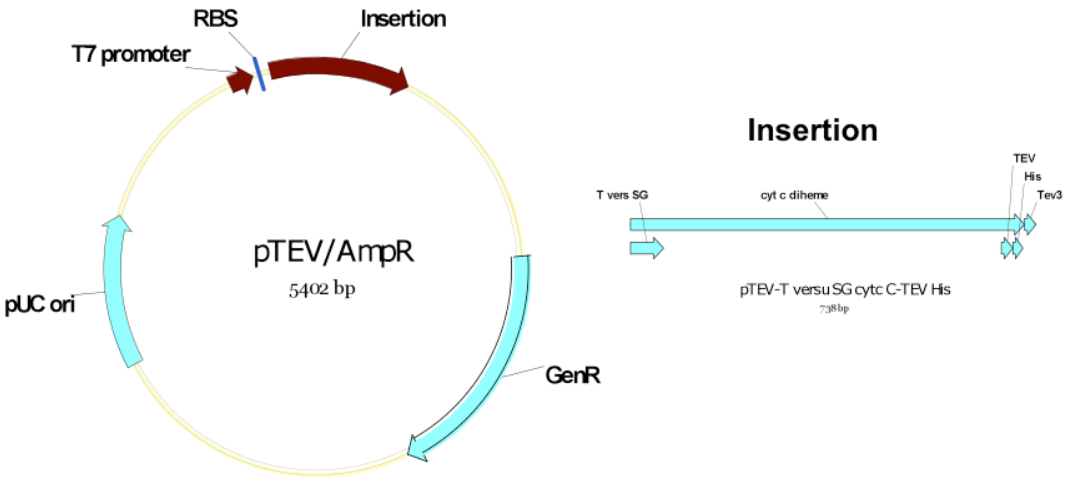

Fig. 2 Expression vector (left) and insertion (right) constructs.

(under gel electrophoresis resolution), which is consistent with the protein peptide mass without the exogenous *T. versutus* signal peptide plus two heme molecules [7, 16, 17]. After the Co^{2+} affinity chromatography, phenyl sepharose (hydrophobic) column was used to further purify the cytochrome *c* enriched samples and pure recombinant protein was obtained. The coomassie blue stained SDS-PAGE gel is shown in Figure 3c. In the gel, a single 25 kDa band confirmed the high purity of the final product.

UV-Vis spectral analysis

UV-Vis absorption spectra of both reduced and oxidized recombinant diheme cytochrome *c* at room temperature are shown in Figure 4. Upon reduction by adding dithionite to 0.5 mM, the reduced protein exhibits a characteristic *c* type cytochrome γ (Soret) band at 418 nm, β band at 521 nm and α band at 550 nm. In the oxidized protein spectra, the Soret band becomes broader and is blue shifted to 411 nm, and the structured α and β bands are lost. To minimize the influence of the protein backbone vibration on the heme molecules and further investigate the diheme binding pockets, 78 K spectra were also recorded, shown in Figure 4. Compared to its room temperature counterpart, the spectrum of reduced cytochrome *c* at 78 K has an overall blue shift. Although it exhibits more detailed β and α band fine structures, no obvious splitting was observed, which suggests that the two heme binding pockets are very similar.

Determination of c-type heme stoichiometry by pyridine hemochrome analysis

To determine weather the recombinant cytochrome *c* has two covalently bound hemes, pyridine hemochrome analysis (Fig. 5) was performed as described in Materials and Methods. The concentration of hemes was quantified by using an extinction coefficient of 23.97 mM^{-1} cm^{-1}

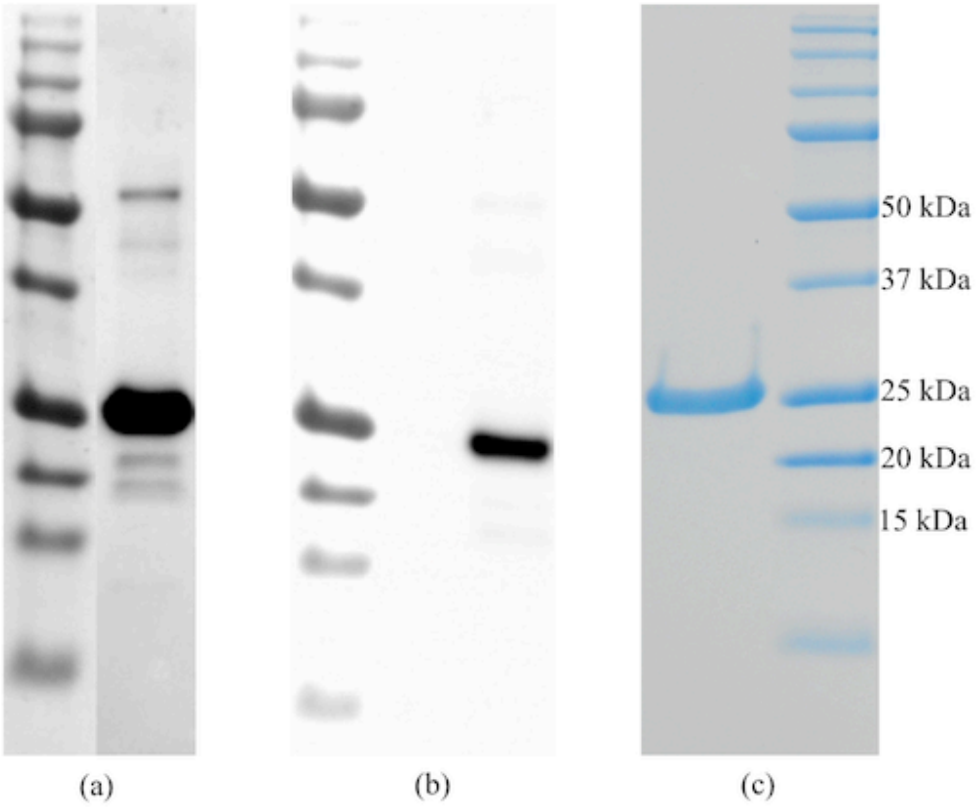

Fig. 3 Affinity column enriched recombinant diheme cytochrome *c* sample was subjected to SDS-PAGE, and then (a) anti-His western blot and (b) Heme staining were performed. The strongest bands on the gels correspond to the recombinant proteins. (c) Coomassie blue stained SDS-PAGE gel of the purified protein.

for *c*-type heme [11]. The protein concentration was determined by BCA assay. By comparing the concentration of hemes and protein, 2 hemes (rounded from 2.1 ± 0.1) are present in each protein molecule. Moreover, by comparing the reduced minus oxidized absorption spectrum of the diheme cytochrome *c* with that of the pyridine hemochrome, we determined that the reduced minus oxidized extinction coefficient is 37.4 mM^{-1} cm^{-1} for the wavelength pairs 551-536 nm. The extinction coefficient for the reduced form of diheme cytochrome *c* is 46.9 mM^{-1} cm^{-1} for the wavelength pairs 551-580 nm. This value reflects both heme groups.

Mass spectrometry

An ESI mass spectrum of the recombinant diheme cytochrome *c* is shown in Figure 6. The mass of the protein is 24,981 Da. The calculated mass of the apoprotein (without signal peptide and hemes) is 23,751 Da. The mass difference is 1,230 Da, equals two heme groups (615 Da per heme). To further investigate whether the hemes are correctly linked to the protein backbone, trypsin digested protein was subjected to MALDI-TOF mass spectroscopic analysis (Fig. 7). In the resulting spectrum, only the two peptides, each bearing a *c*-type heme-binding motif and actually linked with heme, were detected (summarized in the table in Fig. 7). The mass of just the two peptides without hemes, on the other hand, did not appear in the spectrum. Taken together, this evidence is a strong indication of the presence of correctly expressed and assembled diheme cytochrome *c*.

Redox potentiometry

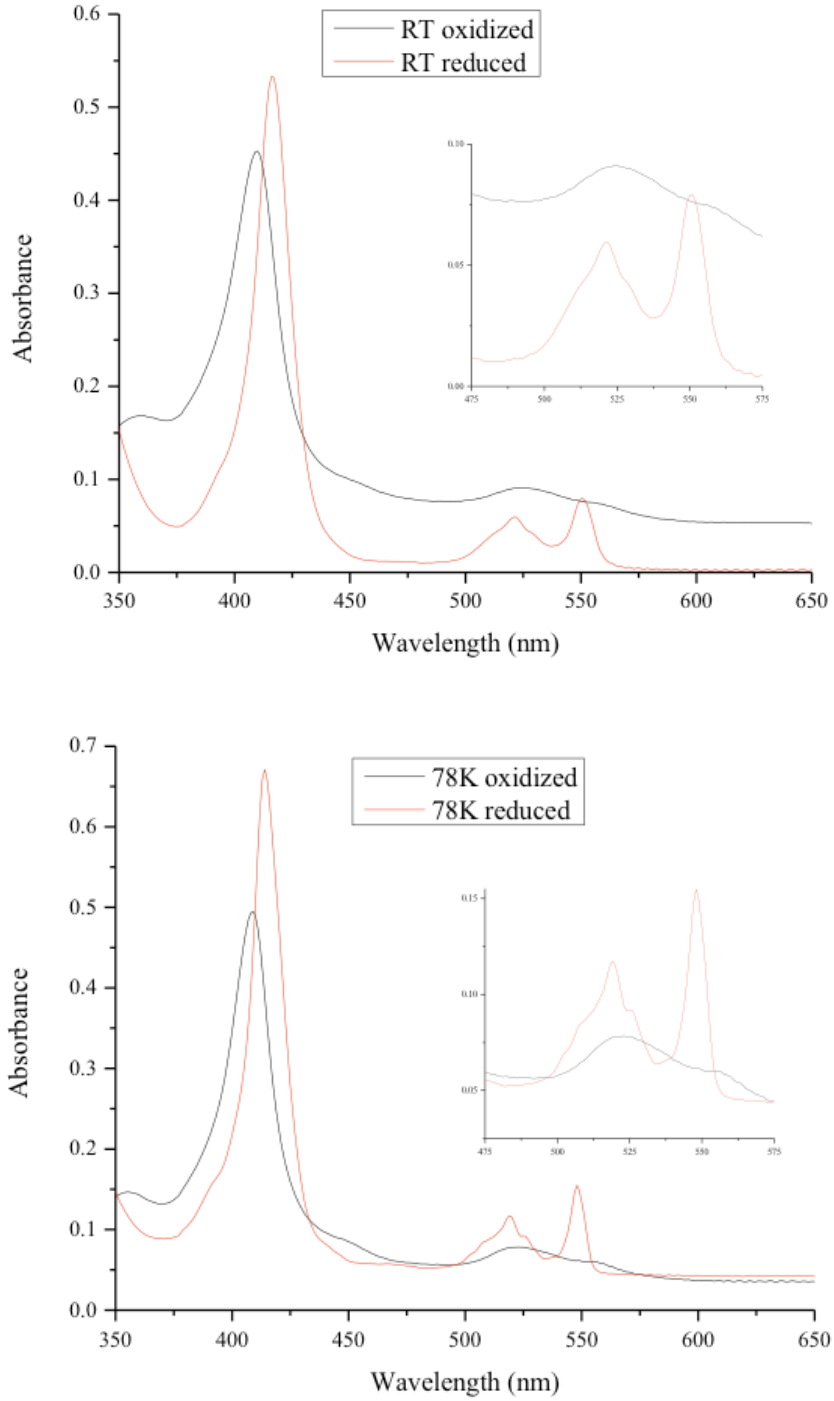

Fig. 4 UV-Vis absorption spectra of both reduced and oxidized recombinant diheme cytochrome *c* at room temperature (RT, upper panel) and 78K (lower panel).

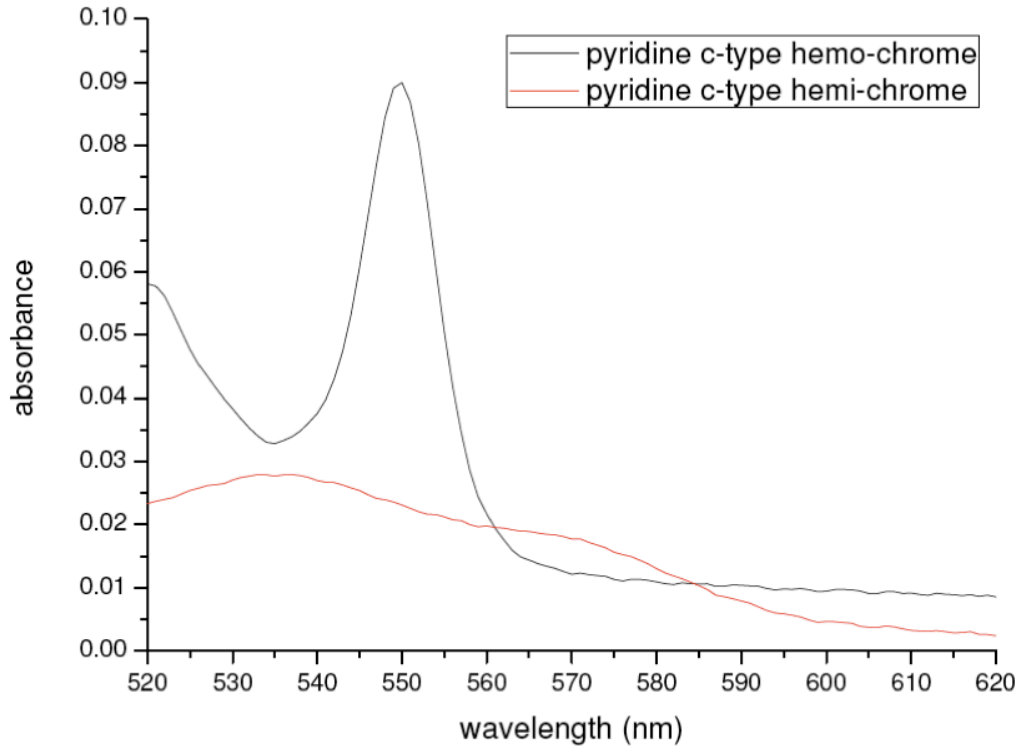

Fig. 5 Spectra of pyridine hemi-chromes *c* (red) and pyridine hemo-chrome *c* (black) at room temperature.

The midpoint redox potential of recombinant diheme cytochrome *c* was determined by using an optically transparent thin film electrode with a potentiostat as described in the Materials and Methods. The data were analyzed by the method reported by Bell et al. [13]. With this method, *c*-type hemes were assayed spectrally as a function of the potential. The titration plot (Fig. 8) shows a single E_m for cytochrome *c*, which is +71 mV versus NHE. The standard error in the midpoint potential is ± 2 mV obtained from the ORIGIN fitting analysis. However, the overall error including systematic errors for all sources is estimated to be ±10 mV. The plot shows a reversible Nernstian behavior corresponding to a one-electron reduction/oxidation reaction (Fig. 9).

Discussion

Similar to that found in the cytochrome c_1 in the cytochrome bc_1 complex and cytochrome *f* in the cytochrome b_6f complex, the N-terminal helix of the heliobacterial diheme cytochrome *c* functions as an anchor to fix the protein in the membrane and binds it with the other parts of the complex [19, 20, 21, 22]. Moreover, this helix is probably spatially removed from the protein core and so probably does not have a significant effect on the optical and redox properties of the hemes. Therefore, during the construction of the expression vector, we replaced it with the signal peptide from *Thiobacillus versutus* cytochrome c_{552}, which can be removed by leader peptidase *in vivo* in *E. coli* [17, 18]. One interesting feature is that a small amount of diheme cytochrome *c* was found in the membrane, indicating that the signal peptides of some proteins were not cut off and therefore the protein stayed with the membrane. One explanation is that during the over-expression, the leader peptidases were overwhelmed by the amount of

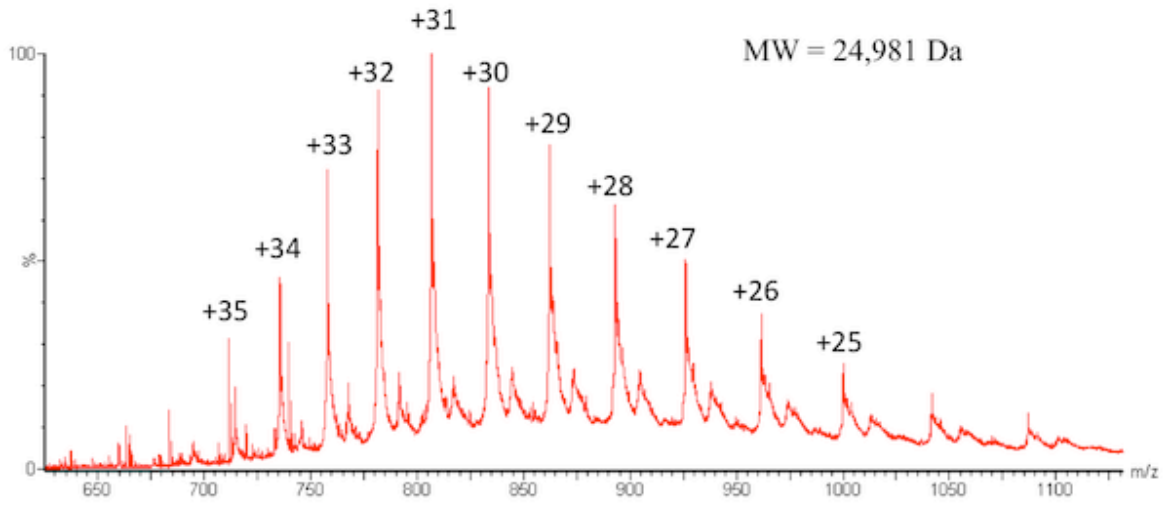

Fig. 6 ESI mass spectrum of diheme cytochrome *c*. The spectrum range is from 650 to 1125 m/z and multiple charged protein peaks were observed and labeled in this spectrum. The molecular mass of the protein is 24,981 Da.

Peptide (trypsin digest)	Calculated peptide mass (Da)	Detected peptide mass (Da)	Mass difference (Da)
THCASCHGEDCK	1244.319	1859.801	615.482
TACAACHGQK	989.132	1604.63	615.498

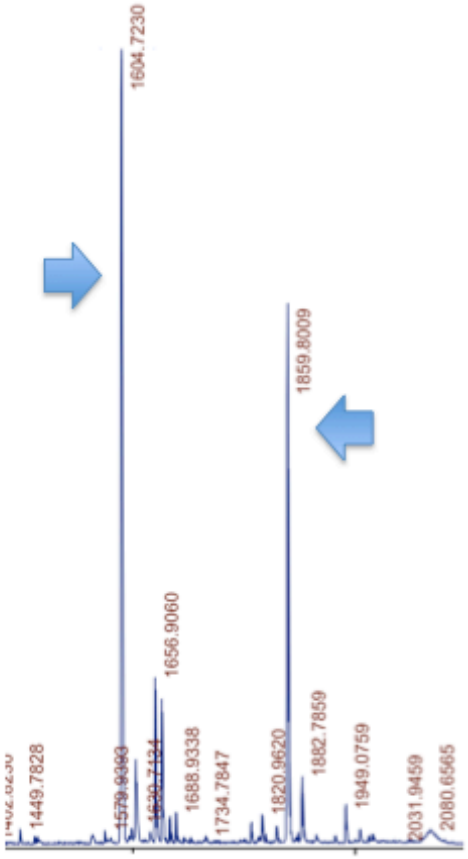

Fig. 7 MALDI-TOF mass spectrum of the trypsin-digested protein. Two heme-binding peptide mass peaks are circled. The table summarizes the calculated and observed results.

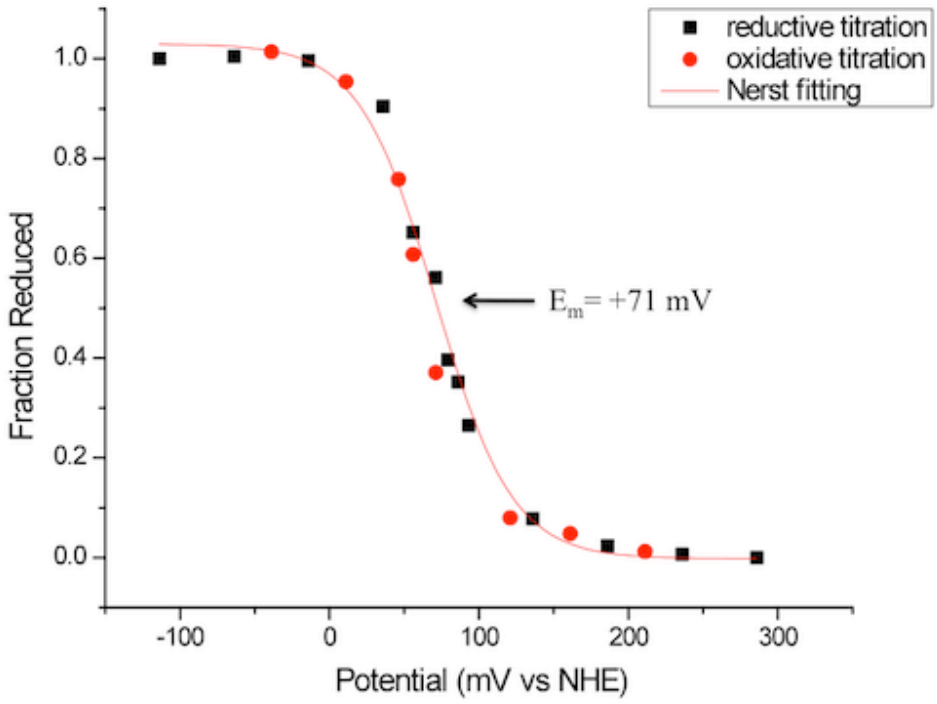

Fig. 8 Potentiometric titration of recombinant diheme cytochrome *c* purified from *E. coli* with squares representing the reductive titration, circles representing oxidative titration, and the solid line representing the Nernst fitting. Standard error for E_m is 1.93 mv, adjusted R^2 value is 0.99 and the reduced chi-squared number is 0.0012.

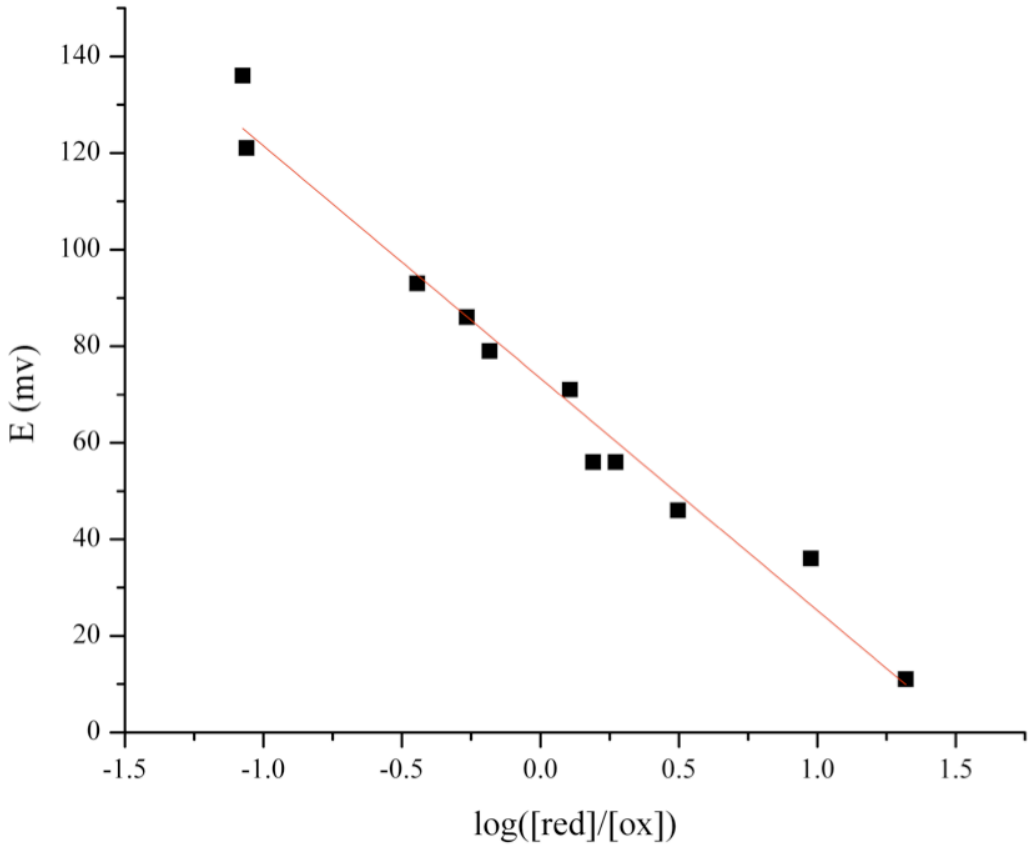

Fig. 9 Nernst curve fitting based on the equation of $E = E_m - (0.059/n)\log([red]/[ox])$, in which [red]/[ox] represents the reduced and oxidized cytochrome *c* concentration ratio, n represents the number of moles of electrons transferred in the reaction. The data were fitted with Origin 8.0 (Origin Lab). The fitted E_m is 72.3 ± 1.8 mv, n is 1.19 ± 0.04, and the adjusted R^2 value is 0.98.

precursor diheme cytochrome *c*. Based on the same logic, the co-transformation of pSysI (*ccmABCDEFGH*) and subsequent *ccm* machinery over-expression are necessary to make the productivity level of the recombinant proteins suitable for biochemical and biophysical studies and lower their misfolding rate [8]. Because of the recombinant cytochrome *c*'s location in the periplasm and electron transfer function, its toxicity (final OD_{600} 1.1-1.2) to host cells is significant during the over-expression. To counteract this negative effect, a low induction temperature, 16 °C, and low IPTG concentration, 300 μM were used. The purified protein yield was 0.2 mg per gram of *E. coli* cell.

In Heliobacteria, menaquinones and membrane-attached cytochrome c_{553} are the electron transfer partners of the cytochrome *bc* comlex. The redox potential of menaquinone is -60 mV [14] and cytochrome c_{553} is +180 mV in *Heliobacerium mobilis* [24]. *H. modesticaldum* diheme cytochrome *c*, as the final step of the inner electron transfer chain of the *bc* complex, passes electrons from the Rieske protein to cytochrome c_{553}. Therefore, a reasonable speculation is that the redox potentials of these three partners would form a gradient from a high value (cytochrome c_{553}) to a low value (Rieske protein) to allow efficient electron transfer. Based on our optical redox titration result, a single E_m of +71 mV was detected for the diheme cytochrome *c*, which implies that the Rieske protein in *H. modesticaldum* cytochrome *bc* complex should have a lower midpoint potential, assuming that the recombinant cytochrome *c* has the same or similar potential as its native form. A previous whole cell redox titration study of flash-induced heme *c* oxidation in *H. mobilis* revealed that three *c*-type hemes with midpoint potentials of +190, +170, and +90 mV became oxidized by the flash-oxidized primary donor [25]. According to our result, the +90 mV value is probably the one midpoint potential reflecting oxidation of the diheme cytochrome *c* of the *H. mobilis* cytochrome *bc* complex. The +190 and +170 mV hemes

might both be due to cytochrome c_{553}, possibly in slightly different environments.

Heliobacterial diheme cytochrome *c* is a cytochrome c_4 type protein, which is found in many different species [17]. It is believed that cytochromes c_4 originated from gene duplication of a monoheme type I cytochrome *c* followed by fusion of the two genes [4]. The same feature can be seen from the sequence similarity of the N- and C- terminal domains of the heliobacterial diheme cytochrome *c* (Fig. 10). Therefore, the structure of its globular heme-binding domains has been modeled based on the crystal structure of cytochrome c_4 from *Pseudomonas stutzerii* (Fig. 11). Unlike cytochrome *f* and cytochrome c_1, whose hemes have distinctive double edges allowing them to accept electrons from one side and pass them to the partners on the other side, heliobacterial diheme cytochrome *c*, as in cytochrome c_4 in general, are predicted to have only one edge of each heme that is accessible toward different sides of the protein respectively. This implies that there must be an intramolecular inter-heme electron transfer in the diheme cytochrome *c*. Some kinetic studies showed that this inter-heme electron transfer is a much faster process compared to the *ms* time range for the electron transfer between diheme cytochrome *c* protein and its partners [14, 27]. In *P. stutzerii* cytochrome c_4, this fast inter-heme electron transfer was attributed to the strong heme-heme hydrogen bond via their propionates, and the same reason was also believed to be responsible for the two different redox midpoint potentials of the two hemes [27]. Whereas, in our study, the heliobacterial diheme cytochrome *c* has only a single observable midpoint potential, indicating two identical or at least spectrally and thermodynamically very similar heme binding pockets. This interesting difference may originate from their different relative geometry and thus different interactions between the two hemes among a variety of diheme cytochromes *c*. The structure of the heliobacterial diheme cytochrome *c* will be an important piece of information to resolve this question.

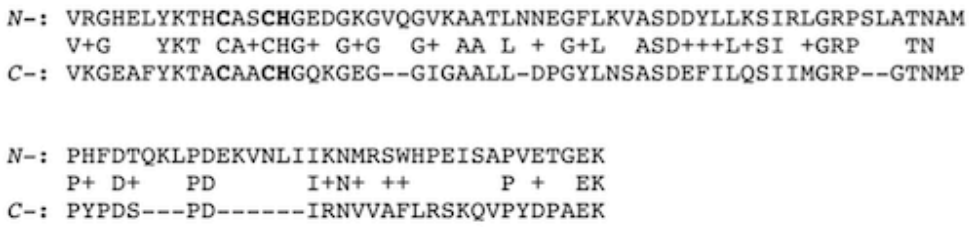

Fig. 10 The alignment of the N- and C- terminal domains of the heliobacterial diheme cytochrome *c*. The two heme-binding motifs are highlighted in bold characters.

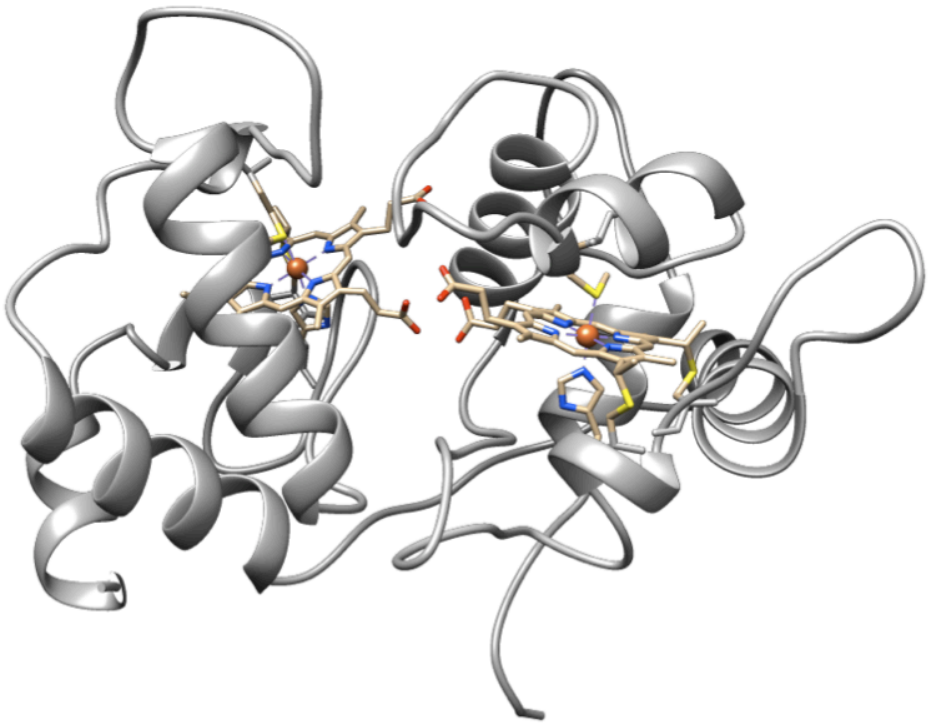

Fig. 11 The diheme cytochrome c without its transmembrane helix as modeled on cytochrome c_4 from *Pseudomonas stutzerii* (pdb: 1ETP) (homology model generated by Modeller 9.11).

In conclusion, as part of the effort to understand the properties of the heliobacterial cytochrome *bc* complex, its unique subunit, the diheme cytochrome *c*, was expressed in *E. coli* and purified. Western blot, heme staining and mass spectrometry results confirmed that two heme-binding motifs covalently linked two *c*-type hemes. The single redox midpoint potential of the recombinant diheme cytochrome *c* strongly suggests that the two hemes are in extremely similar binding environments. This result is quite different from the two distinct midpoint potentials of many cytochromes c_4, which may share the same origin with heliobacterial diheme cytochrome *c*. This is a hint that in heliobacterial diheme cytochrome *c*, the two hemes interact with each other in a different way compared to some other cytochromes c_4. To answer this question and a more intriguing one: what is the relationship between the diheme cytochrome *c* and the rest of the whole cytochrome *bc* complex, crystallographic analysis and more effort trying to purify the intact complex in its native form from Heliobacteria are underway.

Acknowledgement

I am grateful to Mr. Brian San Francisco and Prof. Robert Kranz at Washington University in St. Louis for the *E. coli* strains, *ccm* plasmid and kind suggestions referring to the protein expression. I also want to thank Prof. Michael Gross for the access to the MALDI-TOF mass spectrometer, and Dr. Hao Zhang and Dr. Weidong Cui from Washington University NIH/NCRR MS resource for help with MS sample preparation. This work is supported by grant NNX08AP62G from the Exobiology program of NASA.

References

[1] A. L. Ducluzeau, E. Chenu, L. Capowiez, F. Baymann, The Rieske/cytochrome *b* complex of Heliobacteria, *Biochimica et Biophysica Acta* **1777** (2008), pp. 1140-1146.

[2] D. Baniulis, H. Zhang, T. Zakharova, S. S. Hasan, W. A. Cramer, Purification and crystallization of the cyanobacterial cytochrome b_6f complex, *Methods Mol Bio* **684** (2011), pp. 65-77.

[3] D. Xia, C. A. Yu, H. Kim, J. Z. Xia, A. M. Kachurin, L. Zhang, L. Yu, J. Deisenhofer, Crystal structure of the cytochrome bc_1 complex from bovine heart mitochondria, *Science* **277** (1997), pp. 60-66.

[4] F. Baymann, W. Nitschke, Heliobacterial Rieske/cyt *b* complex, *Photosynthesis Res* **104** (2010), pp. 177-187.

[5] F. Baymann, E. Lebrun, W. Nitschke, Mitochondrial cytochrome c_1 is a collapsed di-heme cytochrome, *Proc Natl Acad Sci USA* **101** (2004), pp. 17737–17740.

[6] L. K. Kimble, A. K. Stevenson, M. T. Madigan, Chemotrophic growth of Heliobacteria in darkness, *FEMS Microbiol Lett* **115** (1994), pp. 51-55.

[7] C. J. Rocco, K. L. Dennison, V. A. Klenchin, I. Rayment, J. C. Escalante-Semerena, Construction and use of new cloning vectors for the rapid isolation of recombinant proteins from *Escherichia coli*, *Plasmid* **59** (2008), pp. 231-237.

[8] J. A. Fee, Y. Chen, et al, Integrity of *Thermus thermophilus* cytochrome c_{552} synthesized by *Escherichia coli* cells expressing the host-specific cytochrome *c* maturation genes, ccmABCDEFGH: biochemical, spectral, and structural characterization of the recombinant protein, *Protein Science* **9** (2000), pp. 2074-2084.

[9] J. Sambrook, E. F. Fritsch, T. Maniatis, Molecular Cloning: a laboratory manual, 2nd ed.. (1989) Cold Spring Harbor Laboratory Press, Cold Spring Harbor, NY.

[10] D. R. Marshak, J. T. Kadonaga, et al, Strategies for protein purification and characterization, a laboratory course manual. (1996) Cold Spring Harbor Laboratory Press.

[11] E. A. Berry, B. L. Trumpower, Simultaneous determination of hemes *a, b,* and *c* from pyridine hemochrome spectra, *Anal Biochem* **161** (1987), pp. 1-15.

[12] X. Gao, Y. Xin, P. D. Bell, J. Wen, R. E. Blankenship, Structural analysis of complex III in the photosynthetic electron transfer chain of *Chloroflexus aurantiacus*, *Biochemistry* **49** (2010), pp. 6670-6679.

[13] P. D. Bell, Y. Xin, R. E. Blankenship, Purification and characterization of cytochrome c_6 from *Acaryochloris marina*, *Photosynth Res* **102** (2009), pp. 43-51.

[14] H. R. Gibson, C. G.Mowat, et al, Structural and Functional Studies on DHC, the Diheme Cytochrome *c* from *Rhodobacter sphaeroides*, and Its Interaction with SHP, the sphaeroides Heme Protein, *Biochemistry* **45** (2006), pp. 6363-6371.

[15] G. D. Rocco, G. Battistuzzi, et al, Cloning, expression, and physicochemical characterization of a new diheme cytochrome *c* from *Shewanella baltica* OS155, *J Biol Inorg Chem* **16** (2011), pp. 461–471.

[16] J. V. Beeumen, Primary structure diversity of prokaryotic diheme cytochrome *c*, *Biochimica et Biophysica Acta* **1058** (1991), pp. 56-60.

[17] M. Ubbink, J. V. Beeumen, G. W. Canters, Cytochrome c_{550} from *Thiobacillus versutus*:

cloning, expression in *Escherichia coli*, and purification of the heterologous holoprotein, *J. Bacteriol* **174** (1992), pp. 3707-3714.
[18] R. G. Kranz, C. R. Fogal, J. S. Taylor, E. R. Frawley, Cytochrome *c* biogenesis: mechanisms for covalent modifications and trafficking of heme and for heme-iron redox control, *MMBR* **73** (2009), pp. 510-528.
[19] D. Xia, C. A. Yu, H. Kim, J. Z. Xia, A. M. Kachurin, L. Zhang, L. Yu, J. Deisenhofer, Crystal structure of the cytochrome bc_1 complex from bovine heart mitochondria, *Science* **277** (1997), pp. 60–66.
[20] C. Lange, C. Hunte, Crystal structure of the yeast cytochrome bc_1 complex with its bound substrate cytochrome *c*, *Proc. Natl. Acad. Sci. U. S. A.* **99** (2002), pp. 2800–2805.
[21] D. Stroebel, Y. Choquet, J. L. Popot, D. Picot, An atypical haem in the cytochrome b_6f complex, *Nature* **426** (2003), pp. 413–418
[22] G. Kurisu, H. Zhang, J. Smith, W. A. Cramer, Structure of the cytochrome b_6f complex of oxygenic photosynthesis: tuning the cavity, *Science* **302** (2003), pp. 1009–1014.
[23] D. M. Kramer, B. Schoepp, U. Liebl, W. Nitschke, Cyclic electron transfer in *Heliobacillus mobilis* involving a menaquinol-oxidizing cytochrome *bc* complex and an RCI-type reaction center, *Biochemistry* **36** (1997), pp. 4203–4211.
[24] W. Nitschke, B. Schoepp, B. Floss, A. Schricker, A. W. Rutherford, U. Liebl, Membrane-bound *c*-type cytochrome in *Heliobacillus mobillus*. Characterization by EPR and optical spectroscopy in membranes and detergent solubilized material, *Eur J Biochem* **242** (1996), pp. 695–702.
[25] W. Nitschke, U. Liebl, K. Matsuura, D. M. Kramer, Membrane-bound *c*-type cytochrome in *Heliobacillus mobillus*. *In vivo* study of the hemes involved in electron donation to the photosynthetic reaction center, *Biochemistry* **37** (1995), pp. 11831–11839.
[26] J. V. Beeumen, Primary structure diversity of prokaryotic diheme cytochrome *c, Biochimica et Biophysica Acta* **1058** (1991), pp. 56-60.
[27] A. C. Raffalt, L. Schmidt, et al, Electron transfer patterns of the di-heme protein cytochrome c_4 from *Pseudomonas stutzeri*, *J. Inorg. Biochem.* **103** (2009), pp. 717-722.

Chapter 3

A mass spectroscopic study of the diheme cytochrome *c* of the cytochrome *bc* complex in *Heliobacterium modesticaldum*

[Manuscript under preparation]

Abstract

Heliobacterial diheme cytochrome *c* subunit of the cytochrome *bc* complex is an unique and important part of the complex structurally and functionally. As an electron carrier and the last stop of the cytochrome *bc* complex's high potential intramolecular electron transfer chain, information about its structure and redox function is crucial toward the understanding of the function of the entire complex and its role in the heliobacterial cyclic electron transfer. Therefore, in this study, we utilized two mass spectroscopic techniques, hydrogen/deuterium exchange mass spectrometry (HDX-MS) and ion mobility mass spectrometry (IM-MS) to study the diheme cytochrome *c*'s conformations under reduced and oxidized conditions. In HDX kinetics studies, in almost all regions from most of the peptides, the oxidized form shows larger deuterium uptake compared to the reduced form, which indicates that the oxidized form of the diheme cyt *c* has a more open structure or at least higher dynamics. Meanwhile, the oxidized diheme cyt *c* showed longer drift time compared to its reduced form in the IM chamber, indicating a conformation with larger dynamic diameter, which is consistent with the conclusion drawn from HDX-MS experiments. Our experiments show unambiguously that there is a real structural conformational difference between the two different redox states. A smaller or more compact reduced form might have the function of bringing the two hemes closer to facilitate interheme electron transfer, which also implies a mechanism that is possibly sensitive to the distance between hemes.

Introduction

Different from cytochrome c_1 in the cytochrome bc_1 complex, or cytochrome *f* in the cytochrome b_6f compelx, a diheme cytochrome *c* plays the role of the terminal electron acceptor in the high potential electron transfer chain of the *bc* complex in heliobacteria [1, 2]. Therefore, studying the structure and function, particularly the redox properties of this unique subunit is crucial to the understanding of the function of the entire heliobacterial cyt *bc* complex.

In general, cytochrome *c* is a class of electron transport hemoproteins that covalently bind with heme group(s) through two thioether bonds between the vinyl groups of heme ring and cysteine sulfhydryls of the CXXCH heme-binding motifs [3]. Its main function is mediating single-electron transfer reactions between protein electron donors and acceptors [4, 5], during which time its heme iron(s) is reversibly oxidized and reduced between the Fe^{2+} and Fe^{3+} oxidation states. The axial coordination of heme iron plays key roles in determining redox, electron transfer, and other properties of cyt c [6, 7, 8]. Redox-dependent conformations of cyt *c* have been subjected to extensive study for decades using various biochemical and biophysical techniques [9-16]. Although some comparative X-ray crystallographic studies of cyts *c* have shown little or no difference between the backbone structures of the two redox states [17, 18], almost all solution based studies showed a clear conformational change between the two redox states [19, 20, 21]. Specifically in the case of horse heart cyt *c*, the radius dimension of the oxidized form is significantly larger than that of the reduced form [20].

Studying details of the redox-dependent conformational change is crucial to the elucidation of the mechanisms of biological electron transfer in metalloproteins, including cytochromes. For proteins with multiple metal centers, mutual orientation and distance between the centers ensures facile intramolecular electron transfer either directly or after conformational

triggering. The electron transfer step involving a given center induces electrostatic or conformational changes in other centers, either enhancing or lowering the rate constants of the subsequent electron transfer steps [22]. Prokaryotic diheme cyts *c*, as the representatives of the electron transfer proteins with two iron centers, have been studied with various spectroscopic methods [23, 24, 25]. For example, cyt c_4 from *Pseudomonas stutzeri*, which also shares the same origin and amino acid sequence similarities with heliobacteria diheme cyt *c* of the *bc* complex [26], the strong hydrogen bond via propionate groups between the two heme groups is the key for inter-heme (intramolecular) electron transfer [27].

Although numerous spectroscopic techniques have been powerful tools to study redox state related conformational changes of cyts *c* in the past, there are limitations. For instance, the biophysical techniques usually require large amount of sample, which is not always available, and the resolution is relatively low [28]. Modern mass spectrometry (MS), on the other hand, is well known for its exquisite sensitivity in probing the details of protein dynamics. In terms of studying protein conformations, hydrogen/deuterium exchange (HDX) or ion mobility (IM) coupled with MS are particularly effective [29, 30]. HDX refers to the exchange between the amide hydrogen in the protein backbone and the deuterium in D_2O in the solution. This is a kind of chemical labeling that can offer a topographical mapping of the protein surface, and the physical conditions of the proteins being probed. The mass shift, which works as a reporter, can be read by mass spectrometer, which eventually provides valuable information about protein dynamics [31-34]. IM is a technique that separates ions, e.g. ionized proteins, based on their mobility, or the ability to move through a certain medium. This is highly dependent on the charge and shape of an ion [35, 36]. Coupled with MS, which gives information on the mass to charge ratio (m/z), IM-MS can identify the mass of the ions, and their overall structure, e.g.

conformation and size, can also be determined simultaneously.

Previously, HDX coupled with infrared spectroscopy has been used to study the conformations of reduced and oxidized horse heart cyt *c* [37]. Viala and co-workers [38] reported the only HDX-MS study of the same system. There has been no HDX-MS or IM-MS study of the diheme cyt *c* system. We have proposed a working mechanism of the diheme cyt *c* subunit of the heliobacterial cyt *bc* complex, which involves a more closed conformation upon reduction, and more opened structure in the oxidized state [39]. Therefore, in this chapter, we report a MS based conformation study of the reduced and oxidized forms of the heliobacterial diheme cyt *c* for the first time, and offer amino acid resolution of the structural change details, which sheds light on the structure function relationship of this protein.

Materials and methods

Reduced and oxidized diheme cytochrome c sample preparation for ion mobility mass spectrometry.

The diheme cytochrome *c* was expressed and purified as described in chapter two [39]. 50 μL of approximately 5 μM diheme cyt *c* in 20 mM Tris-HCl, pH 7.5 solution was used for reduced and oxidized sample preparation respectively. By adding sodium dithionite (reductant) or potassium ferricyanide (oxidant) to the samples, they are either reduced or oxidized instantly. A Zeba spin desalting column (Thermo Scientific, IL, USA) was used to remove the extra sodium dithionite or potassium ferricyanide and the samples were exchanged into 200 mM ammonium acetate pH 6.8 buffer using a Vivaspin 500 ultrafiltration device (Vivaproducts,

Littleton, MA).

Ion mobility (IM) mass spectrometry experiment and data processing.

Samples were delivered by offline emitter (PicoTip, New Objective, Wohurn, MA) at the flow rate of ~10 nL/min. The sample solution was injected to a hybrid ion-mobility quadrupole time-of-flight mass spectrometer (Q-IM-TOF, Synapt G2 HDMS, Waters Inc., Milford, MA). All samples were acquired under the same, gentle instrument conditions (capillary voltage 1.5-2.1 kV, sampling cone 50 V, extraction cone 2 V, source temperature 30 °C, trap collision energy 40 V and transfer collision energy 5 V). The pressure of the backing region was 5 mbar. For the IM, the helium cell and the IMS gas flows were 120 mL/min and 50 mL/min, respectively, the IMS wave velocity was 450 m/s, and the IMS wave height was 20 V. Nitrogen was the carrier gas. An IM spectrum was acquired every 1 s, after external calibration to 8000 m/z with NaI solution. Peak picking and data processing were by Masslynx (v 4.1) and DriftScope software (Waters Inc., Milford, MA). The ion-mobility signal was averaged for 10-15 min.

Hydrogen/Deuterium exchange (HDX) experiment of reduced and oxidized diheme cytochrome c samples.

Differential, solution Hydrogen/Deuterium (HDX) experiments were performed in the cold room at 4 °C. Approximately 25 μM of diheme cyt *c* in 20 mM Tris-HCl, pH 7.5 solution was incubated with either sodium dithionite, or potassium ferricyanide (oxidant) to a final

concentration of 25 mM also at 4 °C, prior to HDX experiments. Continuous labeling was initiated by incubating 2 μL of the 25 μM protein, together with the reductant or oxidant, with 18 μL of D_2O; the incubation lasted for a predetermined time (0.17, 0.5, 1, 2, 15, 60, 240 min). The exchange reaction was quenched by mixing the solution with 30 μL of 3 M urea, 1% trifluoroacetic acid (TFA) at 0 °C. If not being used immediately, the mixture was frozen in liquid nitrogen right after the quenching and stored at -80 °C for less than 48 hours before use.

The mixture was then digested by passing through a custom-packed pepsin column (2 mm x 2 cm) at 200 μL/min, and captured by a C8 trap column (2 mm x 1 cm, Agilent Inc., Santa Clara, CA, USA) and desalted with a 3-min flow. Peptides were then separated by using a C18 column (2.1 mm x 5 cm, 1.9 mm Hypersil Gold, Thermo Fisher Scientific, Waltham, MA, USA) with a 5 min linear gradient of 4% - 40% CH_3CN in 0.1% formic acid. Protein digestion and peptide separation were carried out in an ice-water bath to minimize back exchange. Mass spectrometric analyses were with a hybrid LTQ Orbitrap (Thermo Fisher Scientific, CA, USA) with capillary temperature at 225 °C, and data were acquired with a mass resolving power of 100,000 for ions of m/z 400. Each experiment was performed in duplicate.

Peptide identification and HDX data processing

MS/MS experiments were performed with the LTQ Orbitrap mass spectrometer. Product-ion spectra were acquired in a data-dependent mode, and the six most abundant ions were selected for product-ion analysis. The MS/MS *.raw data files were converted to *.mgf files (MassMatrix Mass Spectrometric Data File Conversion Tools, Version 3.9) and then submitted to MassMatrix (Version 2.4.2) for peptide identification [40, 41]. Peptides included in

the set used for HDX had a MassMatrix score of 10 or greater, using peptide and MS/MS tolerance as 10 ppm and 0.8 Da, respectively. The MS/MS MassMatrix search was also performed against a decoy (reverse) sequence, and ambiguous identifications were ruled out. The product-ion (MS/MS) spectra of all peptide ions from the MassMatrix search were manually inspected, and only those verifiable were used in the following steps. The centroid masses of isotopic envelopes were calculated with HDX WorkBench [42]: deuterium level (%) = {[m(P) – m(N)]/[m(F) – m(N)]} x 100%, where m(P), m(N), and m(F) are centroid values of partially deuterated peptide, nondeuterated peptide, and fully deuterated peptide, respectively. To accommodate situation where a fully deuterated control is not available, m(F) was determined with m(F) = m(N) + (n-p-2)/z, where n is the number of amino acids in the peptide, p is the number of prolines, and z represents charge. Prolines, with no amide hydrogen, were not considered. The value "2" is subtracted within the equation because the first two amino acids do not retain deuterium. No correction was made for back exchange because all values are relative and susceptible to the same back exchange.

Results

HDX kinetic curves of all digested peptides

After pepsin treatment, diheme cytochrome *c* protein was digested into hundreds of peptides, in which around fifty with high signal/noise ratio were picked for the subsequent peptide mapping. The coverage rate is 100% (Fig. 1). Fig. 2 shows the kinetic curves of all the peptides used for HDX mapping of both reduced (solid line) and oxidized (dash line) states of the diheme cyt *c*. We submitted both reduced and oxidized protein to HDX under identical

conditions, so changes in HDX rates would reliably reflect any oxidation-induced changes. In most of the peptides, the oxidized form shows larger deuterium uptake compared to the reduced form, which indicates that the oxidized form of the diheme cyt *c* is more accessible to deuterium, thus more dynamic and opened. The most dramatic changes happened to the heme binding peptides (shown in Fig. 2, peptides 1-29, 1-32, 98-109, 109-127, 109-129, 110-127), indicating a significant conformational change of the heme binding pockets between the two redox states. Some regions of the protein, on the other hand, showed little difference between the oxidized and reduced forms, including peptides 45-49, 78-91, 130-138, 143-149, 169-172, 209-218. Except for peptides 78-91 and 209-218, which showed no difference in the level of deuterium uptake for both redox states, the other, however, showed hardly any deuterium uptake at all, indicating a near-protein-core location. Peptide 209-218 covers the His-tag, and the fact that there is no change of it shows that the His-tag influences little to the protein structure and dynamics.

HDX analysis of diheme cyt c on its homology model

A homology model of the diheme cyt *c* (His- tag not included) was generated with the software Modeller 9.10 using the cyt c_4 from *Pseudomonas stutzerii* as the template, and the percentage of deuterium levels for all peptides was mapped with color for each exchange point in Fig. 3. Since the oxidized and reduced forms of the template protein share exactly the same structure (pdb code 1M6Z and 1M70), and homology modeling alone cannot predict the different conformations of diheme cyt *c* at different redox states, a single predicted structure was calculated and used for HDX kinetics mapping, which can still provide valuable information about the secondary structure features and the protein environment of the hemes. Although the

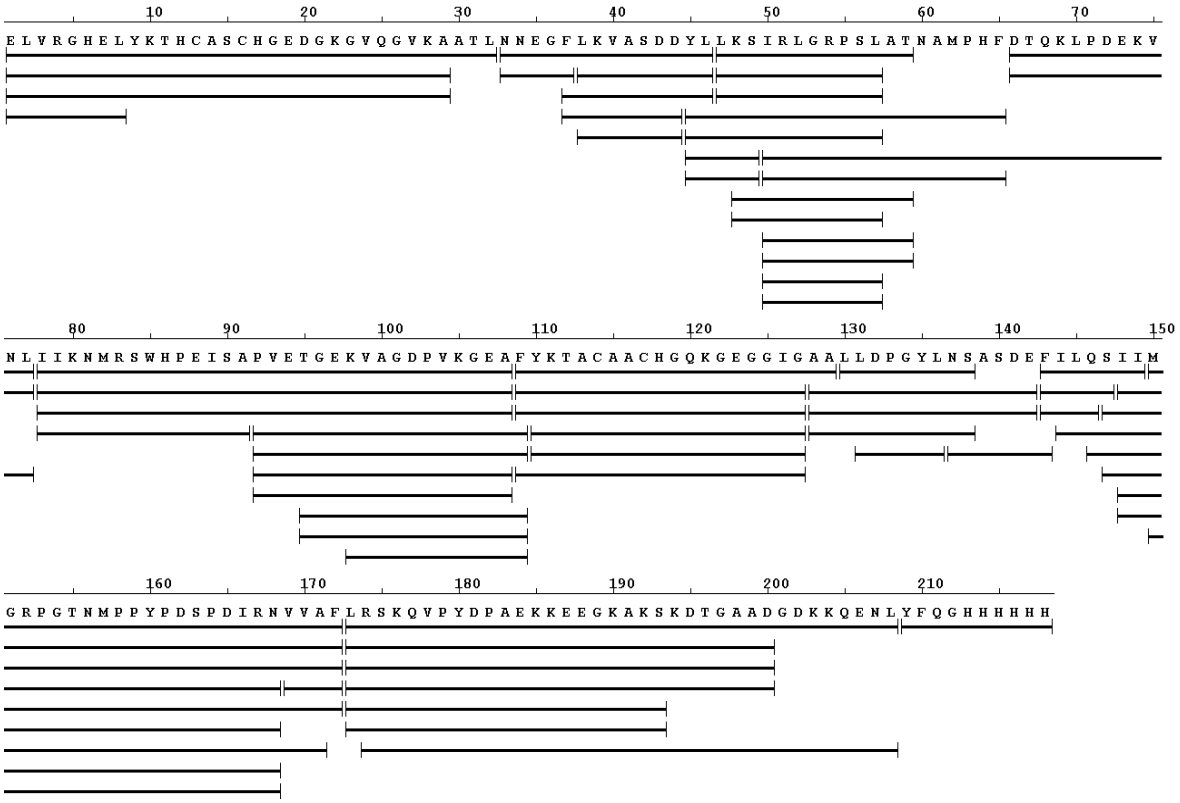

Fig. 1 HDX peptide coverage map for diheme cyt *c*. All amino acids from N to C terminus are covered. The same peptides with different charge states are also shown here.

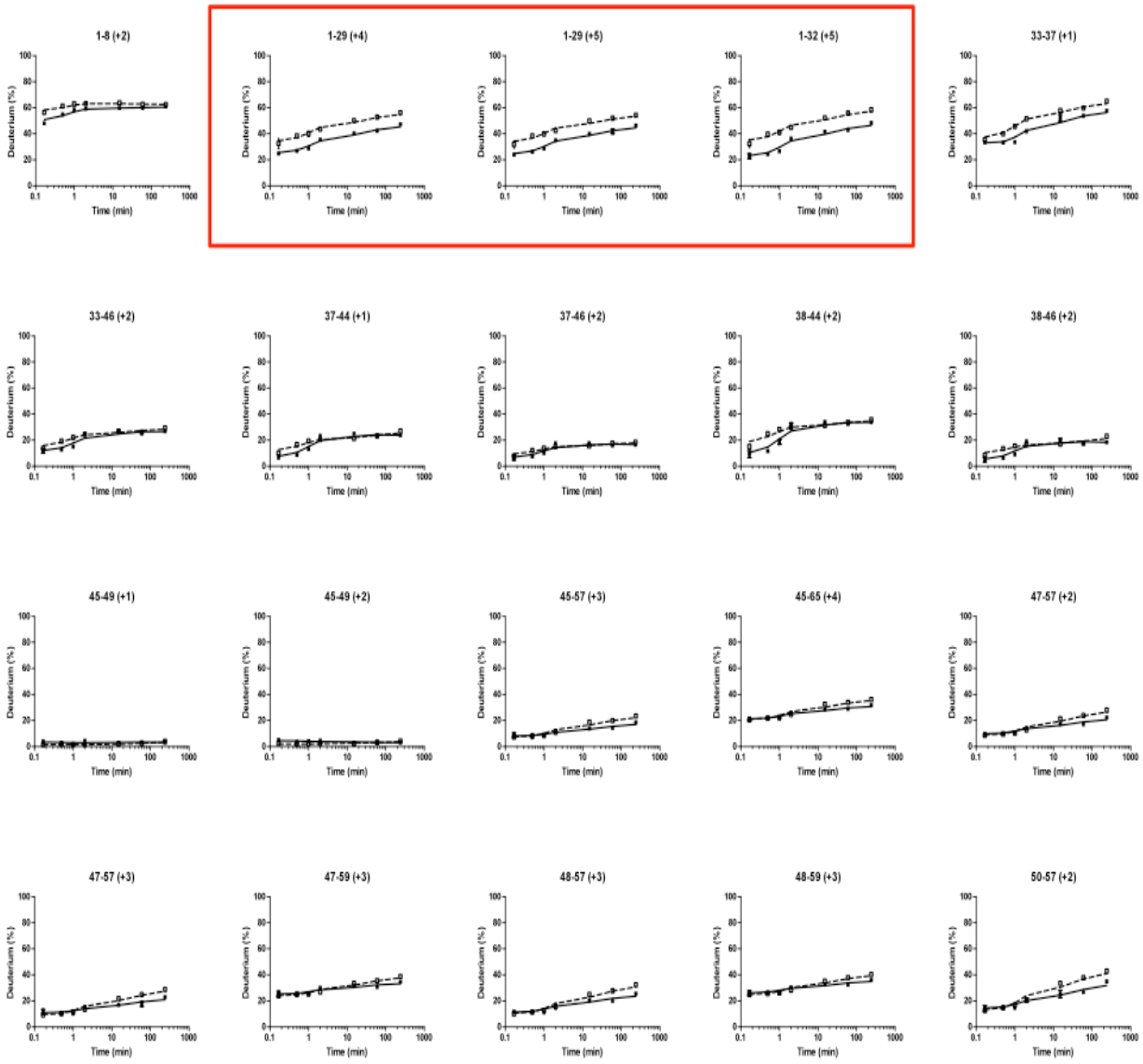

(Fig.2 continues to the next page)

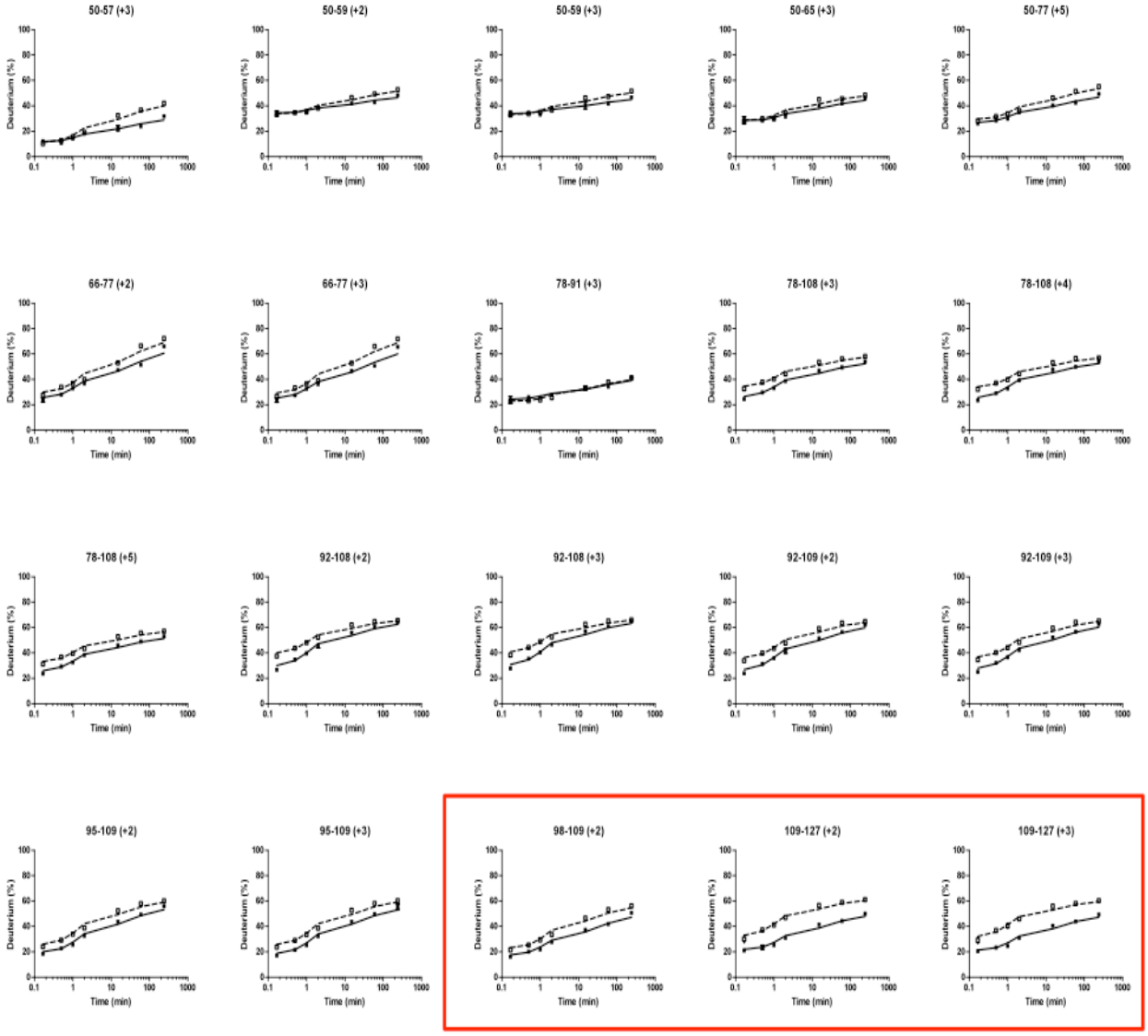

(Fig.2 continues to the next page)

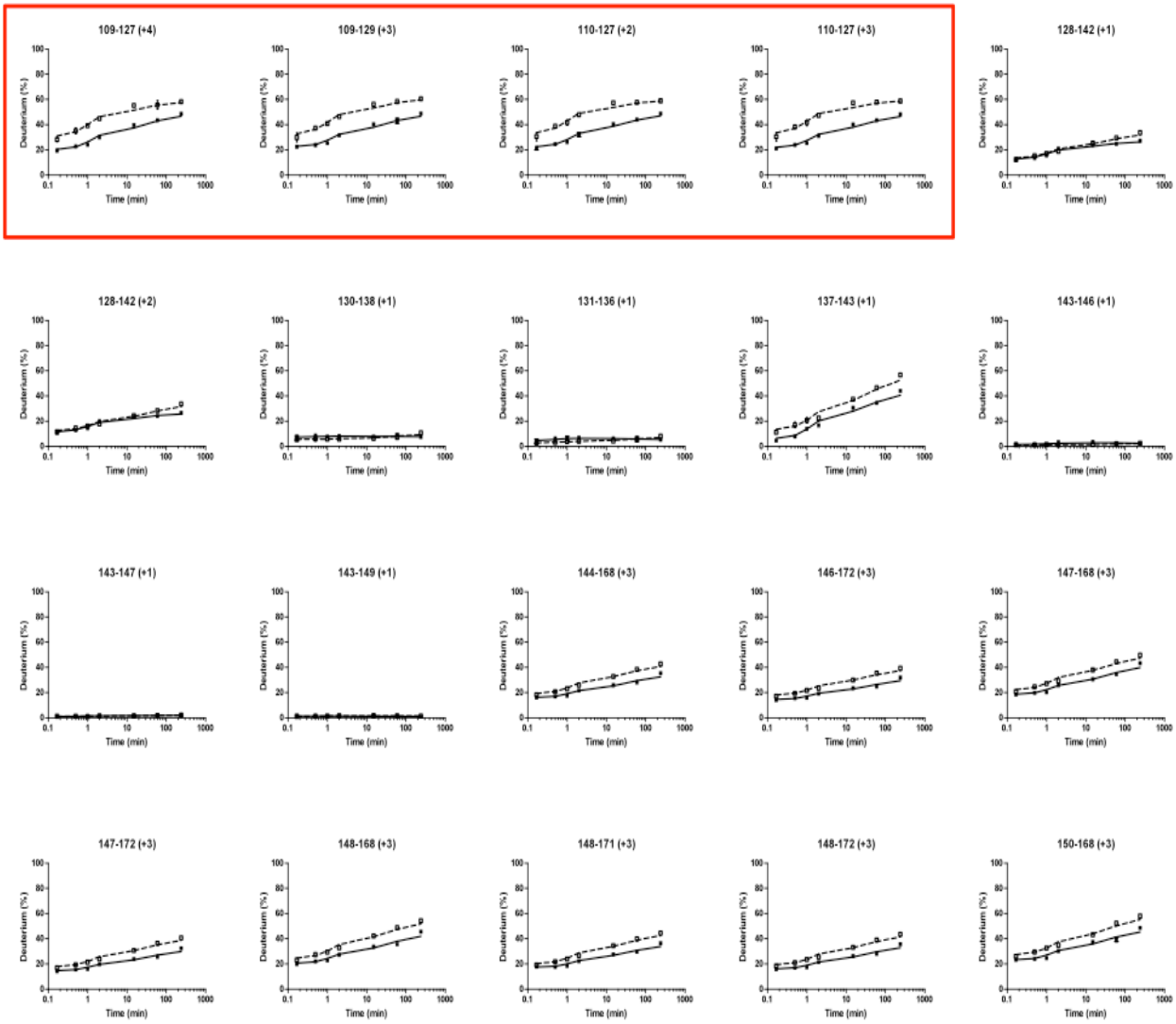

(Fig.2 continues to the next page)

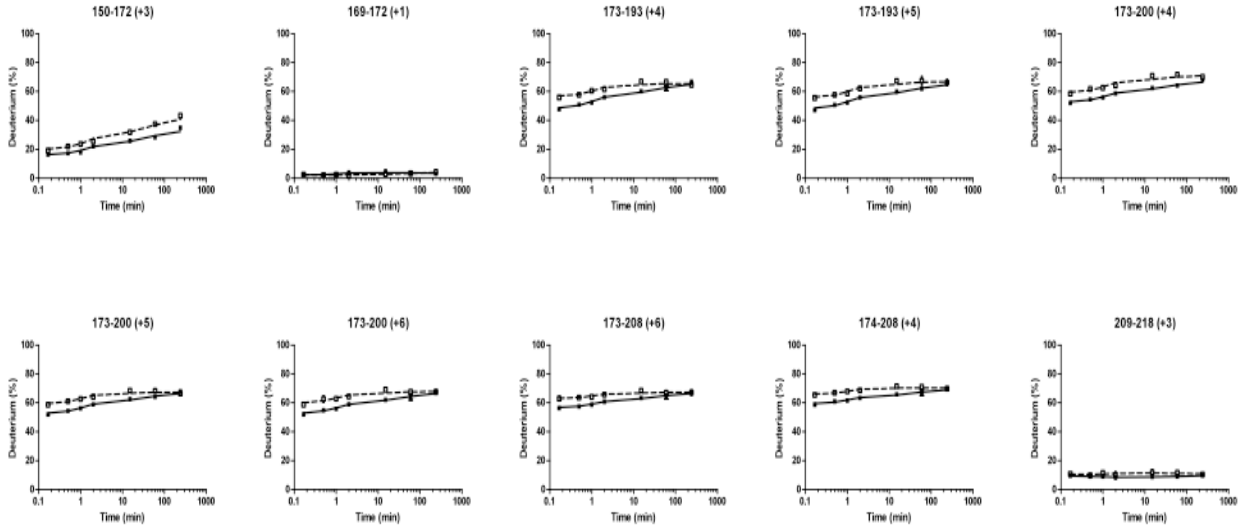

Fig. 2 Kinetic curves of all the peptides used for HDX mapping for reduced (solid line) and oxidized (dash line) states of the diheme cyt *c*. The peptides involved in heme *c* binding pockets are highlighted in red frames. The number range is the amino acid sequence (start from 1 at N-terminus and 218 at C-terminus). The numbers in parenthesis with "+" sign in front are the charge states of the peptides.

two heme binding domains share high sequence similarity and so do their secondary structures, in terms of deuterium exchange levels between reduced and oxidized states, there are some differences. Interestingly, compared to all other alpha helices around the hemes, one alpha helix in the N-terminal heme binding domain shows very low HDX level regardless of the redox state, implying a certain resistance to deuterium exchange. From the kinetic curves in Fig. 2, we observe that the oxidized form has a higher overall deuterium uptake. The kinetic information of both reduced and oxidized forms was mapped onto the homology structure (Fig. 3a and 3b, respectively). Warmer color means higher deuterium uptake. The loop regions have generally higher uptake even at shorter HDX time due to their intrinsic flexibility; but they are not the ones with the highest level, indicating a certain structural restriction. The differences between the oxidized and reduced form of diheme cyt *c* in terms of their uptake level (i.e., average of differences at every time point) are mapped in Fig. 4 onto the homology model. Most alpha-helical and loop regions around the hemes show higher exchange level for the oxidized form, suggesting a more opened structure and higher dynamics. The most significant difference happens to the loop and one short alpha helix close to the C-terminal heme (colored in deep blue in Fig. 4). The biggest structural changes based on the homology modeling, though not as significant as the ones close to the C-terminal heme, happen to the two alpha helices close to the N-terminal heme. These loop or alpha helical structures are all on the same sides of axial direction of the hemes' porphyrin plane, suggesting the possibility of allosteric interaction.

Diheme cyt c native mass spectroscopy.

To study the native conformation of the diheme cyt *c* protein with IM-mass spectrometry,

its native mass spectrum was first collected. The protein sample in 200 mM ammonium acetate was injected into the mass spectrometer and the spectrum is shown in Fig. 5. The protein was in nearly the native state, which is in a folded conformation with relatively few positive side chains on the surface compared to the denatured unfolded form. The major peak was observed at m/z = 2502.4 for 10+ charge state. The charge state distribution of diheme cyt *c* protein confirmed the near native folded state of the protein. There was some denatured unfolded protein signal observed in the low m/z region. We focused on the near native state of protein for the further investigation, which was reflected in the 10+ and 9+ charge states.

Diheme cyt c redox conformation study by IM-mass spectrometry.

IM gives a global view of conformational differences of proteins [43]. The electrical mobility of a protein ion, measured and represented by its drift time pass through a chamber filled with electrical field and inert gas, depends mainly on its charge state and collision cross section area. The larger the ion's collision cross section area is, the slower it will move in the chamber, thus giving a longer drift time. Yet in reality, when dealing with protein ions, it is usually more complicated. Fig. 6 shows the two-dimenstional IM-mass spectrum of diheme cyt *c*. The ions with the charge states 10+ and 9+ share almost the same drift time, although there is a one positive charge difference and ideally the one with higher charge should move faster in the electrical field. An explanation for this phenomenon is that the 10+ state protein ion has one more positively charged side chain on its surface compared to the 9+ one, which will lead to a more opened conformation relative to the lower charge state ion. This effect may counteract the more charges the ion bears in Fig. 6 and the same drift time is the result. Therefore, for redox

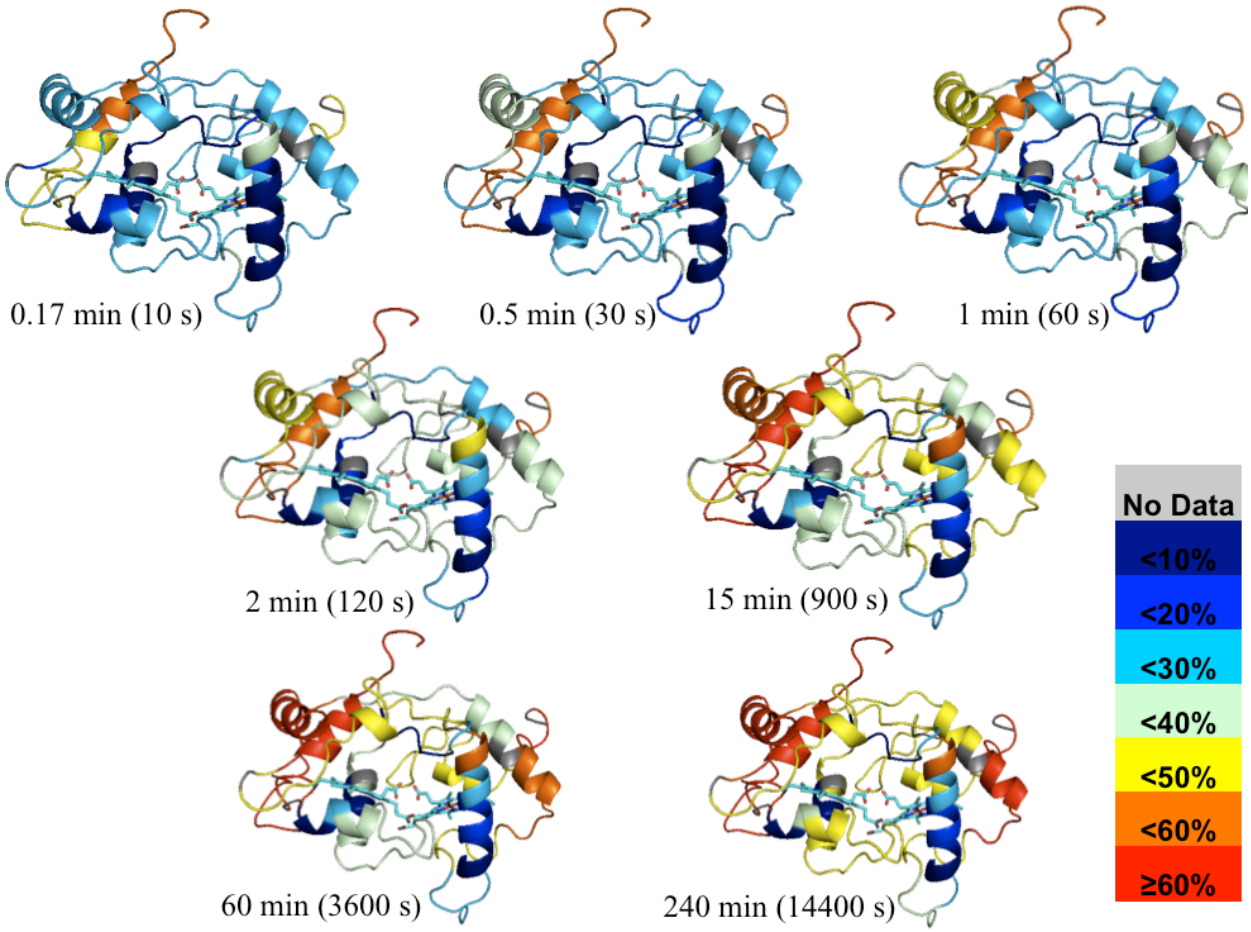
0.17 min (10 s)
0.5 min (30 s)
1 min (60 s)
2 min (120 s)
15 min (900 s)
60 min (3600 s)
240 min (14400 s)
No Data
<10%
<20%
<30%
<40%
<50%
<60%
≥60%

(a)

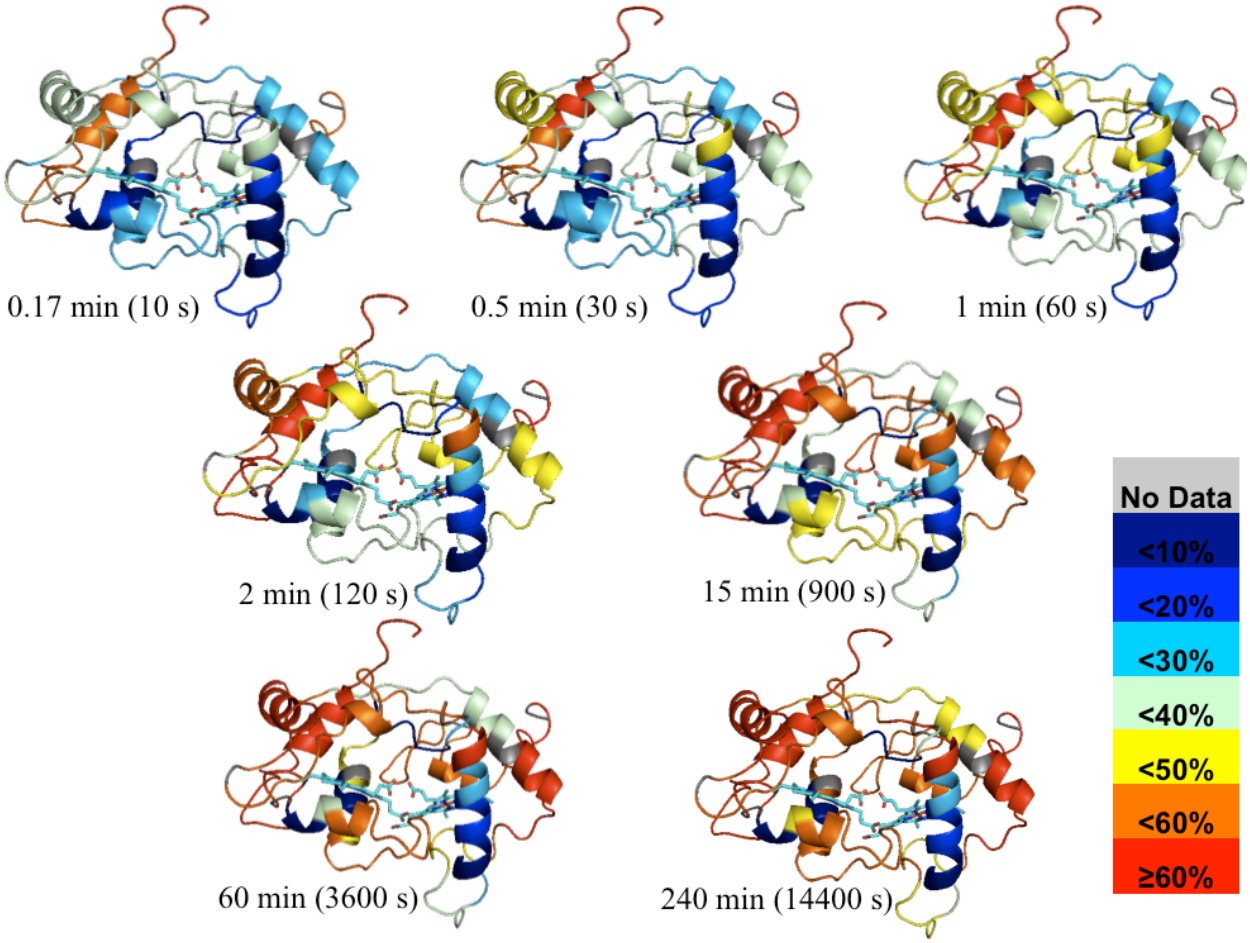

(b)

Fig. 3 The percentage of deuterium levels for all peptides was mapped with color for each exchange point onto the homology model of diheme cyt *c*; the color code is explained on the right of the figure. (a) Reduced form HDX kinetics. (b) Oxidized form HDX kinetics.

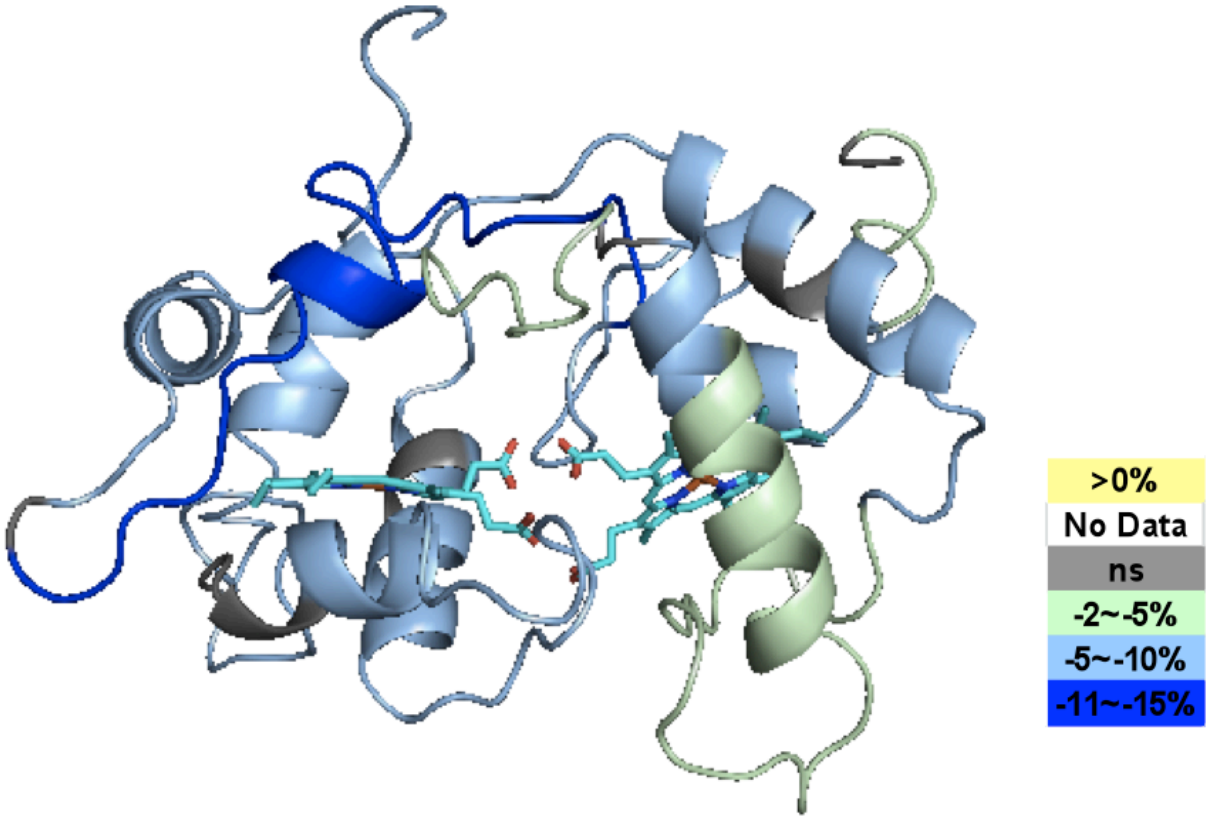

Fig. 4 The differences between the oxidized and reduced form of diheme cyt *c* in terms of their deuterium uptake are mapped onto the homology model. Color code shows the differences (reduced form subtracted by the oxidized form).

state related conformational change IM study, we picked up one single charge state ion as the target for analysis, which in this case the 9+ state due to its higher signal/noise ratio (data not shown here).

We then treated the samples with different sodium dithionite concentrations, 0, 250 μM, 500 μM, and injected them into the IM-mass spectrometer. For each sample, we could clearly detect two different forms of ions, with two different drift times, from the same charge state, 9+. Fig. 7 shows the drift time profiles of samples with different amount of the reductant. With the increase of dithionite concentration, the ion species with a shorter drift time increased as well, which indicates that this is the reduced form of the diheme cyt *c*. The other species had a decreased population at the same time, which means that it must be the oxidized form. Because the reduced form has a shorter drift time compared to the oxidized form, so the reduced protein has a more compact conformation, and the oxidized one has a more opened structure.

Discussion

Although numerous solution-based spectroscopic and computational studies showed that there is a conformational change between the reduced and oxidized forms of cyt *c*, these results were in apparent conflict with high-resolution crystallographic data on cyt *c* that shows the crystal structures of the two forms being very similar [44]. It is highly possible that the X-ray structures are both reduced forms. There can be radiation-induced reduction of oxidized metal proteins in an X-ray beam, and this clearly happens to the oxygen-evolving complex (OEC) in Photosystem II. Another proposed mechanism is that while the time-averaged structures of oxidized and reduced cyt *c* are the same, their dynamics are different, in that the oxidized form

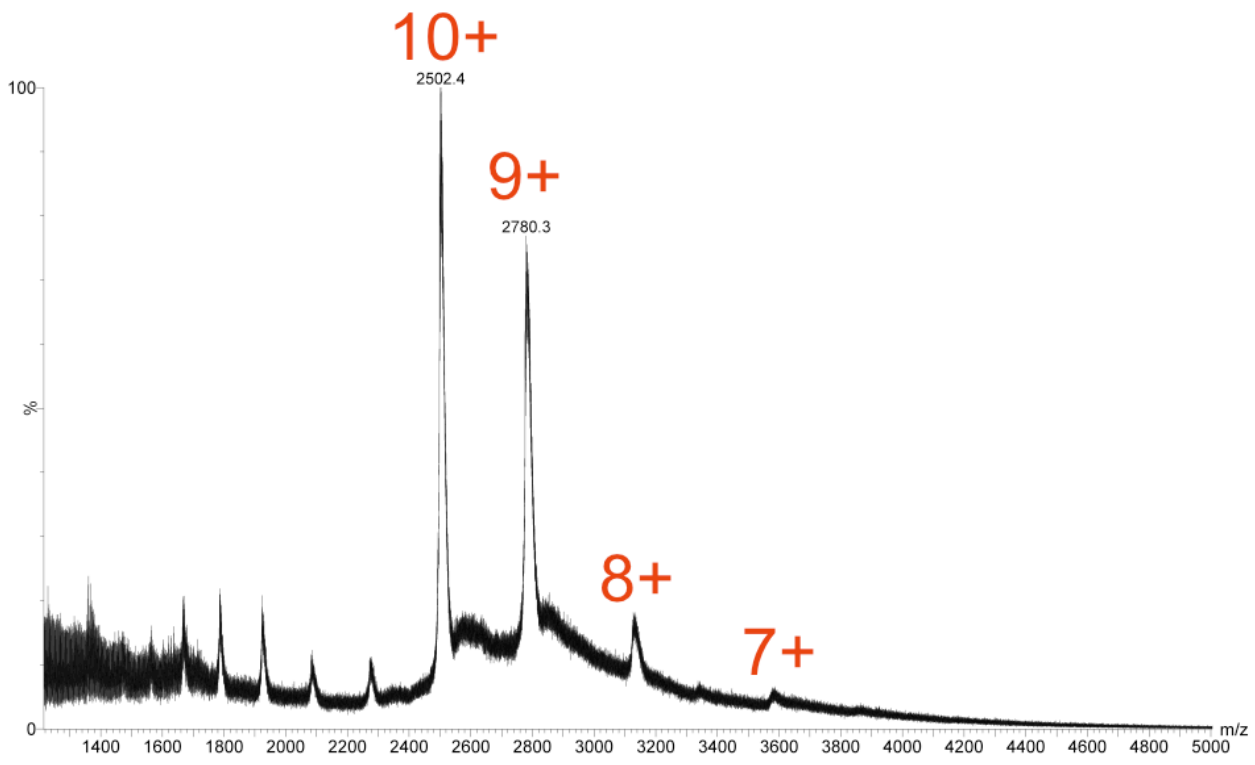

Fig. 5 Native mass spectrum of diheme cyt *c* in 200 mM ammonium acetate. Red numbers with "+" signs represent charge states of the ion species.

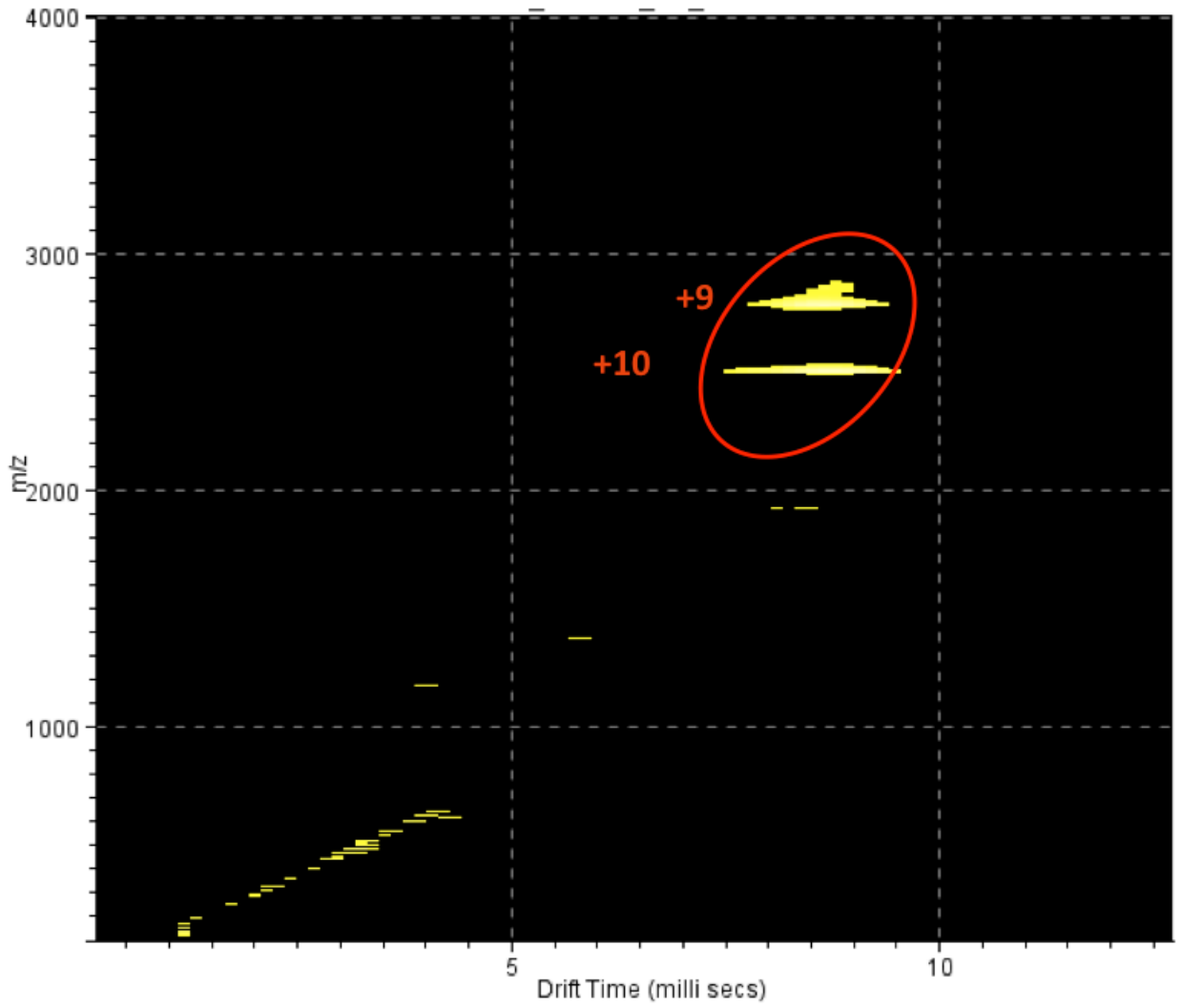

Fig. 6 Two-dimensional IM-mass spectrum of diheme cyt *c*. The protein was introduced into gas-phase (filled with N_2) by native ESI. The near native folded state of protein was observed. The ion mobility separation was plotted on the x-axis (drift time in ms) and the mass spectrum on the y-axis (m/z).

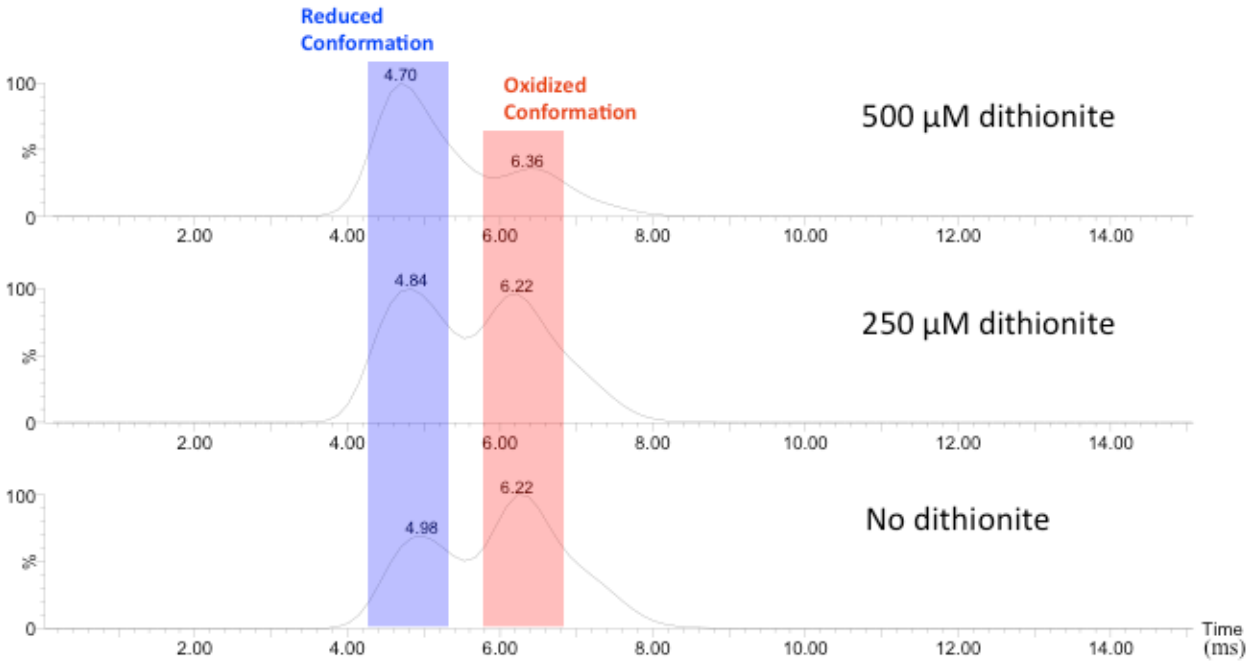

Fig. 7 Ion mobility measurement of diheme cyt *c* (9+ species) with different concentrations of reducing agent. The native IM mass spectra were acquired for samples with different sodium dithionite concentrations. The drift time profile for each experiment was extracted and plotted. The same instrument parameters were applied to all samples. Two species were observed in single charge state (9+). One is more open in the conformation, the other is more closed, labeled in different color.

undergoes more low-frequency, large-amplitude motions than the reduced form [45]. However, this cannot explain the overall yet unevenly distributed higher HDX for all peptides of the oxidized-form of diheme cyt *c* in our study. Besides, the IM-MS results clearly showed a more open structure or larger diameter of the oxidized form. Therefore, our study suggests that there are real structural differences between the two different redox forms. The most dramatic changes between the two redox states happen to the peptides directly linked to the hemes *c*, indicating that the main driving force of protein conformational change is the redox state change of the heme groups. Since the recombinant diheme cyt *c* we used in this study does not have the N-terminal transmembrane helix in its native form *in vivo* [39], so it is difficult to assess its influence toward the conformations at different redox states. It is possible, due to its closeness to the N-terminal heme binding motif, that it will impose some structural rigidity to the N-terminal heme binding domain and make this heme *c* a possible electron transfer partner with the Rieske iron-sulfur protein subunit of the *bc* complex.

For monoheme cytochromes, the electron transfer is a two-step process. First the electron donor binds with and reduces the cytochrome, then the cytochrome binds with the electron acceptor and passes the electron to it. For diheme cytochromes, on the other hand, one more step, the intramolecular interheme electron transfer, is added. In most diheme cyts *c*, the two hemes usually possess two distinct macroscopic redox potentials, e.g. 240 mV and 330 mV for the cyt c_4 from *P. stutzeri*, which follows expectations from the negative and positive electrostatic charges of the two domains [22]. And the electron will flow along with the direction of the electrostatic field inside the protein. The diheme cyt *c* from the heliobacterial cyt *bc* complex, however, only has one redox midpoint-potential [39], indicating two very similar heme binding pockets and similar protein charge distributions between the two domains, thus a

possible different intramolecular electron transfer mechanism. The observed significant protein conformational changes in both HDX- and IM-mass spectrometry studies may not only be triggered by the internal conformational change and charge distribution of the hemes upon reduction [4], but also work to facilitate the intramolecular interheme electron transfer, indicating a mechanism sensitive to distance between the hemes. The existence of an intramolecular "electrical wire" allows for an electron transfer function analogous to that of cytochrome *f* or cytochrome c_1. Our results points toward a more closed-up structure upon reduction of the protein, implying that closer distance between the two hemes can facilitate interheme electron transfer, either through the hydrogen bond between propionate groups, or bonds comprising the chain structures of the protein.

A conclusion is thus that there is a real difference between the structure of the reduced and oxidized form of diheme cyt *c*, and the oxidized conformation is more dynamic and opened comparing to the reduced form. The redox state driven conformational change is probably crucial to the intramolecular interheme electron transfer. To further understand the structure and function of the diheme cyt *c*, we crystallized the protein and the crystal diffracts at 2.0 Å. After the structure is solved, combined with our HDX- and IM-mass spectroscopic studies, there will be a clearer picture of the redox state triggered conformational change. The study of how this conformational change relates to the binding of electron donor (Rieske protein in the cyt *bc* complex) and electron accepter (cyt c_{553}), and its influence to the binding affinity will provide more information about the function of the diheme cyt *c* subunit and the *bc* complex in *H. modesticaldum* photosynthetic electron transfer chain.

Acknowledgement

We would like to thank Ms. Ying Zhang from Prof. Gross group at Washington University in St. Louis for her contribution to the HDX-MS part of the work, Dr. Hao Zhang in our lab for his contribution to the IM-MS part of the work, and Ms. Erica Majumder for her kind help in generating the homology models.

References

[1] A. L. Ducluzeau, E. Chenu. L. Capowiez, F. Baymann, The Rieske/cytochrome *b* complex of Heliobacteria, *Biochim. Biophys. Acta* **1777** (2008), pp. 1140-1146.

[2] J. Xiong, K. Inoue, C. E. Bauer, Tracking molecular evolution of photosynthesis by characterization of a major photosynthesis gene cluster from *Heliobacillus mobilis*, *Proc. Natl. Acad. Sci. U. S. A.* **95** (1998), pp. 14851-14856.

[3] E. Margoliash, Primary structure and evolution of cytochrome *c*, *Proc. Natl. Acad. Sci. U. S. A.* **50** (1963), pp. 672-679.

[4] G. W. Pettigrew, G. R. Moore, Cytochrome *c* – biological aspects, *Springer Verlag, Berlin, Heidelberg,* (1987).

[5] R. A. Scott, A. G. Mauk, Cytochrome *c* – A multidisciplinary approach, *University Science Books, Sausalito, CA,* (1997).

[6] D. S. Wuttke, H. B. Gray, Protein engineering as a tool for understanding electron transfer, *Curr. Opin. Struct. Biol.* **3** (1993), pp. 555-563.

[7] G. R. Moore, G. W. Pettigrew, Cytochrome *c*: evolutionary, structural and physicochemical aspects, *Springer Verlag, Berlin, Heidelberg,* (1990).

[8] C. J. Wallace, I. Clark-Lewis, Functional role of heme ligation in cytochrome *c*. Effects of replacement of methionine 80 with natural and non-natural residues by semisynthesis, *J. Biol. Chem.* **267** (1992), pp. 3852-3861.

[9] E. Margoliash, A. Schejter, Cytochrome *c*, *Adv. Protein Chem.* **21** (1966), pp. 113-286.

[10] F. R. Salemme, Structure and function of cytochrome *c*, *Annu. Rev. Biochem.* **46** (1977), pp. 299-329.

[11] G. A. Mines, T. Pascher, S. C. Lee, J. R. Winkler, H. B. Gray, Cytochrome *c* folding triggered by electron transfer, *Chem. Biol*. **3** (1996), pp. 491-497.

[12] T. Pascher, J. P. Chesick, J. R. Winkler, H. B. Gray, Protein folding triggered by electron transfer, *Science* **271** (1996), pp. 1558-1560.

[13] B. A. Feinberg, X. Liu, M. D. Ryan, A. Schejter, C. Zhang, Direct voltammetric observation of redox driven changes in axial coordination and intramolecular rearrangement of the phenylalanine-82 histidine variant of yeast iso-1-cytochrome *c*, *Biochemistry* **37** (1998), pp. 13091-13101.

[14] S. Baddam, B. E. Bowler, Tuning the rate and pH accessibility of a conformational electron transfer gate, *Inorg. Chem*. **45** (2006), pp. 6338-6346.

[15] S. Bandi, S. Baddam, B. E. Bowler, Alkaline conformational transition and gated electron transfer with a Lys79-His variant of iso-1-cytochrome *c*, *Biochemistry* **46** (2007), pp. 10643-10645.

[16] S. Bandi, B. E. Bowler, Probing the bottom of a folding funnel using conformationally gated electron transfer reactions, *J. Am. Chem. Soc*. **130** (2008), pp. 7540-7541.

[17] T. Takano, R. E. Dickerson, Conformation change of cytochrome *c*. I. Ferrocytochrome *c* structure refined at 1.5 Å resolution, *J. Mol. Biol*. **153** (1981), pp. 79-94.

[18] T. Takano, R. E. Dickerson, Conformation change of cytochrome *c*. II. Ferricytochrome *c* refinement at 1.8 Å and comparison with the ferrocytochrome structure, *J. Mol. Biol*. **153** (1981), pp. 95-115.

[19] J. F. Calvert, J. L. Hills, A. Dong, Redox-dependent conformational changes are common structural features of cytochrome *c* from various species, *Arch. Biochem. Biophys.* **346** (1997), pp. 287-293.

[20] J. Trewhella, V. A. P. Carlson, E. H. Curtis, D. B. Heidorn, Differences in the solution structures of oxidized and reduced cytochrome *c* measured by small-angle X-ray scattering, *Biochemistry* **27** (1988), pp. 1121-1125.
[21] S. Oellerich, H. Wackerbarth, P. Hildebrandt, Spectroscopic characterization of nonnative conformational states of cytochrome *c*, *J. Phys. Chem. B* **106** (2002), pp. 6566-6580.
[22] A. C. Raffalt, L. Schmidt, E. M. Christensen, Q. Chi, J, Ulstrup, Electron transfer patterns of the di-heme cytochrome c_4 from *Pseudomonas stutzeri*, *J. Inorg. Biochem.* **103** (2009), pp. 717-722.
[23] J. van-Beeumen, Primary structure diversity of prokaryotic diheme cytochrome *c*, *Biochim, Biophys. Acta* **1058** (1991), pp. 56-60.
[24] G. D. Rocco, G. Battistuzzi, C. A. Bortolotti, M. Borsari, E. Ferrari, S. Monari, M. Sola, Cloning, expression, and physicochemical characterization of a new diheme cytochrome *c* from *Shewanella baltica* OS155, *J. Biol. Inorg. Chem.* **16** (2011), pp. 461-471.
[25] H. R. Gibson, C. G. Mowat, C. S. Miles, B. R. Li, D. Leys, G. A. Reid, S. K. Chapman, Structural and functional studies on DHC, the diheme cytochrome *c* from *Rhodoacter sphaeroides*, and its interaction with SHP, the *sphaeroides* heme protein, *Biochemistry* **45** (2006), pp. 6363-6371.
[26] F. Baymann, W. Nitschke, Heliobacterial Rieske/cyt *b* complex, *Photosynth. Res.* **104** (2010), pp. 177-187.
[27] A. Kadziola, S. Larsen, Crystal structure of the diheme cytochrome c_4 from *Pseudomonas stutzeri* determined at 2.2 Å resolution, *Structure* **5** (1997), pp. 203-216.
[28] A. Thijs, M. Jorg, Biophysical techniques in photosynthesis, *Advances in Photosynthesis and Respiration,* **26** (2008).
[29] A. J. Percy, M. Rey, K. M. Burns, D. C. Schriemer, Probing protein interactions with hydrogen/deuterium exchange and mass spectrometry-A review, *Analytica Chimica Acta* **721** (2012), pp. 7-21.
[30] B. C. Bohrer, S. I. Merenbloom, S. L. Koeniger, A. E. Hilderbrand, D. E. Clemmer, Biomolecule analysis by ion mobility spectrometry, *Annu. Rev. Anal. Chem.* **1** (2008), pp. 293-327.
[31] H. Xiao, S. J. Eyles, I. A. Kaltashov, Indirect assessment of small hydrophobic ligand binding to a model protein using a combination of ESI MS and HDX/ESI MS, *J. Am. Soc. Mass Spectrom*. **14**, (2003), pp. 506-515.
[32] X. Yan, D. Broderick, M. E. Leid, M. I. Schimerlik, M. L. Deinzer, Dynamics and ligand-induced solvent accessibility changes in human retinoid X receptor homodimer determined by hydrogen deuterium exchange and mass spectrometry, *Biochemistry* **43** (2004) pp. 909-917.
[33] E. A. Komives, Protein-protein interaction dynamics by amide $H/^2H$ exchange mass spectrometry, *Int. J. Mass Spectrom*. **240** (2005), pp. 285-290.
[34] G. N. Betts, P. van der Geer, E.A. Komives, Structural and functional consequences of tyrosine phosphorylation in the LRP1 cytoplasmic domain, *J. Biol. Chem.* **283** (2008), pp. 15656-15664.
[35] C. Uetrecht, R. J. Rose, E. van Duijn, K. Lorenzen, A. J. R. Heck, Ion mobility mass spectrometry of proteins and protein assemblies, *Chem. Soc. Rev.* **39** (2010), pp 1633-1655.
[36] E. Jurneczko, P. E. Barran, How useful is ion mobility mass spectrometry for structural biology? The relationship between protein crystal structures and their collision cross sections in the gas phase, *Analyst* **136** (2011), pp. 20-28.

[37] D. D. Ulmer, J. H. R. Kagi, Hydrogen-deuterium exchange of cytochrome *c*. I. Effect of oxidation state, *Biochemistry* **7** (1968), pp. 2710-2717.
[38] E. N. Viala, C. Thiery, P. Calvet, J. M. Thiery, Hydrogen-isotope exchange of oxidized and reduced cytochrome *c*. A comparison of mass spectrometry and infrared methods, *Eur. J. Biochem.* **61** (1976), pp. 253-258.
[39] H. Yue, Y. Kang, H. Zhang, X. Gao, R. E. Blankenship, *Arch. Biochem. Biophys.* **517** (2012), pp. 131-137.
[40] H. Xu, M. A. Freitas, A mass accuracy sensitive probability based scoring algorithm for database searching of tandem mass spectrometry data, *BMC Bioinformatics* **8** (2007), pp. 133.
[41] H. Xu, M. A. Freitas, MassMatrix: A database search program for rapid characterization of proteins and peptides from tandem mass spectrometry data, *Proteomics* **9** (2009), pp. 1548-1555.
[42] B. D. Pascal, S. Willis, J. L. Lauer, R. R. Landgraf, G. M. West, D. Marciano, S. Novick, D. Goswami, M. J. Chalmers, P. R. Griffin, HDX workbench: software for the analysis of H/D exchange MS data, *Journal of the American Society for Mass Spectrometry* **23** (2012), pp. 1512-1521.
[43] C. Uetrecht, R. J. Rose, E. van Duijn, K. Lorenzen, A. J. R. Heck, Ion mobility mass spectrometry of protein and protein assemblies, *Chemical Society Review* **39** (2010), pp. 1633-1655.
[44] S. Rackovsky, D. A. Goldstein, On the redox conformational changes in cytochrome *c*. *Proc. Natl. Acad. Sci. U. S. A.* **81** (1984), pp. 5901-5905.
[45] D. Eden, J. B. Matthew, J. J. Rosa, F. M. Richards, Increase in apparent compressibility of cytochrome *c* upon oxidation, *Proc. Natl. Acad. Sci. U. S. A.* **79** (1982), pp. 815-819.

Chapter 4

In vitro quantification of the reaction center (RC) and cytochrome *bc* complex in *Heliobacterium modesticaldum*

[Manuscript under preparation]

Abstract

Photosynthetic light reactions establish cyclic electron transfer (CET) in the cytoplasmic membrane in *Heliobacterium modesticaldum*, leading to the production of ATP and NADH, which participate in carbon assimilation and nitrogen fixation. Therefore, it is important to understand its mechanism, especially the dynamic interaction between two key components of the CET chain, the reaction center (RC) and the cytochrome *bc* complex. Determining their stoichiometry is a crucial step toward building a more accurate heliobacterial CET model. We determined the amount of RC in *H. modesticaldum* whole cells by measuring the absorption spectrum of the cell methanol extract. The cytochrome *bc* complex content was calculated based on quantitative Western blot, using an antibody raised against recombinant diheme cytochrome *c* subunit of the complex. A stoichiometry of 14 to 8 RCs per cytochrome *bc* complex catalytic center was estimated, a much larger number than previously reported, indicating a higher turnover number of the *bc* complex.

Introduction

Light-induced cyclic electron transfer (CET) in Heliobacteria involves two integral membrane protein complexes, the reaction center (RC) and the cytochrome *bc* (Rieske/cytochrome *b*) complex, each encompassing several redox centers and embedded in the cytoplasmic membrane, plus the membrane attached cytochrome c_{553} that shuttles electrons between them [1, 2, 3]. The direct outcome of this light-induced CET is the translocation of protons from the cytoplasm to the periplasm and the formation of a trans-membrane potential, which ultimately drives the ATP synthesis via the ATP synthase. Part of the energy is used to produce reducing power, e.g. the producing of NADH, which is the driving force for linear electron pathway and carbon/nitrogen fixation [4]. Therefore, CET is crucial for a proper balance of ATP and NADH in Heliobacteria [5].

The main steps of the light-induced CET in Heliobacteria can be outlined as follows. After the absorption of a photon by the Bchl *g* pigments, the excitation induces a charge separation in the RC complex [6, 7, 8]. Electrons within the RC core polypeptide homodimer PshA are eventually shuttled to a [4Fe-4S] cluster, and subsequently donated to the terminal Fe/S dicluster F_A/F_B within PshB, a [4Fe-4S] ferredoxin that associates with PshA on the cytoplasmic side of the membrane [9, 10, 11]. Then PshB may pass the electrons to a second ferredoxin, which supplies reducing equivalents for cytoplasmic reactions primarily focused on carbon assimilation and nitrogen fixation, or may dissociate and fulfill this function. Meanwhile, the menaquinols in the membrane pool are oxidized via turnover of the cytochrome *bc* complex through the Q-cycle mechanism. The electrons will then be passed to the cytochrome c_{553} and eventually the RC core complex [2]. Protons will be translocated from cytoplasm to periplasm at the same time via Q cycle in the cytochrome *bc* complex [12]. NADH:menaquinone

oxidoreductase (complex I) will re-reduce the menaquinone pool together with cytochrome *bc* complex to complete the cycle.

Many attempts over the past three decades dedicated to the understanding of heliobacterial CET, investigations are complicated by the extreme oxygen sensitivity of the organism due to a high proportion of the unsaturated lipids [13] and the presence of Bchl *g* [14], which is transformed to farnesol-Chl *a* upon contact with oxygen [15]. Furthermore, it seems that electron transfer reactions beyond the RC itself can only be studied in intact, living cells since membrane preparation disrupts the electron transfer chain [16]. Nitschke and coworkers [17], using absorption difference spectra recorded on whole cells poised to different redox conditions by addition of chemicals (ferrocyanide, ascorbate, phenazine methosulfate) and flash-induced absorption difference spectra, determined a stoichiometry of 5-6 hemes *c* and 1-3 hemes *b* per RC in *H. mobilus*. Kramer and coworkers [18] estimated a stoichiometry of 0.6-0.75 cytochrome *bc* complexes per RC based on light-induced redox changes in whole cells under anaerobic and aerobic conditions also for *H. mobilus*. Though variable depending on species and growth conditions, the stoichiometric ratios between the components of the photosynthetic chain are generally in the order: quinones > RC > mobile cytochrome > cytochrome *bc* complex [19]. Moreover, the complexity of whole cell systems and a serious of assumptions made for these calculations reported in the earlier reports imposes challenges to the model building for the heliobacterial CET, and no similar study has been done in *H. modesticaldum* cells. Therefore, in this study, we determined *H. modesticaldum* RC quantity based on the absorption spectra of Bchl *g* (Bchl *g'*) directly extracted from whole cells. The cytochrome *bc* complex quantity in the same amount of cells was determined by quantitative Western blot, using the antibody raised against its diheme cytochrome *c* subunit as the probe and recombinant diheme cytochrome *c* as internal

standard. These data were used to estimate the stoichiometry of the RC and cytochrome *bc* complex, and the implications of ratio for the current heliobacterial CET model are discussed.

Materials and methods

Growth of H. modesticaldum and cell lysis sample preparation

H. modesticaldum was grown in PYE medium inside the Coy anaerobic chamber at temperatures ranging from 40–45 °C in the light (10 ± 1 W/m^2). To prepare the sample for cytochrome *bc* complex quantification, 250 μL of overnight (20 hours) culture was harvested by centrifugation at 13,000 rpm and re-suspended into the SDS denaturing buffer, which is composed of 150 mM Tris-HCl, 4% SDS, 5% 2-mercaptoethanol, 0.05% coomassie blue G250, 30% glycerol, pH=7.0. The final volume is 100 μL. Sonication is needed for cell lysis. The mixture is incubated at room temperature for 1 hour, then centrifuged at 13,000 rpm for 3 min to precipitate the insoluble material, and ready for SDS PAGE. To prepare the sample for reaction center quantification [20], 250 μL of cell culture, taken from the same one used for cytochrome *bc* complex quantification, was harvested by centrifugation. The liquid was removed thoroughly, 1 mL of methanol, degassed and kept in the anaerobic chamber, was added. Then the mixture was subjected to vigorous shake for 1 min and centrifuged at 13, 000 rpm for 3 min to remove the cell debris. The yellow-greenish supernatant contained all the extracted pigments from the cells, which is used for UV-Vis spectroscopy measurement. The entire operation was conducted inside a Coy anaerobic chamber to avoid oxygen.

HPLC purification of Bchl g and Bchl g' and their extinction coefficient determination with UV-Vis spectroscopy

H. modesticaldum cells from 1 mL of overnight culture was disrupted with degased 100% methanol and the pigments in the cells were extracted. Then the Bchl *g* (Bchl *g*') was purified using an Agilent 1100 HPLC system equipped with a Zorbax Eclipse XDB-C18 reverse phase column (250 mm × 4.6 mm) with the flow rate of 1 ml/min and two mobile phase gradients: methanol from 100% to 98% and THF from 0 to 2% from 0 to 5 min, then methanol from 98% to 90% and THF from 2% to 10% from 5 to 10 min. The fraction of the peak from 6.5 to 7.0 min was pure Bchl *g* (Bchl *g*') and collected. Then the collected solution was quickly dried by N_2 gas flow and dissolved with degased acetone. Then, to 1 mL of degased methanol and diethyl ether solvent in two separate UV cuvettes, 20 μL of the Bchl *g* (Bchl *g*') acetone solution were added to each one respectively. The absorbance profiles were measured with a Shimadzu UV-1800 UV-Vis spectrophotometer.

Room temperature UV-Vis spectroscopy for Bchl g (Bchl g') and RC quantification

The UV-Vis spectra of the pigments methanol extract was taken with a Shimadzu UV-1800 UV-Vis spectrophotometer inside the anaerobic chamber. A 0.5 cm pathlength cuvette was used for the measurements. The spectrum was analyzed by Shimadzu software pack and Origin 7.5 (OriginLab).

Protein concentration assay, SDS-PAGE and Western blot

The concentration of recombinant diheme cytochrome *c* was determined by pyridine hemochrome method described in chapter two. The standard samples with known concentrations were mixed with SDS denaturing buffer, which was used for cell lysate denaturing, and incubated for 1 hour at room temperature before being loaded onto a SDS gel for electrophoresis. The SDS-PAGE procedure is addressed in Chapter two. After SDS-PAGE, the gel was taken out, and the proteins were blotted onto a nitrocellulose membrane using a Pierce Fast Semi-Dry Blotter in the transfer buffer (25 mM Tris, 192 mM glycine, 10% methanol) at 4 °C for 50 min with a constant voltage of 15 V. Then the membrane was treated with 3% H_2O_2 for 10 min, and rinsed with water three times, each for 3 min. After thoroughly rinsed, the membrane was put into 10% (w/v) non-fat milk TBS buffer (10 mM Tris-HCl, pH 7.4, 0.9% (w/v) NaCl) overnight at 4 °C for blocking. The anti diheme cytochrome *c* polyclonal antibody, raised in rabbit and purified by protein A and G, was diluted 10,000 times into TBS buffer with 5% non-fat milk. The membrane was then incubated for 2 hours at room temperature with mild shaking. After primary antibody incubation, the membrane was washed with TBS buffer for 4 times on a shaker, 8 min each. The secondary antibody, anti-rabbit IgG-peroxidase produced in goat, was diluted 10,000 times in TBS buffer with 5% milk. The membrane was then incubated with secondary antibody for 1 hour, also at room temperature on a shaker. Then pour out the buffer and wash the membrane with TBS buffer for 4 times, 10 min each, and followed by water 3 times, 1 min each. The membrane was carefully dried briefly with Kimwipe without disturbing the surface attached with proteins. Then the SupperSignal West Femto Maximum Sensitivity Substrate kit (Thermo Scientific) was used to develop the membrane. The chemiluminescence signals were detected and analyzed by a LAS-4000 detection system and ImageQuant TL software pack (GE).

Results

Bchl g and Bchl g' extinction coefficient in methanol determination

Based on Beer's law, $A=\varepsilon cl$ (ε extinction coefficient, c concentration of the compound in solution, l pathlength of the sample), calculating the concentration of Bchl *g* (Bchl *g*') thus RC in solution requires known extinction coefficient. Methanol is the most commonly used organic solvent to extract pigments from whole cells, but the ε of Bchl *g* (Bchl *g*') in 100% methanol has yet been reported. Since we use methanol to determine the RC concentration, the first step is to measure the ε of Bchl *g* (Bchl *g*') in methanol. Moreover, ε of Bchl *g* (Bchl *g*') in diethyl ether was well known [21], therefore, we chose it as the reference. The UV-Vis absorption spectra of HPLC purified Bchl *g* (Bchl *g*') in diethyl ether and methanol are shown in Fig. 1. The maximum Q band absorption of Bchl *g* (Bchl *g*') in diethyl ether is 0.359 at 767 nm, and 0.21 at 750 nm in methanol. The ε of the Q band in diethyl ether is 100 $mM^{-1}cm^{-1}$, so the ε of the Q band in methanol is calculated to be 58.5 $mM^{-1}cm^{-1}$.

H. modesticaldum reaction center quantification

In *H. modesticaldum* membrane, under photosynthetic growth conditions, reaction center is the dominant component [22]. The major pigments it contains, Bchl *g* and Bchl *g*', have unique and characteristic absorbance at higher wavelengths above 730nm in organic solvents. Therefore, in terms of reaction center quantification, comparing to direct protein peptide measurement, which requires complete and accurate, usually difficult separation of the RC from the membrane, extracting and measuring Bchl *g* (and Bchl *g*') pigments with organic solvent

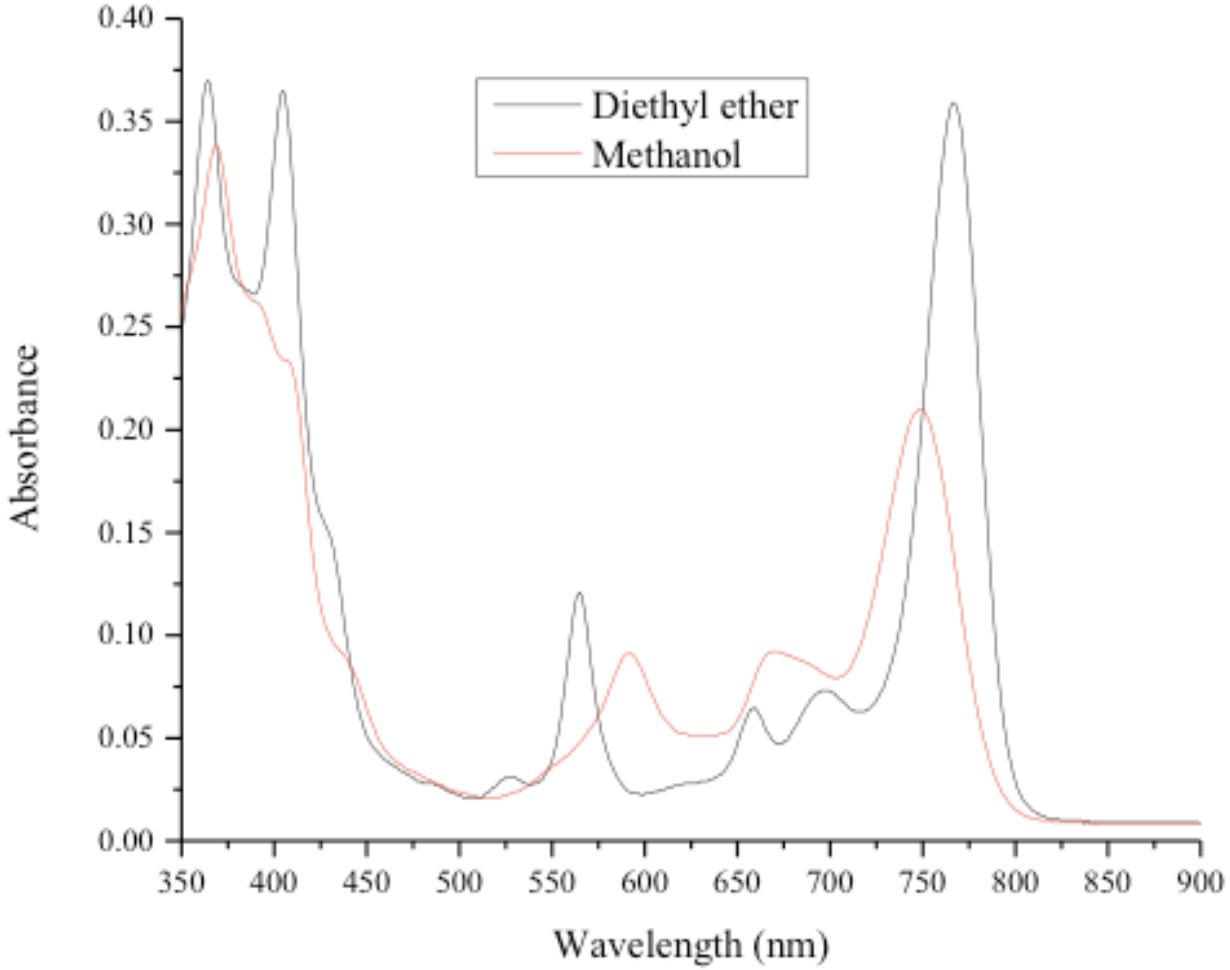

Fig. 1 UV-Vis absorption spectra of HPLC purified Bchl *g* (Bchl *g*') in diethyl ether (black) and methanol (red).

offers two main advantages: (1) Less technical challenges. Though being the main component in the membrane (mass wise), purifying RC is still labor intensive and could take days to weeks. Small-scale purification with HPLC system is faster, but very high purity is difficult to achieve. (2) Higher result accuracy. Bchl *g*'s UV-Vis absorption Q band is at 788nm when bound with protein, within the range from 740nm to 790nm in organic solvent, which has no interference from any other pigment in *H. modesticaldum*. Besides, pigments extraction can be done by using whole cells, which avoids the inevitable loss during any purification process. However, caution must be used since Bchl *g* is extremely sensitive to oxygen. Therefore, we conducted every step of the procedure inside an anaerobic chamber with O_2 level of < 1 ppm. The spectrum of cell pigment extracts from 250 μL was shown in Fig. 2. We chose the absorbance at 850 nm as the baseline, thus the absorbance at 750 nm is 0.05. Based on the extinction coefficient we calculated, 58.5 $mM^{-1}cm^{-1}$, we can further calculate the concentration of both pigments from 250 μL cell culture is 1.7 μM.

Much work has been done on figuring out the number of Bchl *g* and Bchl *g*' bound in *H. modesticaldum* RC complex; a broad range of numbers were reported, from 22 to 40 [9, 23-25]. Due to this unsettled issue, we decided to use 22 and 40 to calculate the number of RCs and generate a range instead of a single number. Therefore, the RCs in the cells from 250 μL cell culture is from 42.7 to 77.7 pmol.

H. modesticaldum cytochrome bc complex quantification

Quantitative Western blotting was used to determine the amount of cytochrome *bc* complex in the cell lysate from 250 μL cell culture. Meanwhile, RC's quantities in the same

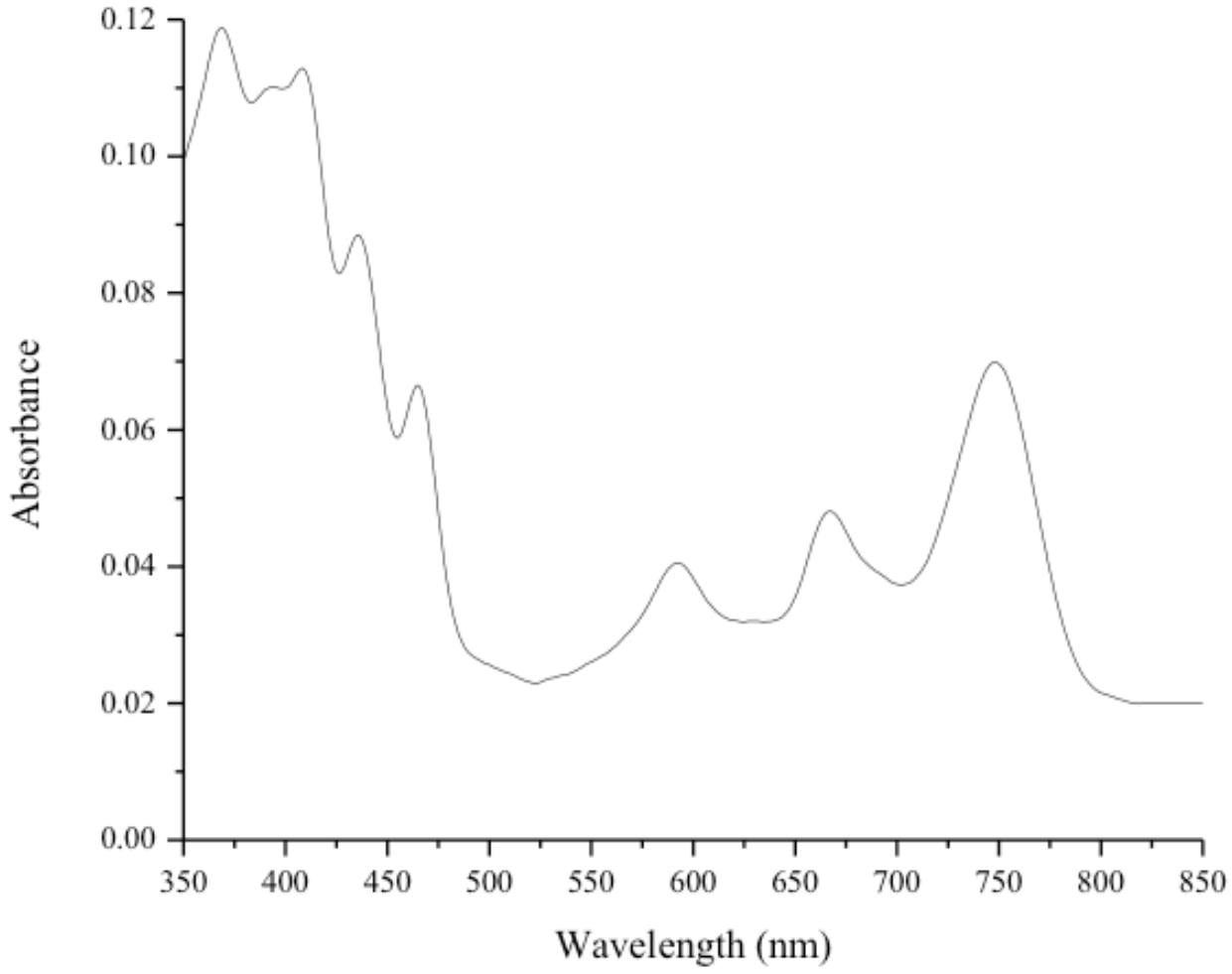

Fig. 2 UV-Vis absorption spectra of cell pigment extracts from 250 μL cell culture.

volume/mass of lysate from 250 μL cell culture. Meanwhile, RC's quantities in the same volume/mass of cells was already measured by UV-Vis spectroscopy and calculated. Since diheme cytochrome *c* is one of the four subunits of the *H. modesticaldum* cytochrome *bc* complex, using antibodies raised against diheme cytochrome *c* to probe that subunit can also provide quantitative information about the complex. A stock solution of expressed diheme cytochrome *c* with unknown concentration (measured by pyridine hemochrome method described in chapter two) was diluted into five separate samples with different factors and their western blot chemiluminescence signals were used to generate calibration curve. To minimize experimental error and increase consistency, cell lysate sample from 250 μL cell cultures, after denaturation, was loaded onto the same SDS gel with the standard diheme cytochrome *c* samples. The developed western blot membrane of serial dilutions of recombinant diheme cytochrome *c* and cell lysates is shown in Fig. 3(a); the calculated loading moles and chemiluminescence signal readings of the samples are summarized in Fig. 3(b). Band intensities on the blot (shown in Fig. 3) were analyzed by spot densitometry and then plotted against recombinant diheme cytochrome *c* amount to generate a standard curve within the linear range of recombinant diheme cytochrome *c* (Fig. 4). Based on the fitting function, the pixel reading of the cell lysate sample from the cells in 250 μL culture, we can calculate that there is 5.39 pmol diheme cytochrome *c* subuni. Although *H. modesticaldum* cytochrome *bc* complex has a similar general organization to that of the cytochrome b_6f complex thus it most likely is also a heterodimer complex, functionally, the two monomers work somewhat independently as two catalytic centers. Therefore, in cells from 250 μL culture, there is 5.39 pmol cytochrome *bc* complex catalytic centers.

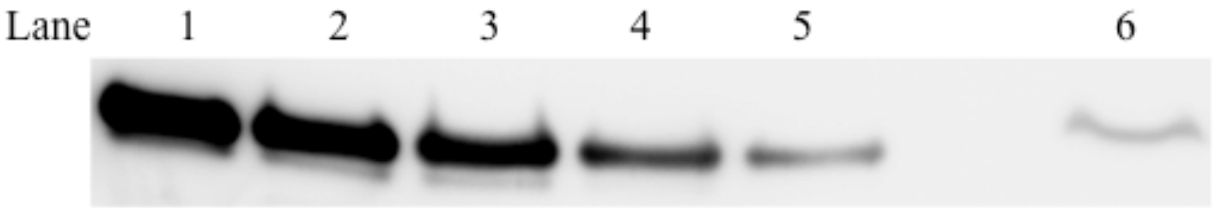

(a)

Lane	**Sample**	**Loaded** (pmol)	**Pixels**
1	standard 1	25.4	47979900
2	standard 2	20.2	32495100
3	standard 3	12.2	20928500
4	standard 4	5.10	10693400
5	standard 5	2.54	4157540
6	cell lysate	TBD	1871323

(b)

Fig. 3 Quantification of diheme cytochrome *c* subunit of cytochrome *bc* complex in different cell lysate samples. (a) Chemiluminescence signals from the western blot of standard samples (serial dilutions of recombinant diheme cytochrome *c*, lane 1-5) and cell lysate (lane 6) with exposure time of 5 seconds. (b) Gel loading amount (pmol) and signal strength (pixels, background subtracted) of all samples.

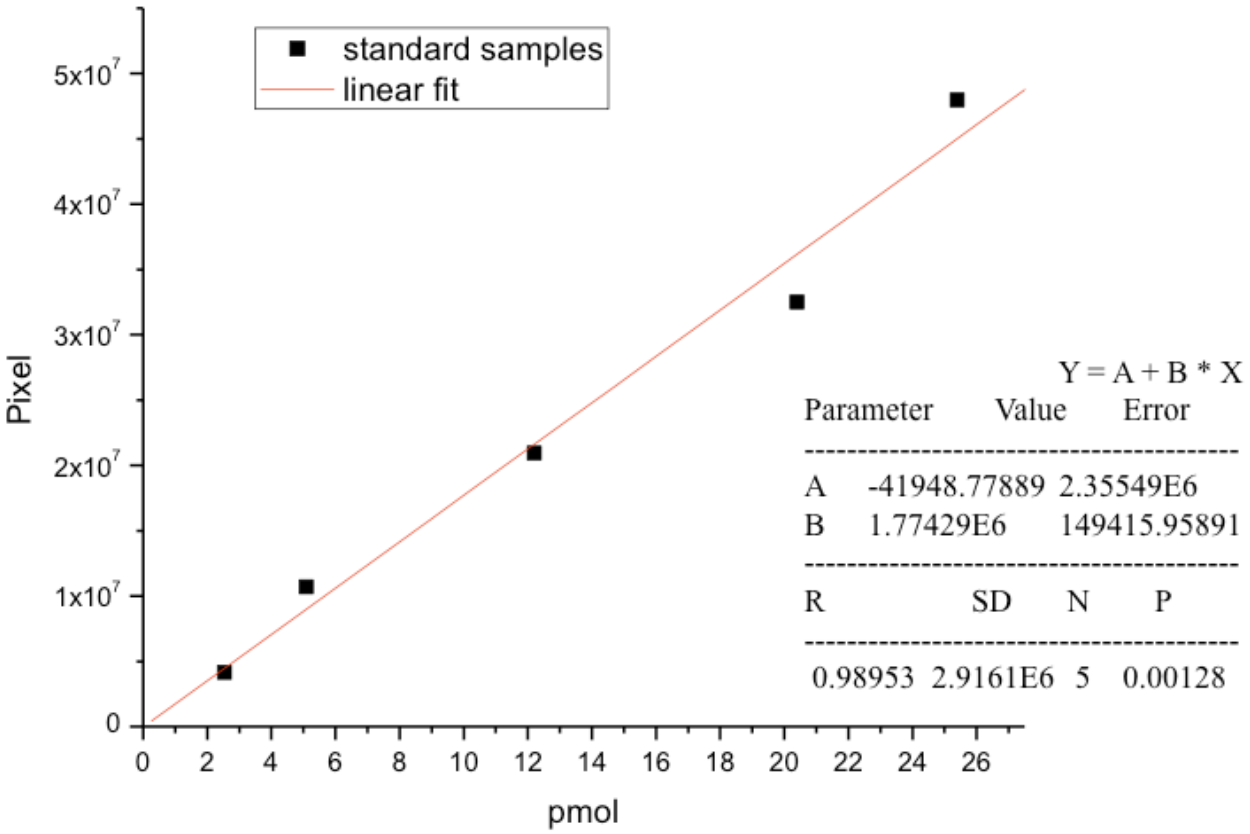

Fig. 4 Calibration curve of serial dilutions of recombinant diheme cytochrome *c* with known quantity. The data were fitted with Origin 7.5 (OriginLab) and the fitting parameters were shown in the chart.

H. modesticaldum RC/cytochrome bc complex catalytic center ratio

To make the results comparable, we took the same amount of cells from the same overnight culture (250 μL), to measure the moles of RC and cytochrome *bc* complex. The calculation shows that there are 42.7 to 77.7 pmol of RCs and 5.39 pmol cytochrome *bc* complex catalytic centers in the cell membrane. The ratio is 14 to 8 RCs per cytochrome *bc* complex catalytic center.

Discussion

Although classical Western blotting is typically used for qualitative purposes, it also can be used for quantitative analysis of proteins [26, 27, 28], provided that specific controls are included. To generate linear calibration curve, a variety of recombinant diheme cytochrome *c* solution concentrations were tested. We found that the loading amount from 1 pmol to 30 pmol, under our current experimental and material conditions, can give an acceptable linear calibration curve. More than 30 pmol of sample loading will saturate the densitometrical signals and cause artifact and nonlinear calibration curves. At the same time, the cell lysate sample must contain sufficient cytochrome *bc* complexes (diheme cytochrome *c* subunit proteins), so that its amount will be within the standard curve range. After exploring with the amount of cells taken from overnight cell cultures, we settled with the cells from 250 μL culture mixture.

As shown in the results, the ratio is determined as 14 to 8 RCs per cytochrome *bc* complex catalytic center in *H. modesticaldum*, whereas a number around 1 – 2 RC per cytochrome *bc* complexes in *H. mobilis* was reported in earlier literatures [17, 18]. This

significantly lower number we determined is in line with our observations during the cytochrome *bc* complex purification attempts that comparing to RC, which shows in the native and denatured gels as the most abundant component in membrane, the cytochrome *bc* complex, mainly its diheme cytochrome *c* subunit, can only be detected with very sensitive staining techniques, e.g. silver staining or Western blot. As reviewed in the introduction section, the RC : cytochrome *bc* complex stoichiometry was calculated from light-induced redox changes in whole cells from *H. mobilis* recorded under anaerobic and aerobic conditions. The authors had to make several assumptions, e. g. all photooxidizable cytochrome *c* appears in the light-dark difference spectrum in the anaerobic conditions, all oxidizable cytochrome *b* appears in the anaerobic-aerobic dark difference spectrum, and cytochrome *b* and *c* have equal extinction coefficients at their respective α-bands, ignoring the complexity of the heliobaterial whole cell system. Indeed, although *H. mobilis* and *H. modesticaldum* share very high similarity in general, it does not mean that they should have exactly the same photosystem and RC to cytochrome *bc* complex ratio, therefore the previous results might be still correct in *H. mobilis*. However, in terms of methodology, we believe the most accurate way to determine this number is through direct detection of the proteins or pigments contained inside the complexes, as shown in this chapter.

The 14 to 8 RCs per cytochrome *bc* complex catalytic center ratio, which is much higher than the roughly 1 : 1 in the previous literatures, indicates that the cytochrome *bc* complex in *H. modesticaldum* may have a high catalytic turnover number. In the heliobacterial cyclic electron transfer system [29], the proposed electron transport cycle starts with charge separation in the RC, resulting in oxidation of menaquinol in the membrane via turnover of the cytochrome *bc* complex; and electrons from the RC (reducing side) complete the cycle by re-reducing the menaquinone via NADH:menaquinone oxidoreductase (complex I). To explain the low

percentage of the cytochrome *b* being oxidized while cytochrome *c* being reduced despite the almost stoichiometric relationship between RC and the *bc* complex reported in the previous papers [17, 18], in their model, the authors proposed a mechanism in which a significant fraction of the menaquinone produced at the Q_o site of the cytochrome *bc* complex must be re-reduced by the NADH:menaquinone oxidoreductase, whereas, in chloroplasts of plants or algae, most of the quinones produced at the Q_o site are re-reduced at the Q_i site. Based on our study, the presence of fewer cytochrome *bc* complexes per RC indicates a much faster turnover of the *bc* complex, thus the significance of the involvement of complex I protein in terms of re-reducing menaquinone is decreased. Therefore, functionally, the cytochrome *bc* complex in *H. modesticaldum* might share more similarity to the ones in chlorophlasts in plants or algae than previously thought.

In conclusion, as part of the effort to understand the function of the *H. modesticaldum* cytochrome *bc* complex, its relationship to RC, and the role of the dynamics of these two key components of the entire photosystem, we determined that there are 8 to 14 RCs per cytochrome *bc* complex catalytic center with quantitative Western blot and absorption spectroscopy. This much larger number than previously reported result suggests that the cytochrome *bc* complex has a high turnover number, thus higher efficiency in terms of menaquinone re-reducing. More functional studies of the whole cells could reveal more detail of the cyclic electron transport mechanism. Transcriptomic (qPCR) studies are underway to further illustrate the expression of different components of the photosystem on the mRNA level.

Acknowledgement

I would like to thank Dr. Deriusz Niedzwiedzki and Dr. Haijun Liu in my lab for the kind help and discussion over the determination of the extinction coefficient of Bchl *g* (Bchl *g*') and quantitative Western blot.

References

[1] M. Heinnickel, J. H. Golbeck, Heliobacterial photosynthesis, *Photosynth. Res*. **92** (2007), pp. 35-53.

[2] W. M. Sattley, M. T. Madigan, W. D. Swingley, P. C. Cheung, K. M. Clocksin, A. L. Conrad, L. C. Dejesa, B. M. Honchak, D. O. Jung, L. E. Karbach, A. Kurdoglu, S. Lahiri, S. D. Mastrian, L. E. Page, H. L. Taylor, Z. T. Wang, J. Raymond, M. Chen, R. E. Blankenship, J. W. Touchman, The genome of *Heliobacterium modesticaldum*, a phototrophic representative of the Firmicutes containing the simplest photosynthetic apparatus, *J. Bacteriol.* **190** (2008), pp. 4687-4696.

[3] W. M. Sattley, R. E. Blankenship, Insights into heliobacterial photosynthesis and physiology from the genome of *Heliobacterium modesticaldum*, *Photosynth. Res*. **104** (2010), pp. 113-122.

[4] K. H. Tang, H. Yue, R. E. Blankenship, Energy metabolism of *Heliobacterium modesticaldum* during phototrophic and chemotrophic growth, *BMC Microbiology* **10**, (2010), pp. 150

[5] D. M. Kramer, T. J. Avenson, G. E. Edwards, Dynamic flexibility in the light reactions of photosynthesis governed by both electron and proton transfer reactions, *Trends Plant Sci.* **9**, (2004), pp. 349-357.

[6] R. C. Fuller, S. G. Sprague, H. Gest, R. E. Blankenship, A unique photosynthesis reaction center from *Heliobacterium chlorum*, *FEBS Lett.* **182**, (1985), pp. 345-349.

[7] R. C. Prince, H. Gest, R. E. Blankenship, Thermodynamic properties of the photochemical reaction center of *Heliobacterium chlorum*, *Biochim Biophys Acta.* **810**, (1985), pp. 377-384.

[8] T. Noguchi, Y. Fukami, H. Oh-oka, Y. Inoue, Fourier transform infrared study on the primary donor P798 of *Heliobacterium modesticaldum* cysteine: S-H coupled to P798 and molecular interactions of carbonyl groups, *Biochemistry*. **36**, (1997), pp. 12329-12336.

[9] F. A. M. Kleinkerenbrink, H. C. Chiou, R. LoBrutto, R. E. Blankenship, Spectroscopic evidence for the presence of an iron-sulfur center similar to F_X of Photosystem I in *Heliobacillus mobilis*, *Photosynth. Res*. **41** (1994), pp. 115-123.

[10] H. Oh-Oka, Type I reaction center of photosynthetic heliobacteria, *Photochem Photobiol.* **83**, (2007), pp. 177-186.

[11] B. Jagannathan, J. H. Golbeck, Unifying principles in homodimeric type I photosynthetic reaction centers: properties of PscB and the F-A, F-B, and F-X iron-sulfur clusters in green sulfur bacteria, *Biochim Biophys Acta.* **1777**, (2008), pp. 1535-1544.

[12] A. R. Crofts, The cytochrome bc_1 complex: function in the context of structure, *Annu Rev Physiol*. **66**. (2004), pp. 689-733.

[13] M. T. Madigan, J. G. Ormerod, *Anoxygenic photosynthetic bacteria. Kluwer, The Netherlands*. (1995), pp. 17-30.

[14] H. Gest, J. Favinger, *Heliobacterium chlorum*, an anoxygenic brownish-green photosynthetic bacterium containing a new form of bacteriochlorophyll, *Arch. Microbiol.* **136**, (1983), pp. 11-16.

[15] T. J. Michalsky, J. E. Hunt, M. K. Bowman, U. Smith, K. Bardeen, H. Gest, J. R. Norris, J. J. Katz, Bacteriopheophytin *g*: properties and some speculations on a possible primary role for bacteriochlorophylls *b* and *g* in the biosynthesis of chlorophylls, *Proc. Natl. Acad. Sci. U. S. A.,* **84**, (1987), pp. 2570-2574.

[16] M. H. Vost, H. E. Klaasen, H. J. van Gorkom, Electron transport in *Heliobacterium chlorum* whole cells studied by electroluminescence and absorbance difference spectroscopy, *Biochim Biophys Acta.* **973**, (1989), pp. 163-169.
[17] W. Nitschke, U. Liebl, K. Matsuura, D. M. Kramer, Membrane-bound *c*-type cytochromes in *Heliobacterium mobilis*. *In vivo* study of the hemes involved in electron donation to the photosynthetic reaction center, *Biochemistry* **34** (1995), pp. 11831-11839.
[18] D. M. Kramer, B. Schoepp, U. Liebl, W. Nitschke, Cyclic electron transfer in *Heliobacterium mobilis* involving a menaquinol-oxidizing cytochrome *bc* complex and an RCI-type reaction center, *Biochemistry* **36** (1997), pp. 4203-4211.
[19] A. R. Crofts, C. A. Wraight, The electrochemical domain of photosynthesis, *Biochim Biophys Acta* **726** (1983), pp.149-185.
[20] D. M. Niedzwiedzki, R. E. Blankenship, Singlet and triplet excited state properties of natural chlorophylls and bacteriochlorophylls, *Photosynth Res* **106** (2010), pp. 227-238.
[21] E. J. Meent, M. Kobayashi, C. Erkelens, P. A. Veelen, J. Amesz, Identification of 8^1-hydroxychlorophyll *a* as a functional reaction center pigment in *Heliobacteria*, *Biochim Biophys Acta* **1058** (1991), pp. 356-362.
[22] J. T. Trost, R. E. Blankenship, Isolation of a photoactive photosynthetic reaction center-core antenna complex from *Heliobacillus mobilis*, *Biochemistry* **28** (1989), pp. 9898-9904.
[23] A. M. Nuijs, R. J. van Dorssen, L. N. M. Duysens, J. Amesz, Excited states and primary photochemical reactions in the photosynthetic bacterium *Heliobacerium chlorum*, *Proc. Natl. Acad. Sci. U. S. A.* **82**, (1985), pp. 6865-6868.
[24] M. Kobayashi, E. J. van de Meent, C. Erkelens, J. Amesz, I. Ikegami, T. Watanage, Bacteriochlorophyll *g* epimer as a possible reaction center component of heliobacteria, *Biochim. Biophys. Acta* **1057** (1991), pp.89-96.
[25] M. Heinnickel, R. Agalarov, N. Svensen, C. Krebs, J. H. Golbeck, Identification of F_X in the Heliobacterial reaction center as a [4Fe-4S] cluster with an $S = {}^3/_2$ ground spin state, *Biochemistry,* **45** (2006), pp. 6756-6764.
[26] D. G. Schiavini, J. M. Puel, S. A. Averous, J. A. Bazex, Quantitative western immunoblotting analysis in survey of human immunodeficiency virus-seropositive patients, *J. Clin. Microbiol*. **27** (1989), pp. 2062-2066.
[27] P. Y. Martin, W. T. Abraham, L. M. Xu, B. R. Olson, R. M. Oren, M. Ohara, R. W. Schriers, Selective V2-receptor vasopressin antagonism decreases urinary Aquaporin-2 excretion in patients with chronic heart failure, *J. Am. Soc. Nephrol.* **10** (1999), pp. 2165-2170.
[28] R. Feissner, Y. Xiang, R. G. Kranz, Chemiluminescent-based methods to detect subpicomole levels of *c*-type cytochromes, *Anal. Biochem.* **315** (2003), pp. 90-94.
[29] A. Kolpasky, U. Muhlenhoff, A. Atteia, W. Nitschke, *Photosynthesis: From Light to Biosphere,* **Vol. II** (1995), pp. 951-954.

Chapter 5

Conclusions and future directions

This dissertation has focused on the structural and functional study of the unique diheme cytochrome *c* subunit of the cytochrome *bc* complex in the photosynthetic bacterium *Heliobacterium modesticalum*, and its further application regarding the relationship between *H. modesticaldum*'s cytochrome *bc* complex and reaction center. By doing so, we hope to shed some light on the ultimate goal, a deeper understanding the structure and function of the heliobacterial cyt *bc* complex, which is unique among all other photosynthetic organisms [1, 2].

Heliobacteria provide some very exciting opportunities for the study of photosynthesis: the simplest known antenna/reaction center system [3], a structurally unique cyt *bc* complex, an interesting carbon fixation system [4], etc. The cyt *bc* complex plays a central role in heliobacterial photosynthesis, transferring electrons between electron carriers reduced and oxidized by the photochemical reaction centers, oxidizing menaquinol and reducing cyt c_{553} while translocating protons via some variation of the Q-cycle mechanism. Structurally, while preserving the mechanistic core consisting of the cyt *b* and Rieske iron-sulfur proteins, it has a very different "third" redox subunit, the diheme cyt *c* compared to the cyt c_1 in the cyt bc_1 and cyt *f* in the cyt b_6f complex. In general, this particular subunit in all *bc* complexes bear phylogenetic markers for the species in which the proteins reside [5].

The use of diheme cyt *c* in the *bc* complex separates heliobacteria from all other photosynthetic organisms, and groups it with Gram positive actinobacteria and Gram negative ε-proteobacteria. This cytochrome is of the c_4 type, and the sequence comparisons of the two monoheme domains suggest that it probably results from gene duplication and subsequent gene fusion. Most cyt c_4 proteins are soluble electron carriers that might interact with membrane proteins as electron transfer partners. However, in heliobacteria, there is no soluble cytochrome; the diheme cyt *c* has a N-terminal transmembrane helix, which helps to anchor the protein in the

membrane and thus be a subunit of the *bc* complex.

The first part of the thesis (Chapter 2) described the construct of a heliobacterial diheme cyt *c* expression system in *E. coli* and the protein purification and characterization. Because the diheme cyt *c* is a subunit of the *bc* complex, direct purification of the whole complex and subsequent fractionation is probably not the best strategy to acquire it. To sustain the following biochemical and biophysical, especially crystallographic studies, a large amount of protein is needed. Therefore, establishing an expression system is a key step. Herein, in this part of our work, the diheme cyt *c* was expressed in *E. coli* and purified. Western blot, heme staining and mass spectrometry results confirmed that two heme-binding motifs of the protein are covalently linked with two *c*-type hemes. The single redox midpoint potential of the recombinant diheme cyt *c* strongly suggests that the two hemes are in extremely similar protein binding environments. This result is quite different from the two distinct midpoint potentials of many cyts c_4, which share the same origin with heliobacterial diheme cyt *c*. This is a hint that in the heliobacterial diheme cyt *c*, the two hemes interact with each in a different way compared to some other cyts c_4. The structural model of the protein shows that for each heme group, only one edge is exposed toward the different sides of the protein respectively. Some structural arrangement of the protein must allow intramolecular interheme electron transfer to happen so that this subunit can behave similarly to cyt c_1 or cyt *f* as a functional analog. In other words, some kind of structural rearrangement or conformational change may happen upon reduction or oxidation to facilitate the intramolecular electron transfer between the two hemes.

To further elucidate the relationship between diheme cyt *c*'s different redox states and its conformations, in Chapter 3 of this dissertation, we utilized two mass spectroscopic techniques, hydrogen/deuterium exchange mass spectrometry and ion mobility mass

spectrometry. HDX-MS can theoretically offer single amino-acid resolution about protein chain dynamics; and IM-MS, especially coupled with native protein MS, will provide information about the proteins' global conformation under different physical conditions. In HDX kinetics studies, in almost all regions from most of the peptides, the oxidized form shows larger deuterium uptake compared to the reduced form, which indicates that the oxidized form of the diheme cyt *c* has a more open structure or at least higher dynamics. Meanwhile, the oxidized diheme cyt *c* showed a longer drift time comparing to its reduced form in the IM chamber, indicating a conformation with larger dynamic diameter, which is consistent with the conclusion drawn from HDX-MS experiments. Our experiments showed unambiguously that there is a real structural conformational difference between the two different redox states. A smaller or more compact reduced form might have the function of bringing the two hemes closer to facilitate interheme electron transfer. Therefore, in terms of the intramolecular electron transfer mechanism, no matter specifically what this mechanism is, it may be sensitive to the distance between hemes.

One key question that remains to be answered is the working mechanism of heliobacterial cyclic electron transfer. To take on this challenge, determining the stoichiometry of its key components, e.g. reaction center, cyt *bc* complex, is crucial information. Yet this seemingly simple study has yet been able to present any conclusive answer due to many challenges, e.g. heliobacteria's extreme sensitivity to oxygen, the electron transfer chain's vulnerability to any cell disruption and membrane preparation [5], etc. The complexity of whole cell studies makes some results non-conclusive. Therefore, in Chapter 4, we determined the ratio between *H. modesticaldum* RC and *bc* complex using direct protein quantification methods. We measured RC quantity based on the absorption spectra of Bchl *g* (Bchl *g'*) directly extracted

from whole cells. The cytochrome *bc* complex quantity in the same amount of cells was determined by quantitative Western blot, using the antibody raised against its diheme cyt *c* subunit as the probe and recombinant diheme cyt *c* as internal standards. Therefore, 14 to 8 RCs per cytochrome *bc* complex catalytic center was determined. Compared to the previously reported 1 - 2 RC per cytochrome *bc* complexe, this much larger number suggests that the cyt *bc* complex has a high turnover number, thus higher efficiency in terms of menaquinone re-reduction.

Despite the significant progress we made on this system, there are many intriguing questions that remain to be answered in order to obtain a complete picture of the structure and function of heliobacterial diheme cyt *c*, the cyt *bc* complex, and their exact role in the cyclic electron transfer chain. One study that is underway is to acquire the X-ray crystal structure of the recombinant diheme cyt *c* protein, in collaboration with Prof. Noam Adir from the Technion University, Israel. To this end, we already crystallized the protein and the crystal diffracted at 2.0 Å, shown in Fig. 1. Right now, we are working on solving the structure. With the crystal structure, we will be able to know the exact geometry of the hemes relative to the protein backbone, the heme binding pockets' structure and their physical and chemical environment, the surface charge distribution across the two heme binding domains, and we will be able to map the HDX kinetics more accurately with respect to the protein structure. Another research also underway is the transcriptomic (qPCR) study for the comparison of the mRNA levels of some key heliobacterial photosynthetic proteins and protein complexes, e.g. RC, cyt *bc* complex, NADH:menaquinone oxidoreductase (complex I), etc. As addressed in Chapter 4, the stoichiometry between key photosynthetic proteins is crucial to the understanding of the cyclic electron transfer mechanism in heliobacteria. Yet due to a shortage of the availability of the

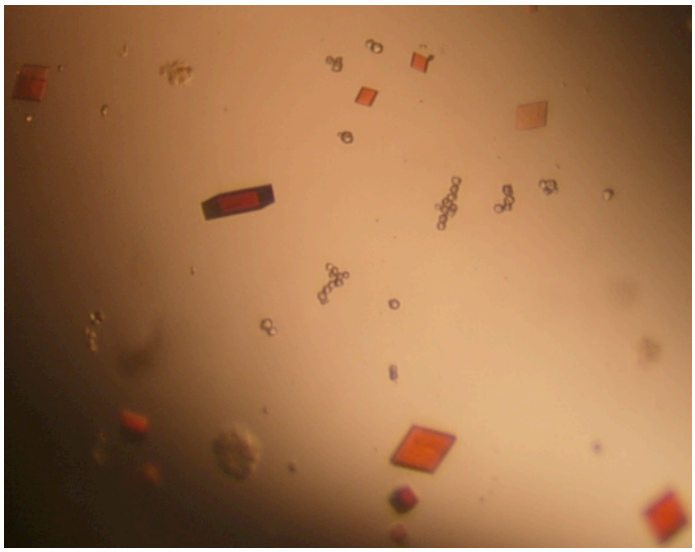

(a)

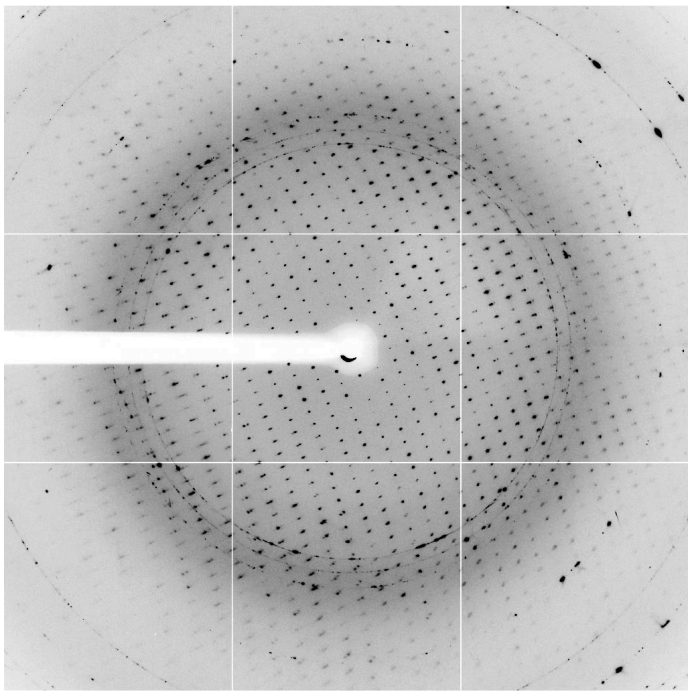

(b)

Fig. 1 Diheme cyt *c* crystals (a) and its diffraction pattern (b).

antibodies raised against those proteins or protocols to purify intact proteins, quantitative western blot is not feasible in every case. Since the bacterial genetic system is relatively simple, mRNA level can be used to represent the protein expression level *in vivo* with relatively high certainty. In our studies, almost all other proteins' genes behave normally in the qPCR experiments except the *pshA* gene, which encodes the RC core protein PshA: there was almost no detectable cDNA level from *pshA* transcripted mRNA. We are now doing trouble-shooting to exclude any experimental errors and optimizing protocols.

Ultimately, we would like to purify the intact cyt *bc* complex and crystallize it. Much effort has been committed to its purification yet no protocols that will generate intact enzymes have been successfully developed so far. Nevertheless, we have made important progress in terms of understanding its crucial subunit, the diheme cyt *c*, which provided valuable information about not only the subunit, but also the entire complex and its relationship with the rest of the heliobacterial photosystem. However, much remains to be explored. All in all, we are still left with more questions than answers.

References

[1] A. L. Ducluzeau, E. Chenu, L. Capowies, F. Baymann, The Rieske/cytochrome *b* complex of Heliobacteria, *Biochim. Biophys. Acta* **1777** (2008), pp. 1140-1146.
[2] F. Baymann, W. Nitschke, Heliobacterial Rieske/cyt *b* complex, *Photosynth. Res.* **104** (2010), pp. 177-187.
[3] M. Heinnickel, J. H. Golbeck, Heliobacterial photosynthesis, *Photosynth. Res.* **92** (2007), pp. 35-53.
[4] C. von Mering, P. Hugenholtz, J Raes, S. G. Tringe, T. Doerks, L. J. Jensen, N. Ward, P. Bork, Quantitative phylogenetic assessment of microbial communities in diverse environments. *Science* **315** (2007), pp. 1126-1130.
[5] M. H. Vost, H. E. Klaassen, H. J. van Gorkom, Electron transport in *Heliobacterium chlorum* wholecells studied by electroluminescence and absorbance difference spectroscopy, *Biochim. Biophys. Acta* **973** (1989), pp. 163-169.